People's Democratic Republic of Algeria

Ministry of Higher Education and Scientific Research

University of Amar Thelidji-Laghouat

FACULTY of TECHNOLOGY

DEPARTMENT OF ELECTRICAL ENGINEERING

Dissertation of MASTER

Presented by:

Chouireb Saad

DOMAIN: TECHNOLOGY

FACULTY: ELECTRICAL ENGINEERING

OPTION: ELECTROMECHANICS

Theme

Sensorless control of PMSM drive for electric vehicle applications

defense jury :

last name and first names	Grade	quality
Hajaj Chafiq	**Prof**	President
Bougrine Djamel Eddine	**MCB**	Examiner
Bendjedia Bachir	**MCA**	Supervisor

Promotion : 2021-2022

ملخص

تركز هذه المذكرة على تحسين أداء سلسلة الجر لسيارة كهربائية في حال حدوث عطب على مستوى مستشعر السرعة. في الواقع ، توجد بالفعل مستشعرات حالية في سلاسل الجر ومع ذلك ، فإنها تولد تكاليف إضافية كبيرة بسبب فشلها المتكرر والحاجة إلى الاستبدال. وبالتالي ، فإن التحكم بدون مستشعر في أنظمة تشغيل المحركات يسمح بإزالة المستشعرات وبالتالي تجنب تكلفتها. الهدف من المذكرة هو تطوير طرق جديدة ترافق التحكم في المحرك لضمان أداء أفضل لسلسلة الجر في حال غياب او حدوث عطب على مستوى مستشعر السرعة.

تم التطرق لثلاث طرق مختلفة لاستشعار السرعة الميكانيكية للمحرك التزامن ذو المغناطيس الدائم وهي كالتالي (MRAS)والتي تعتمد على اتباع طريقة النظام المرجعي التكيفي ، ومراقب الوضع المنزلق (SMO) ومرشح كالمان الممتد (EKF). تم استخدام الطرق الثلاثة مع التحكم الشعاعي في سلسلة الجر في حالتين ’الاولى هي غياب مستشعر السرعة في وضع عادي .والثانية في حالة حدوث عطب على مستوى مستشعر السرعة يتم استبدال هذا الأخير بأحد انظمة المراقبة الثلاثة لضمان استمرارية تشغيل المحرك وبالتالي تحسين اداء سلسلة الجر لسيارة الكهربابية.

كلمات مفتاحية السيارة الكهربائية. مستشعر السرعة. عطب. محرك التزامن ذو مغناطيس دائم (EKF) (SMO) (MRAS) بدون مستشعر .

Abstract

This these focuses on improving the reliability of a traction chain for electric vehicle applications, If there is a failure in the speed sensor In fact, there are already existing sensors in the traction chains however, they generate significant additional costs due to their frequent failure and the need for replacement. Thus, speed sensorless control of the AC drive systems allows the elimination of the sensors of the machine and therefore to avoid their cost, the objective of the thesis is to develop new methods that accompany the motors control to ensure better performance of the traction chain in the absence or failure of the speed sensor

In this thesis, the observers is presented by model reference adaptive system method (MRAS), the sliding mode observer (SMO) and the extended Kalman filter (EKF) to be used in the control of the conversion chain

The three methods were used with vector control of the traction chain in two cases. The first is the absence of the speed sensor in a normal condition. The second is when the failure happen at the speed sensor, which is replaced by one of the three observers systems to ensure the continuity of drive operation and thus improve the performance of the traction chain of the electric vehicle

Keywords: Electric machine, sensorless control, MRAS, SMO, EKF, electric vehicle, observers, Permanent magnet motor

ACKNOWLEDGMENTS

First of all, we would like to thank "ALLAH" for giving us the strength and the courage to carry out this modest work, also we thank our parents very much, and who encouraged and helped us to reach this stage of our training. .

We would like to thank all those who contributed to finalize this modest work.

Our thanks go to Dr. Bendjedia Bachir our supervisor for guiding me in the realization of this project.

Many thanks to the members of the jury for honoring me by accepting to judge the modest work I have done, to Mr. Hajaj Chafik for accepting to preside over this jury, and Mr. Djamel Eddine Bougrine,to be Examiner

We sincerely thank our comrades. And Mr. Kamel Tounsi for their moral and educational support throughout the preparation period.

We would like to thank our professors from the electrical engineering department who did not hesitate our education.

Finally, I would like to thank all those who helped and assisted me during my studies.

Dedication

This work is wholeheartedly dedicated to my beloved parents

To my dear father,

To my dear mother,

Who have never ceased, to formulate prayers for me, to support me and help me achieve my goals

To my brothers and sisters

TO all my family

Especially my uncle Omar, May God have mercy on him, and make him enter Jannah al-Firdaws, "Amen"

GLOSSARY

EV:	*electric vehicle*
BEVs:	*battery electric vehicles*
HEV:	*hybrid electric vehicles*
FCEV:	*fuel cell electric vehicle*
PHEVs:	*plug-in hybrid electric vehicles*
ICE:	*the internal combustion engine*
PWM:	*pulse width modulation*
NEDC:	*north european driving cycles*
UDC:	*urban driving cycle*
EUDC:	*extra urban driving cycle*
SFTP:	*supplemental federal test procedures*
FOC:	*field oriented control*

Nomenclature

in the sequel, v can be a, b, c, α, β, 0, d or q.

u_v:	*Voltage across winding v*
v_v:	*electric potential of the point v*
t:	*time.*
i_v:	*Current of winding v.*
r :	*motor resistance per phase.*
j :	*motor moment inertia.*
P:	*number of the motor pole pair.*
$P(\theta)$:	*park transformation matrix*

$\boldsymbol{P_{EV}}$: *The power at the wheel*

$\boldsymbol{\Omega_{roll}}$: *The rotation speed of the wheel*

r: *the radius of the wheel*

$\boldsymbol{B_m}$: *Viscous coefficient of friction*

$\boldsymbol{K_{C2T}}$: *Torque constant*

$\boldsymbol{t_d}$: *Time constant*

$\mathbf{t_m}$: *electromagnetic torque.*

θ: *rotor electric position.*

$\boldsymbol{\hat{\theta}}$: *rotor electric estimated position*

$\boldsymbol{\varphi_v}$: *magnitude of the magnet flux.*

$\boldsymbol{\lambda_m}$: *Permanent magnet flux amplitude in dq0 and αβ0 frame.*

L : *Self-inductance per phase in the abc frame.*

$\mathbf{L_d}$: *d- Axis inductance.*

lq : *q- Axis inductance.*

$\boldsymbol{\omega_r}$: *The measured speed*

$\boldsymbol{\widehat{\omega_r}}$: *The estimated speed*

$\boldsymbol{\widehat{I_q}}$: *d- Axis estimated current*

$\boldsymbol{\widehat{I_d}}$: *q- Axis estimated current*

$\boldsymbol{e_d}$: *d- Axis back electromotive force*

$\boldsymbol{e_q}$: *q- Axis back electromotive force*

η: *Popov integral variable*

.

List of figures

List of tables:

Summary

CHAPTER I: State of the art on electric vehicles

CHAPTER II: Modelling and Field Oriented Control of PMSM

CHAPITREIII: *Speed Sensorless Vector Control of PMSM*

Chapitre IV: Electric Vehicle Application with a Driving Cycle

General Introduction

General Introduction

Electric mobility and zero emission vehicles are key factors for sustainable transport. In the wake of the technological advances, automotive suppliers are focusing their efforts on reducing CO2 emissions and on the "intuitive driving", which combines the connected vehicle, autonomous driving and the man-machine interface, making them accessible to all.
Mechanical actuators are being replaced by electric power systems which have faster time response. Despite that the automotive industry is cost sensitive, there are strong incentives to increase system costs in order to improve the level of safety with new risk-based safety standards. Naturally, proper operations of certain functions are of utmost importance and their failure cannot be tolerated since this would drastically compromise safety. Moreover, the dependence on a continuous power supply causes problems with vehicle propulsion and an electric energy source must be carried on-board, which is usually heavy and expensive (storage battery, rotating generator with internal combustion engine, fuel or solar cells). This requires the embedded energy to be smartly used and to cope with faults that highly increase energy consumption (e.g. a sensor fault which induces an over-current).

Electrical drives adopting permanent-magnet synchronous machines (PMSM) are suitable for a wide range of applications in cars. These applications include not only propulsion but also steer and brake-by-wire systems, active suspension, electrical compressors and other electrical subsystems. For PMSM drives used for propulsion, it is evident that increasing the level of reliability that goes with a significant with cost cannot be motivated if a fault is not significantly increasing the accident risk or if a post-fault strategy cannot be economically motivated for the specific vehicle model. That's the main difference aerospace domain where a high safety level is requested and then, needs on solutions are more justified, and well suited to increase the reliability, the availability and the continuous operation of electromechanical systems [1].

This study focuses on electric vehicle drive the term *drive* pertains to both the electric machine as well as its corresponding inverter although faults can arise in other parts including sensors

Generally, mechanical position/speed sensor with high resolution is a prerequisite for excellent control, which also adds to the cost and complexity and impairs the reliability of drive systems. Therefore, the control system without mechanical position sensors, or known as position/speed sensorless control of AC motors has been studied and applied increasingly in both industries and household appliances.

The objective of this thesis is to detect and isolate the sensors faults at their incipient stage and perform a post-fault reconfiguration if possible by Estimation. To this purpose, the work goes from theoretical studies toward experimental validations through the model simulation. The outline of the thesis is summarized as follows:

- In chapter 1, state of the art electric vehicle, Its Architecture, and configurations, an Overview of Electric Vehicles Sensors, electrical drives challenges, Consequences of the faults in the drive operation and the existing solutions proposed to overcome these faults

- In chapter 2, is devoted to the modeling part of the different components of the traction chain. First, we presented the synchronous motor with magnets permanent as well as its modelling. And converter modelling and control types of PMSM FOC method control with speed sensor and overview about sensorless FOC control.

- In chapter 3, we apply the vector control of the permanent magnets synchronous machine with the observers first is MRAC observer and SMO observer then finally we have EKF observer. In order to improve the performance of the system, we propose to do the parametric variation tests and Torque variation in terms of robustness. A comparative study between vector control with speed sensor and without speed sensor that by speed and precision is presented.

- In chapter 4, we will present the application of one of the three control strategies on the traction chain. For this, a dynamic model of the vehicle with a driving cycle are presented. This allows us to have the speed and load torque setpoints for a real vehicle. The two control techniques are compared in terms of performance dynamic and static for the electric vehicle application.

Chapter I

STATE OF THE ART ON ELECTRIC VEHICLES

I.1 Introduction:

With the increasing interests on energy efficiency, energy cost, and environmental protection, the development of Electric Vehicles (EVs) technology has been obvious nowadays. The technologies involved in EVs are diversified and include electrical and electronics engineering, mechanical engineering, automotive engineering, and chemical engineering. EVs depend on which called electric propulsion, in which an electric motor is used to drive the vehicle instead of the internal combustion engine (ICE) and the energy sources are batteries, fuel cells, or capacitors instead of gasoline or diesel fuel in the conventional ICE vehicles. Thus, power electronics technology plays an important role in the electrical propulsion system in order to efficiently drive the electric motor of the vehicle and control the power converters and the associated electronic circuits. [2]

An overview of the current status of power electronic drives for EVs and recent research trends in EV motors, power converters, and energy storage systems will be discussed. Challenges associated with designing, controlling, and operating the motors and power electronic converters used in EVs will be also discussed showing the latest achievements in this field.

I.2.1. History

While electric vehicles are often considered a modern technology, they have actually been around for quite a long time: more than 150 years, in fact. Table.I.1.A shows most interesting events in the history of electric vehicles [3].

Table.I.1.A. Electric vehicles history

picture	The event	The year
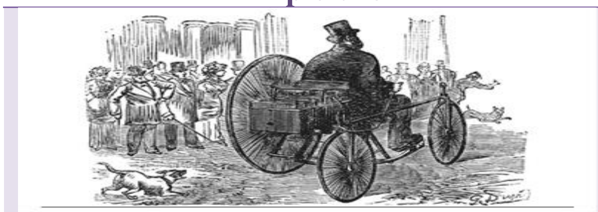	French electrical engineer Gustave Trouvé fits an electric motor to a tricycle, making the first manned electric road vehicle	**1881**
 FIGURE 2.24 The Flocken Elektrowagen.	German inventor Andreas Flocken develops the Flocken Elektrowagen, the first electric car to be widely known	**1888**

	The first vehicle of any kind to reach 60 mph is an electric car, La Jamais Contente , driven by Le Diable Rouge ,. The car has an aerodynamic, torpedo-shaped body made of aluminum alloy, although much of the aerodynamic benefit is ruined by the driver sticking out the top. Driven by two 25-kW motors, it tops out at 65.8mph. While this record will hold for the next three years.	**April 29, 1899**
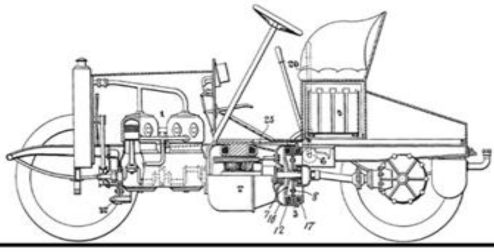	Henri Pieper of Germany develops a parallel hybrid car, which uses an electric motor to supplement the power provided by its weak ICE and batteries charged by the engine while coasting and descending hills The Pieper parallel hybrid starts in electric mode, making it the first ICE vehicle with an electric starter. This is important because until the advent of the self-starter in the early twentieth century,	**1899**
	As a result of more affordable ICE vehicles, the self-starter, improved roads, a rise in interest in longer road trips (known as “touring”), and cheap oil gushing out of the wells, ICEs totally dominate the roads, temporarily driving electric vehicles to extinction	**1910s to 1920s**
	The Henney Motor Company manufactures 100 of the Henney Kilowatt, an electric car based on the Renault Dauphine. Despite a top speed of 60 mph and a range of 60 mi, there is little demand	**1959 to 1960**
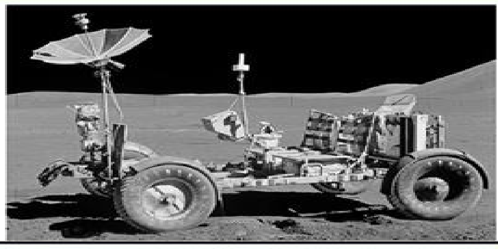	The lunar rovers used by the astronauts of Apollo 15, 16, and 17 are electric. Two 36-V silver-zinc potassium hydroxide primary batteries provide each rover with 57 mi of range Apollo 17 Commander Eugene Cernan sets the unofficial land speed record on the moon: 11.2 mph	**1971 to 1972**
	AC Propulsion demonstrates the tZero, a prototype electric sports car with a 150-kW motor that accelerates from 0 to 60 in 4.07 sec and runs a quarter-mile in 13.24 sec. The original version, using leadacid batteries, has a range of 80 to 100 mi	**1997**

	Tesla releases the Tesla Model S. As of 2020, it has a maximum range of 391 mi (the longest range of any production EV in history, by far), a minimum 0 to 60 time of 2.3 sec (the fastest 0 to 60 time of any production sedan of any kind), and a starting price of $74,990	**2012**
	Tesla announces the Tesla Cybertruck, with a maximum range of over 500 mi, a minimum 0 to 60 time of less than 2.9 sec, a maximum towing capacity of more than 14,000 lb, and a starting price of $39,900. Production is expected to begin in 2021	**2019**

Electric vehicles have had a long and storied history, full of triumphs and tribulations. While it remains to be seen what will happen in the future, one might hope that the newest generation of electric vehicles will finally prevail where previous generations have so far failed

I.2.2. Advantages of Electric Vehicle (EV)

Electric vehicles have other advantages over those powered by combustion engines as follow:

1. No fuel, No pollution.
2. It required less maintenance.
3. Total operation is noise free.
4. It generates high starting torque.
5. We can charge at home.
6. Less Running cost than gasoline powered vehicle.
7. It helps to save fossil fuels.

I.2.3. Challenges:

Electric cars are growing in popularity every day. Just like conventional cars, there are certain benefits and drawbacks of using an electric car. Here are the most important few to consider:

A. Recharge Points:

Electric fueling stations are still in the development stages. Not a lot of places you go to on a daily basis will have electric fueling stations for your vehicle, meaning that if you're on a long trip or decide to visit family in a rural or suburban area and run out of charge, it may be harder to find a charging station. You may be stuck where you are.

B. The Initial Investment is Steep:

As EVs are very new, you may be surprised when you take a look at the sticker price for EVs. Even the more affordable brands can be around $30,000 to $40,000.

C. Short Driving Range and Speed

Electric cars are limited by range and speed. Most of these cars have a range of about 50-100 miles and need to be recharged again. You just can't use them for long journeys as of now, although it is expected to improve in the future.

D. Longer Recharge Time

While it takes a couple of minutes to fuel your gasoline-powered car, an electric car takes about 4-6 hours and sometimes even a day to get fully charged. Therefore, you need dedicated power stations as the time taken to recharge them is quite long. Thus, the time investment and necessary planning do put some people off.

E. Silence as a Disadvantage

Silence can be a bit disadvantage as people like to hear the noise if they are coming from behind them. An electric car is, however, silent and can lead to accidents in some cases

F. Battery Replacement

Depending on the type and usage of battery, batteries of almost all electric cars are required to be changed every 3-10 years [4].

I.2.4 Types of Electric Vehicles:

An EV can be broadly categorized into two types: Battery electric vehicle (BEV) one that runs solely on electricity and the hybrid electric vehicle (HEV) that combines the electric energy with any other source as shown in Fig. I.2. . . [4], Hybrid electric vehicles (HEVs) have an inherent advantage and it can stretch the fuel economy further by combining the best of both battery and an engine. Thus, while in a populated/urban area the vehicle could be operated on battery and then could switch to the engine when outside the city. Hybrids can further be subdivided into plug-in hybrid electric vehicle (PHEV) and fuel cell electric vehicle (FCEV). EVs could therefore, be categorized into:

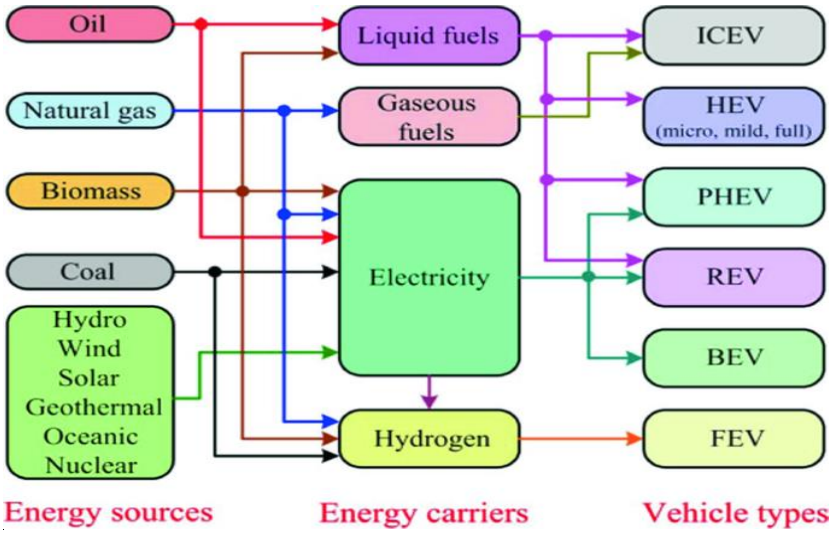

Fig.I.1. Energy diagram of EVs [5]

1. Battery electric vehicles (BEVs),
2. Hybrid electric vehicles (HEVs),
3. Plug-in hybrid electric vehicles (PHEVs),
4. Fuel cell electric vehicles (FCEVs).

	Battery Electric Vehicle (BEV)	**Plug-In Hybrid Vehicle (PHEV)**	**Hybrid Electric Vehicle (HEV)**	**Conventional Vehicle**
Key mechanism	Powered by an electric motor and a battery that can be recharged by plugging into an electric outlet	Powered by a conventional engine (petrol/diesel), along with an electric motor and a battery that can be plugged-into an electrical outlet for recharging	With a conventional (petrol/ diesel) engine, HEVs are powered by an electric motor and a battery that is recharged by regenerative braking	Powered by an Internal combustion engine(petrol/diesel)
Propulsion	Electric motor drive	Electric motor drive; Internal Combustion Engine (ICE)	Electric motor drive; Internal Combustion Engine (ICE)	Internal Combustion Engine (ICE)
Energy source and infrastructure	Charging stations drawing power from electric grids	Charging stations drawing power from electric grids plus Petrol/ diesel stations	Petrol/diesel stations	Petrol/diesel stations
Advantages	Higher efficiency Home/workplace Charging Low engine noise Few auto parts	Higher efficiency Home/workplace Charging Many refueling stations	Higher efficiency Many refueling stations	Wide variety of models Many refueling stations
Disadvantages	Range anxiety Long-time to recharge Fewer charging stations Fewer charging stations	Technologically complex Fewer recharging stations	Tail-pipe emissions Oil dependency engine noise Technologically complex	Low efficiency Tail-pipe emissions Oil dependency engine noise

Table.I.1. B. Pros and cons of different types of electric vehicles and conventional vehicles [6].

I.2.4.A Architectures of HEV:

The HEV powertrain consists of two or more power plants. The ICE is the primary source of energy, responsible for producing most of the vehicle energy and long driving range, while the EM is the auxiliary source, responsible for high-vehicle-power demands and fuel economy of the ICE. The EM charges the batteries from the excess power from ICE when not needed by the vehicle and also from the regeneration of vehicle kinetic energy. The design and control of such powertrain require advanced control algorithms and EMS, which optimizes many objectives, such as the ICE fuel economy and the state of charge (SoC) of the batteries, with the system and driving constraints. The HEV system architecture consists of a drive train, ESS, and a controller unit. The integration of these components gives rise to various HEV configurations that are summarized as follows:

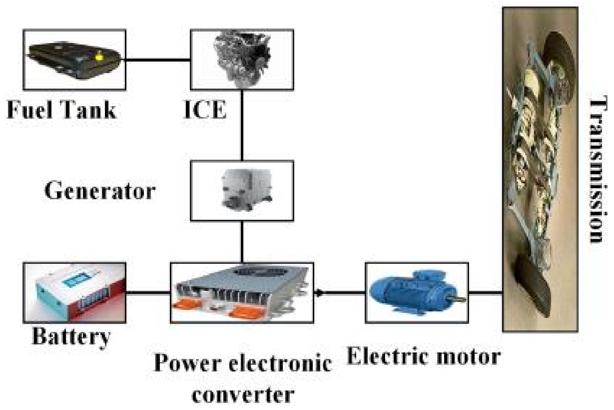

Series HEVs:

-**The EM is** responsible for providing the main traction force for the propulsion of the vehicle**.**
-The ICE power is used to charge the batteries by a generator. The ICE–generator pair can also directly drive the traction EM without charging/discharging the battery.
- **There is** a benefit of traction flexibility by electrically decoupling the ICE from the drive shaft in this configuration, such as in diesel–electric locomotives.

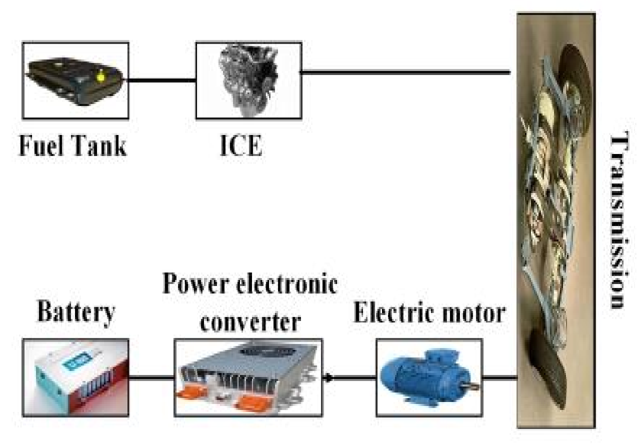

Parallel HEV:

-**The ICE** and EM can additively supply power to drive the wheels. The ICE and EM are coupled to the drive shaft employing two clutches.
-**The traction** power is provided by either ICE or EM, or both. The EM can also serve as a generator, where it can regenerate the vehicle decelerating energy or be driven from the ICE when it powers in excess of that required to drive the wheels [30]. Thus, the parallel
-**One advantage** of this over the series configuration is smaller power ratings of these components, especially the EM, and the electromechanical power losses can be less

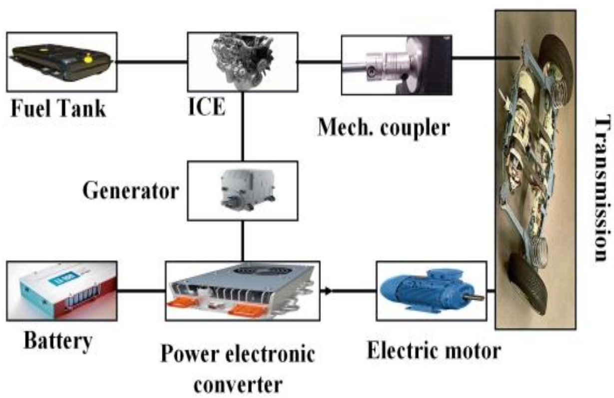

Series–Parallel HEV:

-**The advantages** of both series and parallel HEVs. This configuration has the advantage of smaller size ESS and EM compared to the series and smaller ICE compared to the parallel
-The series and parallel modes are better efficient at low and high speeds, respectively. However, it suffers from higher system complexity and the addition of a planetary gear

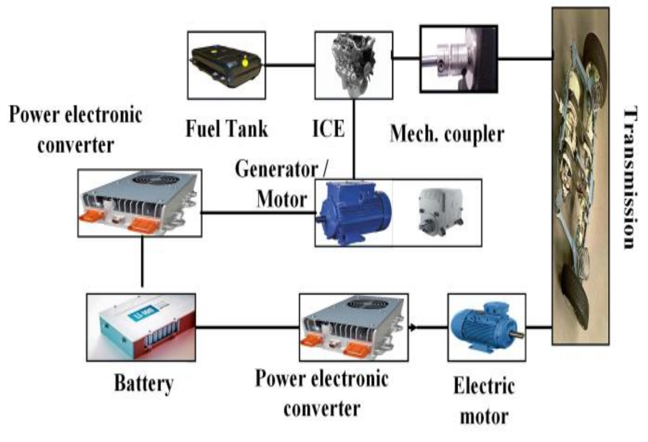

Complex HEV:

The complex HEV is similar to the series–parallel HEV, with the critical difference of having an additional bidirectional converter.
The bidirectional converter provides for bidirectional power flow in the EM. This bidirectional power flow can provide for versatile operating modes, such as the combined ICE and two EMs.
This configuration suffers from complexity and its associated costliness

I.2.4.B. Architecture of Fuel Cell Electric Vehicle (FCEV):

The FCEV uses a hydrogen FC power plant. These vehicles are environmentally friendly, as power is produced by a chemical reaction between hydrogen and oxygen to produce water as the only emission. Hydrogen is used as the energy source, being economically, societally, environmentally, and climatically sustainable and readily available in the water. They have a long driving range and short refueling time. The FCEV is very fuel-efficient compared to the ICE vehicles. There have been several pilot projects launched, but FCEVs have their own set of challenges, including hydrogen safety concerns. Of course, if hydrogen is produced by fossil-fueled energy sources, most of the FCEV advantages disappear.

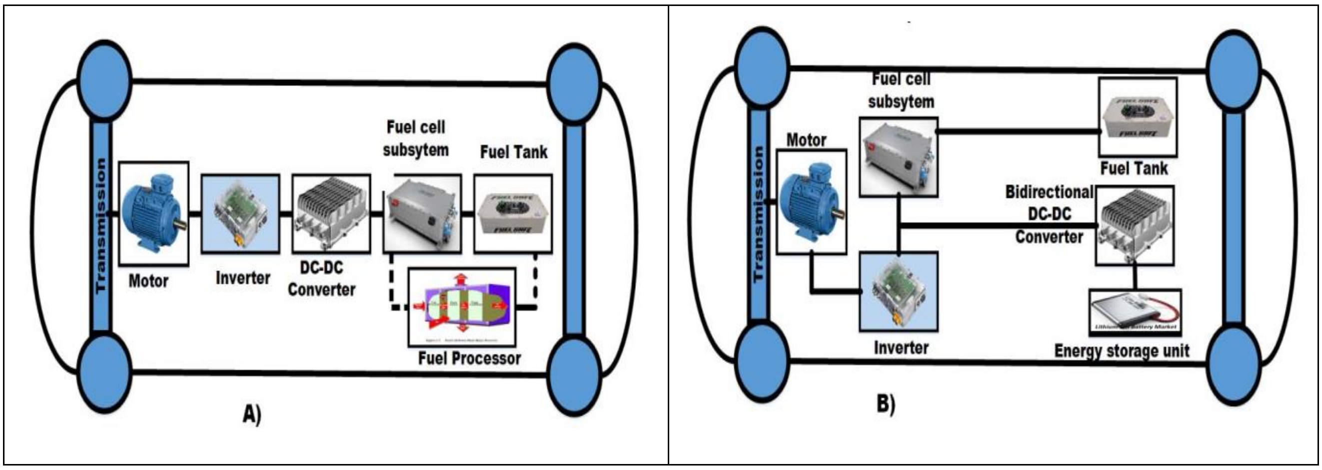

Fig.I.2 Various architectures of (A) FCEV and (B) FCHEV powertrains. [13]

The architecture of FCV has two variants. The first is the basic FCEV, which has the same architecture as the EV. Another variant is the fuel cell hybrid electric, FCHEV. This variant has another ESS assisting the FC. The ESS can be batteries or UC. As in the parallel hybrid, the FC acts as the main energy source. The architectures of FCEV and FCHEV can be seen in Fig.I.3.

I.2.4.C. Battery Electric Vehicle (BEV):

BEVs have a power system structure as shown in Fig.I.4 which mainly consists of a power battery, DC/DC and motor. Current input from lithium batteries flows to DC/ AC after boosting at DC/DC and then into a three-phase AC motor for it to drive EVs to move.

Battery electric vehicles are the vehicles which totally runs on the power. They do not utilize some other fuel (petroleum or diesel) to run. They are 100% all-electric vehicle. The power is put away in the batteries introduced in vehicles (Fig. I.4). they are condition neighborly as they do not discharge any sort of unsafe outflows in nature or we can say that they are zero-emanation vehicle. The charging of the battery electric vehicle is simple as it is very well-finished with the typical home unit supply, or at the charging outlet if accessible. A portion of the instances of battery electric vehicles are Tesla Model 3, Peugeot e-208, MG ZS EV, Nissan Leaf, Renault Zoe, Hyundai Kona Electric, Kia e-Niro, Jaguar I-Pace, and so on [8].

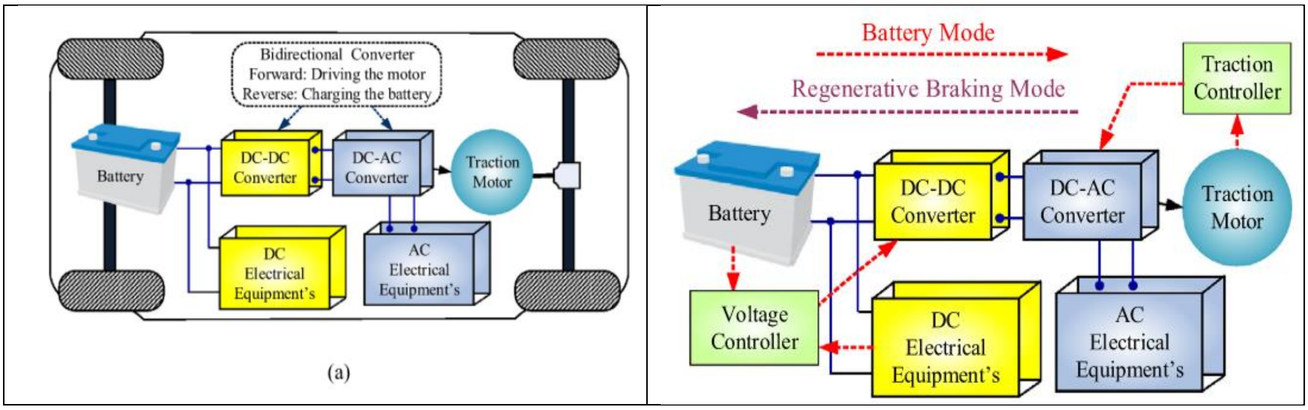

Fig.I.3. Battery Electric Vehicle (a) Typical structure of BEV, (b) Control scheme operating modes of BEV.

I.2.5 EV configurations:

Electric Vehicles (EVs) designers and manufacturers would always want to design a compact and ergonomic car with an incredible performance on all terrains. The designers have to make sure all the required components are mounted on the chassis of the EV do not affect the legroom of the automobile. They must also make sure that electrical components used in the EV are not susceptible to external or internal short-circuit. There are various types of arrangements or configurations used by EV manufacturers and designers.

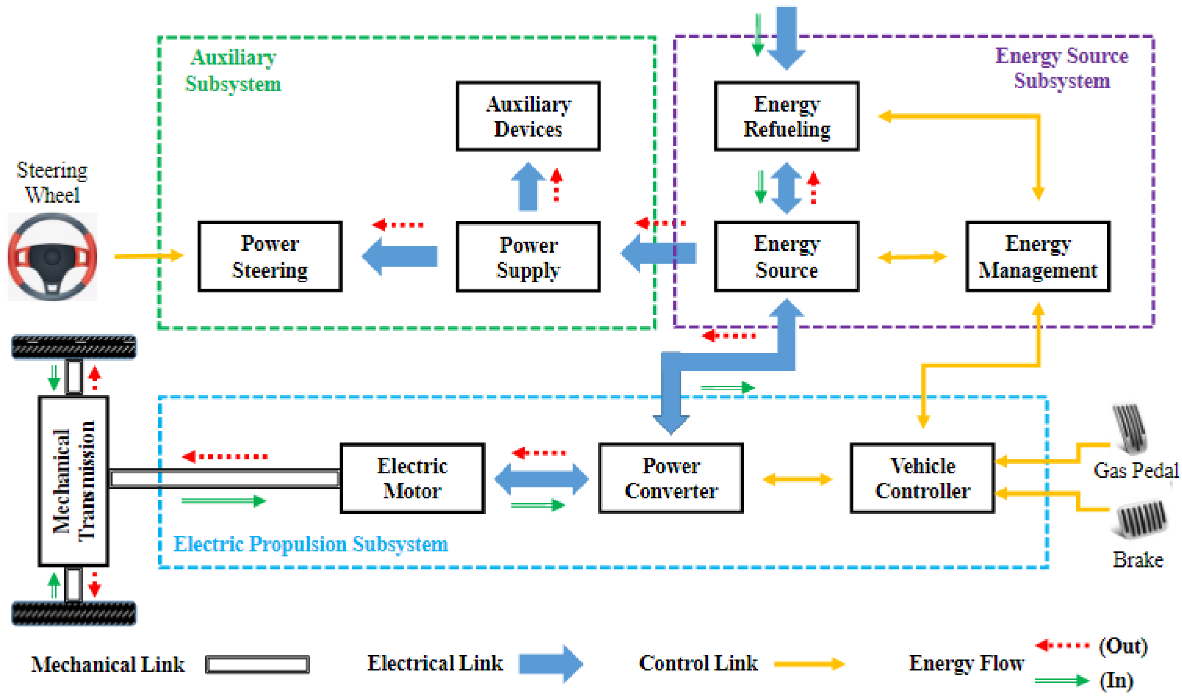

Fig.I.4. A representative configuration of EV.

As shown in fig.I.5, an EV has three major subsystems. They are as follows:

- The electric propulsion subsystem consists of five components. They are:
  - The Electronic Controller
  - Mechanical Transmission
  - Driving Wheels
  - Power Converter
  - Electric Motor
- The energy source subsystem consists of three components. They are:
  - Energy source (ie Battery, Fuel Cell,Ultracapacitor and others)
  - Energy refueling Unit
  - Energy management Unit
- The auxiliary subsystem consists of three components. They are:
  - Power Steering Unit
  - Temperature Control Unit
  - Auxiliary Power Supply

I.2.5.A Powertrain Configurations:

There are various ways of arranging the drivetrain of the electric vehicle. In this section, I will be explaining the six different electric vehicle configurations based on drivetrain arrangements. They are as follows:

➢ **Powertrain Configurations** with clutch, gearbox, and differential;

➢ **Powertrain Configurations** without clutch and gearbox;

➢ **Powertrain Configurations** with fixed gearing, motor and differential;

➢ **Powertrain Configurations** with two Electric Motors (EM);

➢ **Powertrain Configurations** with in-wheel motor and mechanical gear;

➢ **Powertrain Configurations** with in-wheel motor and no mechanical gear [9];

A. Powertrain configuration with clutch, gearbox, and differential:

As shown inf fig.I.5, the clutch is a mechanical device which is used to connect or disconnect power flow from the electric motor to the wheels. The gearbox is another mechanical device which consists of a set of gears with different gear ratios. By incorporating both clutch and gearbox, the driver can shift the gear ratios and hence the torque going to the wheels. The wheels have high torque low speed in the lower gears and high-speed low torque in the higher gears. The differential is a mechanical device which enables the wheels to be driven at different speeds when cornering-the outer wheel covering a greater distance than the inner wheel.

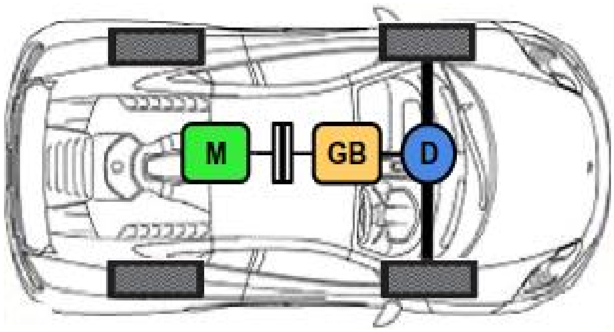

C: Clutch, D: Differential, FG: Fixed Gearing, GB: Gear Box, M: Electric Motor

Fig.I.5. Powertrain configuration with clutch, gearbox, and differential

B. Powertrain configuration without clutch, gearbox and differential:

By replacing the gearbox with fixed gearing and hence removing the clutch, both the weight and size of the mechanical transmission can be greatly reduced. Fig.I.6 shows this arrangement which consists of an electric motor, fixed gearing and a differential. Notice that this EV configuration is not suitable for the ICEV as the engine by itself, without the clutch and gearbox, cannot offer the desired torque-speed characteristics. In this type of configuration, the electric motor needs to be equipped with a complex control system to provide the required amount of torque for the wheels.

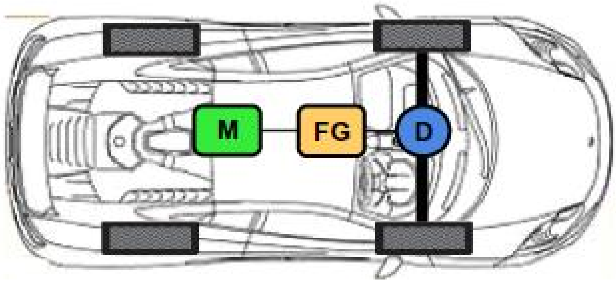

Fig.I.6. Powertrain configuration without clutch, gearbox, and differential

C. Powertrain configuration with fixed gearing, motor and differential:

Similar to the concept of transverse front-engine front-wheel drive of the existing ICEV, the electric motor, fixed gearing and differential are integrated, into a single assembly, while both axles point at both driving wheels. Fig.I.7 show this configuration which is in fact most commonly adopted by modern EVs This is the **Powertrain configuration** that we focus on in our study

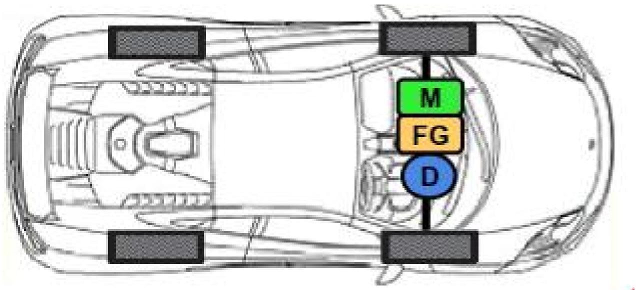

Fig.I.7. Powertrain configuration with fixed gearing, motor and differential

D. Electric Vehicle configuration with two Electric Motors (EM):

Besides the mechanical means, the differential action of an EV when cornering can be electronically provided by two electric motors operating at different speeds. Fig.I.8 shows this dual-motor configuration in which two electric motors separately drive the driving wheels via fixed gearing.

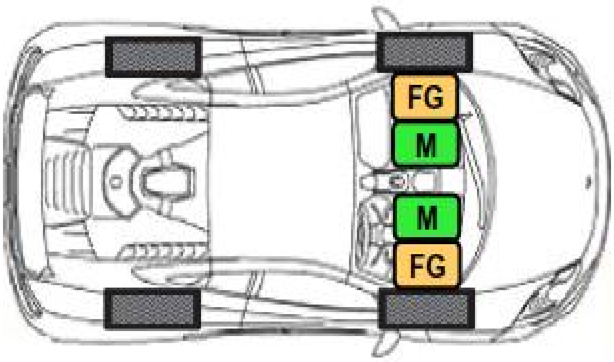

Fig.I.8. Powertrain configuration with two electric motors

E. Electric Vehicle configuration with in-wheel motor and mechanical gear:

In order to further shorten the mechanical transmission path from the electric motor to the driving wheel, the electric motor can be placed inside a wheel. This arrangement is the so-called in-wheel drive. Fig.I.9 shows this configuration in which fixed planetary gearing is employed to reduce the motor speed to the desired wheel speed. It should be noted that planetary gearing offers the advantages of a high speed-reduction ratio as well as an inline arrangement of input and output shafts.

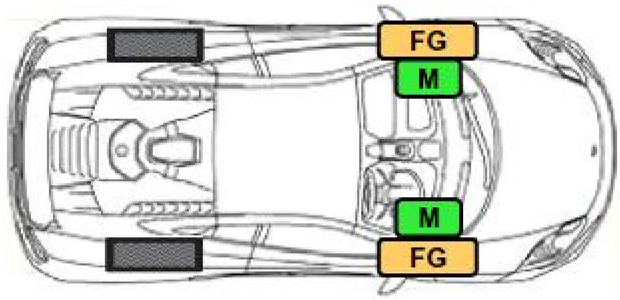

Fig.I.9. Powertrain configuration with fixed gearing, motor and differential

F. Electric Vehicle configuration with in-wheel motor and no mechanical gear:

By fully abandoning any mechanical gearing, the in-wheel drive can be realized by installing a low-speed outer-rotor electric motor inside a wheel. Fig.I.10 shows this gearless arrangement in which the outer rotor is directly mounted on the wheel rim. Thus, speed control of the electric motor is equivalent to the control of the wheel speed and hence the vehicle speed.

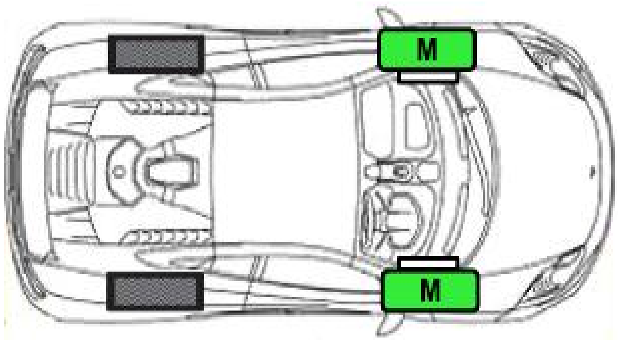

Fig.I.10. Powertrain configuration with in-wheel motor and no mechanical gear [9].

I.2.6 Power train components

Generally, the powertrain contains three parts as the energy storage system, power electronic converters and motors, the propulsion system as shown in figure I.11.

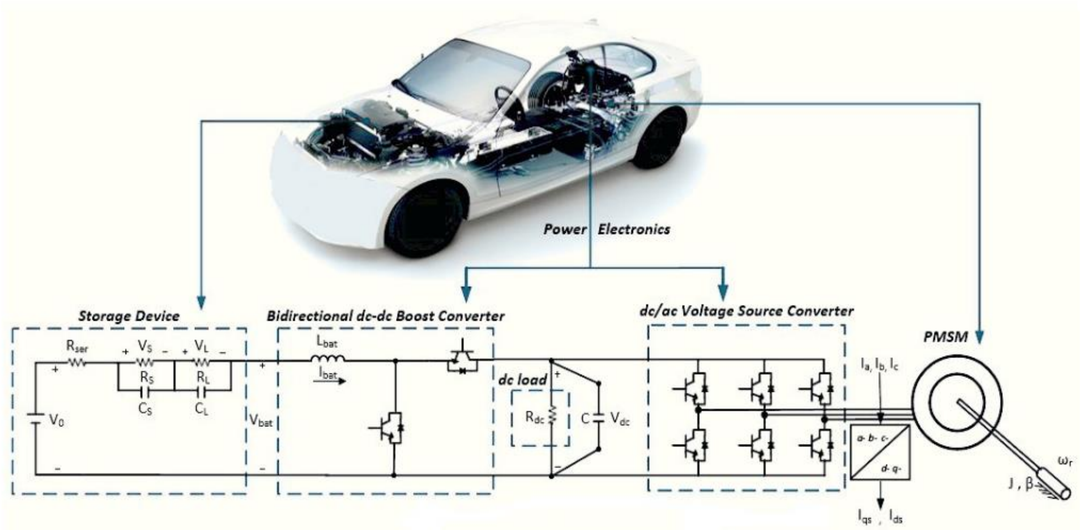

Fig.I.11: Power train components

Electric Propulsion Subsystem

An important goal for electric vehicles is overcoming the disparity between their cost of development, production, and operation, with respect to those of equivalent internal combustion engine vehicles. Customarily, the electric vehicle architecture consists of the main battery and traction subsystem as depicted in the following **Fig.I.12**. In the battery system, the cell modules supply the vehicle with electric energy through the DC bus. More often, half-bridge DC/DC converter is used to adapt the variable voltage from the battery to the quasi-constant voltage in the DC bus. Braking energy is partially recovered during deceleration. The traction subsystem is composed of an electrical motor and a full-bridge Voltage Source Inverter (VSI). Transmission gear is used to adapt the speed ratio between wheels and the motors shaft, followed by a mechanical differential changing the speed ratio between the two traction wheels.

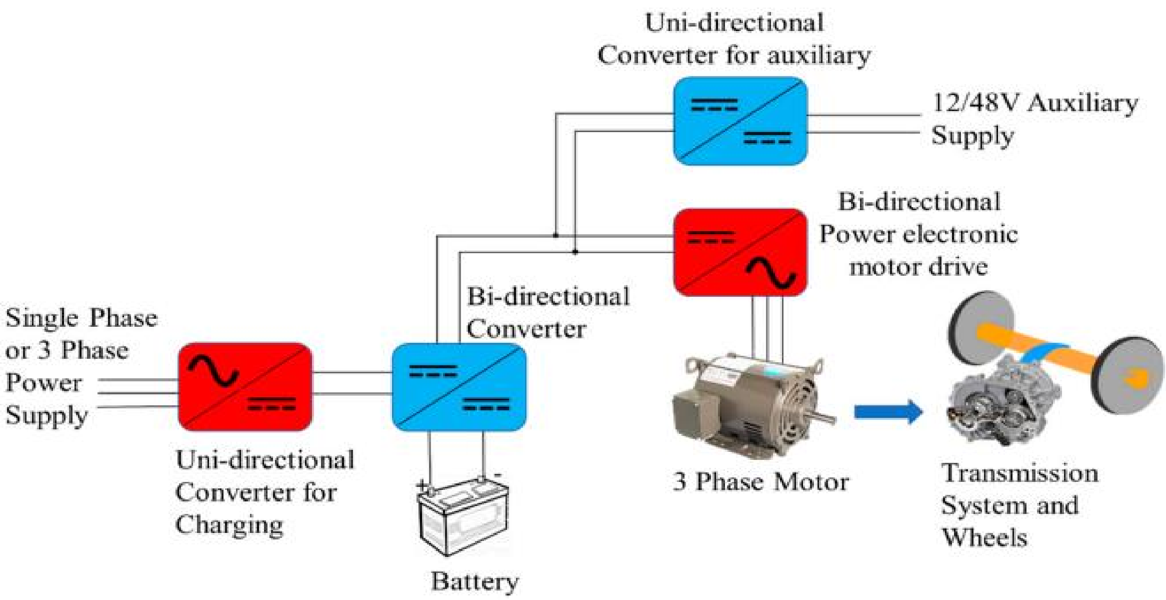

Fig.I.12; Power electronic converter [12]

However, particular attention is paid to the on-board charger's issues such as their low power density, their limited flexibility and etc.

I.2.6 A Battery Pack;

The battery pack is the energy storing device, it must both accept and provide current to the electric machine. Battery packs provide direct current (DC) at their output terminals. Electric machines are controlled by varying an alternating current (AC) waveform

Batteries are electrochemical accumulators that store chemical energy which can be converted into electrical energy and as it is a bidirectional source, electrical energy can be converted into chemical energy. Because of their specific energy and power, reversibility and relatively low cost (regarding other technologies), batteries are one of the most attractive sources to be used in electrical and hybrid electrical vehicles. However, they still require deep research on issues as fabrication, security or recycling. Batteries technologies are commonly based on metals as lead and more recently lithium or nickel.

Characteristics of the Batteries:

Concerning the main characteristics of batteries, we can highlight the following:

-Capacity. The storage difficulty and cost is one of the main problems of electric power. The battery capacity represents the maximum amount of energy that can be extracted from the battery under certain specified conditions. This unit can be expressed in ampere hour (Ah) or in watt hour (Wh)

-Energy Density. Obtaining the highest energy density possible is another important aspect in the development of batteries, in other words, that with equal size and weight a battery is able to accumulate a higher energy quantity, the energy density of batteries is measured as the energy that a battery is able to supply per unit volume (Wh/L).

-Charge cycles. A load cycle is completed when the battery has been used or loaded 100%

-Efficiency. It is the percentage of power that is offered by the battery in relation to the energy charged

Currently, the batteries are the main obstacle to EV wider adoption. The development of better, cheaper, and higher capacity batteries will extend vehicles autonomy, and the users view them as a true alternative to the internal combustion engine vehicles.

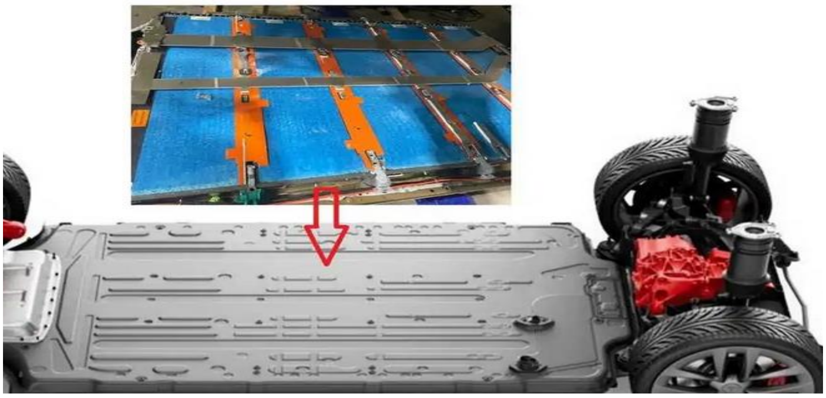

Fig.I.13: Tesla car battery Model

In fact, batteries are a key component in EVs and therefore, there are increasing manufacturers that invest to develop improved and cheaper batteries the motor drive technology is most actively developed in recent years where there are many innovations and advancements in the design, analysis, and control of motor drives. The energy source technology is also actively developed in recent years

In fact, batteries are a key component in EVs and therefore, there are increasing manufacturers that invest to develop improved and cheaper batteries the motor drive technology is most actively developed in recent years where there are many innovations and advancements in the design, analysis, and control of motor drives. The energy source technology is also actively developed in recent years

I.2.6.B. Power electronic converter:

In a recent vehicular system, a three-phase converter acts as an inverter during fuel, battery, split and combine mode whereas rectifier in regenerative mode. The selection of converter mode is sophisticated and controlled by the traction controller unit. The traction controller generates the controlled pulses for the three-phase converter according to the received signal from the traction motor and vehicle drivers. The controlled pulse decides the operation of the three-phase converter as an inverter or rectifier. The voltage control unit controls the SOC of the battery at the maximum and minimum level. The voltage controller continuously receives the SOC (the State of Charge) level signal from the battery and com pare it with the reference voltage signal, consistent with this controlled pulse generate for DC-DC converter to maintain the SOC of the battery to increase its lifespan and avoid power wastage

Broken down into very simple terms, such inverters build up a connection between the direct voltage in the DC link when the momentary alternating voltage in the line is higher than the DC voltage in the link, thus allowing energy intake, and disconnects both from each other when the voltage "out there" is lower. This is the principle of motor operation. For feeding back energy in generator mode the inverter, justifying its name, does the inverse thing: Connect when line voltage is low and disconnect when it is high. In this way the energy can go either way even though the line voltage is constant – and the DC voltage in the link circuit may also be kept at a constant level, depending on design.

The simplified schematic of the classical six-switch VSI is shown in **Fig.I.15**. The mid-point (p) is considered the voltage-reference of the dc-bus (Vd). Thus, the inverter generates three voltage-levels (0, ±V/2) instead of only two-levels (0, +Vd) The simple square-wave control technique is used in this study instead of the pulse-width-modulated (PWM) technique.

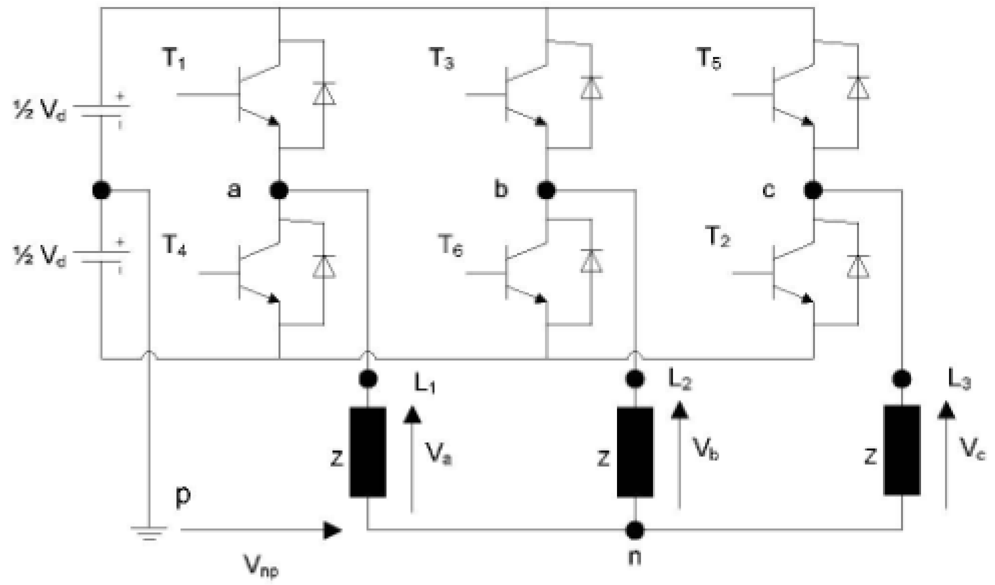

Fig.I.14: the classical six-switch VSI [17].

Voltage source inverters (VSI) are used in electric and hybrid vehicles to control the electric motors and generators. Figure.I.14 shows the power electronic circuits arrangement of a VSI to control induction motors, permanent magnet synchronous motors, and permanent magnet synchronous motors. The switches are usually IGBTs for high- voltage high power hybrid configurations, or MOSFETs for low-voltage designs

This is the most common type of transistors firing, in which, one transistor, per inverter leg, conducts for 180°. So, three transistors remain on at any instant of time. For phase "a", when transistors T1 is switched on, phase "a" is connected to the positive terminal of the dc input voltage, +V/2. When transistor T4 is switched on, phase "a" is connected to the negative terminal of the dc source, -V/2. The same sequence occurs in the other two phases "b" and "c". Six patterns of operation are available in the 2πf-cycle, where the interval of each pattern is 60°. The conducting transistors during each distinct interval, where the rate of sequencing theses patterns specifies the bridge output frequency.

For three-phase wye-connected balanced load controlled with 180° conduction mode, Table 2. Shows respectively, transistors' gating signals, instantaneous line-to-center and line-to-line quasi-square output voltage waveforms, neutral- point voltage, and line-to-neutral (phase) output voltages. The gating signals are shifted from each other by 60° to get three- phase balanced voltages. The phase voltage waveform contains four voltage levels of dc bus (± V/3, ±2 V/3).shown in Fig.I.15.

Interval	Duration	Conducting Devices during interval							
1	$\pi/3$	T_1	T_2	T_3					
2	$\pi/3$		T_2	T_3	T_4				
3	$\pi/3$			T_3	T_4	T_5			
4	$\pi/3$				T_4	T_5	T_6		
5	$\pi/3$					T_5	T_6	T_1	
6	$\pi/3$						T_6	T_1	T_2

Table.I.2: transistors gating signals

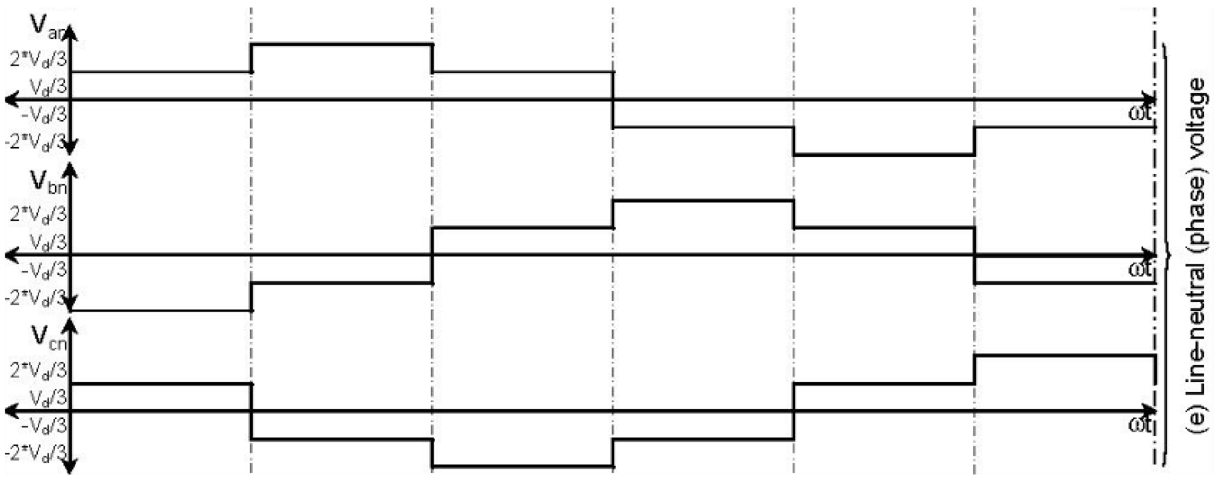

Fig.I.15: Phase output voltages waveforms

I.2.6.C Traction electric motor characteristics:

A review of the state of the art related to electric-traction systems shows that the permanent magnets synchronous motor are the more used machines for electric traction systems. The requirements often encountered in electric traction systems are the following:

(1) High power and high-power density.

(2) High torque at low speed for starting and climbing.

(3) Wide speed range, especially for constant-torque and constant-power operating conditions.

(4) Fast torque response;

(5) High efficiency over wide speed and torque ranges;

(6) High robustness for various vehicle operating conditions

Motors Used: Several types of electric motors can be used for electric vehicles as mentioned in the table.I.2.

Table.I.3. electric motors for electric vehicles [15].

Motor Type	Advantage	Disadvantage	Vehicles Used In
Brushed DC Motor	• Maximum torque at low speed	• Bulky structure • Low efficiency • Heat generation at brushes	Fiat Panda Elettra (Series DC motor), Conceptor G-Van (Separately excited DC motor)
Permanent Magnet Brushless DC Motor (BLDC)	• No rotor copper loss • More efficiency than induction motors • Lighter • Smaller • Better heat dissipation • More reliability • More torque density • More specific power	• Short constant power range • Decreased torque with increase in speed • High cost because of PM	Toyota Prius (2005)
Permanent Magnet Synchronous Motor (PMSM)	• Operable in different speed ranges without using gear systems • Efficient • Compact • Suitable for in-wheel application • High torque even at very low speeds	• Huge iron loss at high speeds during in-wheel operation	Toyota Prius, Nissan Leaf, Soul EV
Induction Motor (IM)	• The most mature commutatorless motor drive system • Can be operated like a separately excited DC motor by employing field orientation control	-that speed control of induction motors are difficult -poor starting torque and high inrush currents	Tesla Model S, Tesla Model X, Toyota RAV4, GM EV1
Switched Reluctance Motor (SRM)	• Simple and robust construction • Low cost • High speed • Less chance of hazard • Long constant power range • High power density	• Very noisy • Low efficiency • Larger and heavier than PM machines • Complex design and control	Chloride Lucas
Synchronous Reluctance Motor (SynRM)	• Robust • Fault tolerant • Efficient • Small	• Problems in controllability and manufacturing • Low power factor	
PM assisted Synchronous Reluctance Motor	• Greater power factor than SynRMs • Free from demagnetizing problems observed in IPM	hard manufacturing and installment process	BMW i3
Axial Flux Ironless Permanent Magnet Motor	• No iron used in outer rotor • No stator core • Lightweight • Better power density • Minimized copper loss • Better efficiency • Variable speed machine • Rotor is capable of being fitted to the	High costs in manufacturing because of longer time	Renovo Coupe

I.3. Electric vehicle sensors and systems

Sensors detect, measure, and transmit information, which help in analyzing performance of vehicles. Sensors are devices that detect events or changes in environment and then provide a corresponding output. They sense physical input such as light, heat, motion, moisture, pressure, or any other entity, and respond by producing an output on a display or transmit the information in electronic form for further processing. It uses integrated circuit (IC) fabrication technology made on silicon wafers. It monitors and controls chemical, physical, and process changes of an automobile.

The EVs sensor system fall into two main categories:

1. Internal sensor systems

2. External sensor systems

1) Internal sensors system monitors the performance of vehicles such as wheel speed, yaw rate, steering inputs, driver inputs, powertrain outputs, or hydraulic braking [11]. For EVs the internal sensors can monitor the battery state of charge (SoC), battery temperature, and battery current and voltage from the Battery Management System (BMS).

2) External sensor systems are focused on enhancing driver safety, perception and autonomous navigation. These systems include a combination of camera, GPS, RADAR, LIDAR, Ultrasonic, and Dedicated Short range Communications etc.

I.3.1 position /speed Sensor based motor control:

In general motor control for PMSM needs information of rotor position in order to make the correct commutation switching for aligning the stator currents for maximum torque production. The position information can either be retrieved by a sensor or using sensorless control algorithms based on back-emf information or signal injection. Sensored solutions have more components added to the system, therefore adding more costs and potential hardware failures. However, the sensorless systems requires higher performance processor and memory. The sensorless motor control algorithms are also more complex, leading to more design and code generation time, which may lead to higher costs compared to a sensored system solution. In this section three commonly used sensored techniques of motor control will be briefly described.

A- Optical encoders

Optical encoders are frequently used for high servo drive systems whereposition and speed is key for high performance in speed or positioning control. The encoder can provide rotor position for the vector control orientation and may be used for feedback for the speed or torque control loop. There are two types of optical encoders, incremental and absolute. The traditional absolute encoder provides absolute position as binary outputs. The rotating unit consists of a disc with coded

elements along the surface which is decoded
by a stationary decoding unit. The decoding units reads the element of the rotating disc, allowing position measurement regardless speed or direction. However, the absolute encoder is expensive and used in application were precision is of utter most importance, such as robotic arms and surveying apparatus. Incremental encoders use incremental steps for pulse generation that can be translated to speed and position. The rotating disc of the encoder has patterns of transparent and impervious sections which generates pulses when the optical light hits the surface of the disc while the shaft is rotating. There are one or two pulse incremental encoders. The one pulse encoder does not track position or direction, but only speed. The two-pulse incremental encoder has two code tracks on the disc which produces binary square pulses, phase A and B which are 90 degrees separated, see Fig I.16

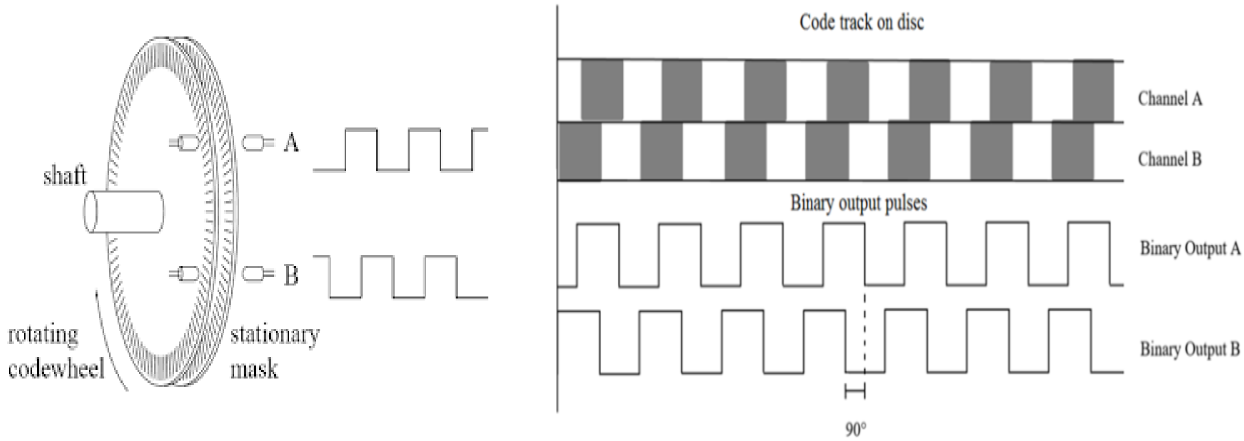

Figure I.16. Visualization of encoder tracks compared with binary output phases of channel A and B of incremental encoders

B- Resolvers

The resolver is an analog position sensor, which looks like a small transformer. The coil of resolver solver has total of three windings, one primary (located on the shaft of resolver) and two secondary (oriented at 90° to each other) shown in Fig. I.17. the sensing mechanism is done by calculating the effective turns ratio and polarity between the two sets of coils. It acts just like a rotary transformer; the data obtained through this mechanism reports the variation in the angle of the shaft as it rotates.
The excitation of resolver coils is done through an AC reference input voltage, which is set at a constant frequency and gets induced in the primary winding. The stator and rotor give the same frequency output with a difference in phase of 90° due to the alignment of coil windings. Due to the 90° phase difference, a signal obtained is sine and cosine. The voltage induced on the windings is equivalent to the reference voltage multiplied by the value of the angle ($\sin\theta$ or $\cos\theta$) between the input shaft and the secondary coils. Here, h denotes the shaft angle

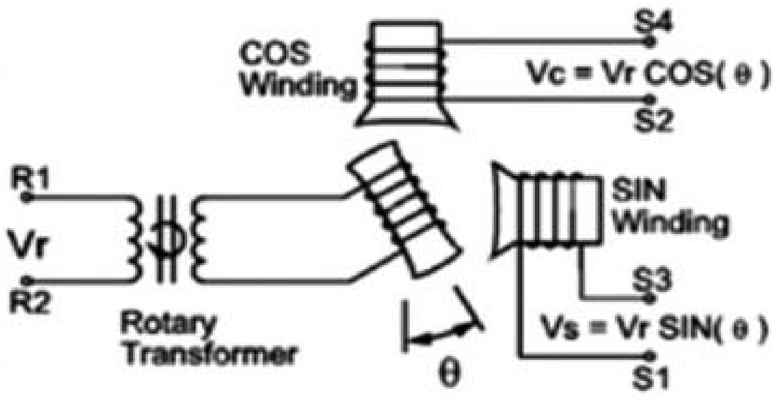

Fig I.17 Components of the resolver. Reprinted with permission from Texas Instruments [14].

C- Hall effect sensors (speed):

Hall sensors are one of the most promising low-cost position sensors for sensor-based motor control. During recent years, PMSM and BLDC drives with hall position sensors has been targeted for plentiful research. The most beneficial property of hall elements is the low cost and its small volume. Hall elements does not require mechanical connection and does not wear down as a resolver or an encoder do. However, the installation of hall elements inside a rotor is sensitive for misplacement and complicated in terms of motor design and fault tolerant control is preferable for reliable position and speed feedback. The hall sensor is implemented by burying one or more hall elements inside the rotor/stator, departed with a certain electric angle between. Usually, 3 hall elements are installed with a 120° mechanical angle separation close to the air gap in the stator. The Hall elements emits current signals that are measured by shunt resistors and the absolute position can be measured as proposed in. The mechanical angle between two signals

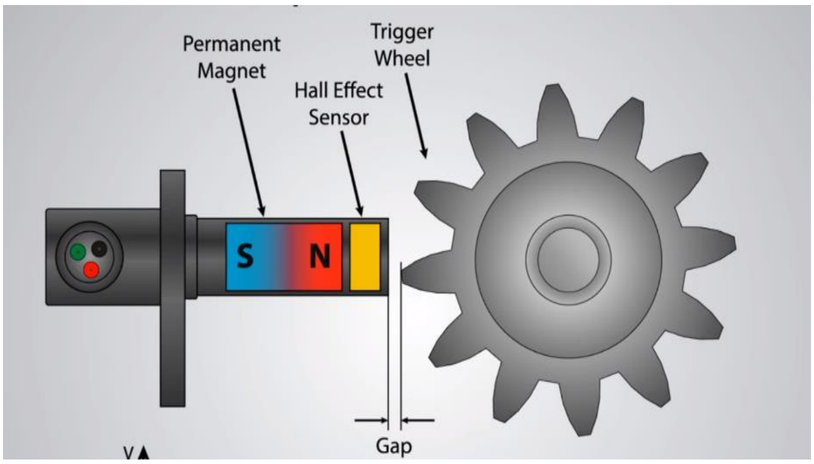

Fig I.18: Hall Effect sensor speed

I.3.2. Speed Sensor Problems: What causes speed sensor failure?

Speed sensor problems can set off a lot of issues in your vehicle. You may now be able to notice the signs or symptoms of speed sensor problems, but what causes the speed sensors to fail? Here are some of the reasons why a speed sensor fails.

- Infernal electrical fault.

Over time, the speed sensors can get internal damages. This could result in having an abnormal output signal or having no signal at all.

- Normal wear and tear.

The sensor itself can become damaged or cracked. Its plastic part can also become brittle after being exposed to the elements. The speed sensor's magnetic part can eventually become worn or damaged.

- Poor car care and maintenance.

Experts always say that proper car care and maintenance can extend the lifespan of the vehicle as well as its components. Following the recommended maintenance schedule can also help prolong the speed sensor's life. Failing to do so can increase the risk of speed sensor failure causing your vehicle to experience speed sensor problems. The sensors will not be able to give accurate readings if its parts become covered in gunk, dirt, and other fluid contaminants.

- Broken wirings and loose connections.

Disconnection of the sensor to the engine control unit can cause problems too. Make sure that you check the connections for loose or broken ones. Check also for corrosions and build ups [11].

I.3.3 An Overview of Sensorless control:

The speed/position sensor may fail any time during the life of the motor. Therefore, when one of the sensors becomes faulty or damaged, motor operation is severely affected and after two sensor failures, the motor comes to a complete stop. Such a scenario may result in very dangerous and life-threatening situations in the aerospace or automotive industries and such situations must be avoided at all costs. In order to maintain the motor operation with the damaged sensor, fault tolerant control system (FTCS) is required. The FTCS keeps the motor operating and functional till the maintenance can be performed or the damaged part can be replaced

I.3.4 D Problem Statement:

If a fault occurs when driving, the faulty component must be immediately excluded from the drivetrain control. The control algorithm has to switch into emergency mode in order to maintain vehicle controllability. This is particularly important for cars equipped with in-wheel electric drives where a fault of a single in-wheel drive may disrupt the balance of propulsive or breaking forces generated on individual wheels, which at high traveling speed can lead to the sudden deprivation of vehicle stability.

The requirements for an emergency-activated sensorless control algorithm are found and studied in this dissertation. A rotor-position estimator based on the derivatives of motor phase currents (DMPCs) is proposed. The estimator is implemented and tested on a Simulink PMSM drive. The results confirm fast emergency activation and stable operation in traction-specific operational conditions, therefore, a set of two estimation methods is typically used. At low speed and at standstill, the rotor position is estimated by the analysis of stator inductances, which vary due to the rotor saliency. An additional high-frequency (HF) signal component, generated by the inverter, is required to measure the inductances. At medium and high speeds, an estimation based on the electromotive force (EMF) observer is more convenient. [16].

I.4 Conclusion:

EVs have great potential of becoming the future of transport while saving this planet from imminent calamities caused by global warming. They are a viable alternative to conventional vehicles that depend directly on the diminishing fossil fuel reserves. The EV types, configurations, energy sources, motors, power conversion and charging technologies for EVs have been discussed in detail in this chapter.

The key technologies of each section have been reviewed and their characteristics have been presented, along with the huge possibilities they hold to promote a better and greener energy system by collaborating with smart grid and facilitating the integration of renewable sources. Limitations of current EVs have been listed along with probable solutions to overcome these shortcomings.

A brief overview of the sensors of speed’s EV. Finally, an overview of sensorless control has been presented to prove the necessity this type of control; in case of speed sensor failure.

CHAPTERII

MODELLING AND FIELD ORIENTED CONTROL OF PMSM

II.1 Introduction:

Permanent magnet (PM) synchronous motors are widely used in low and mid power applications such as computer peripheral equipment, robotics, adjustable speed drives and electric vehicles.

The growth in the market of PM motor drives has demanded the need of simulation tools capable of handling motor drive simulations. Simulations have helped the process of developing new systems including motor drives, by reducing cost and time. Simulation tools have the capabilities of performing dynamic simulations of motor drives in a visual environment so as to facilitate the development of new systems.

In this work, the simulation of a field oriented controlled PM motor drive system is developed using Simulink. The simulation circuit will include all realistic components of the drive system. This enables the calculation of currents and voltages in different parts of the inverter and motor under transient and steady conditions. The losses in different parts can be calculated facilitating the design of the inverter.

A closed loop control system with a PI controller in the speed loop has been designed to operate in constant torque and flux weakening regions. Implementation has been done in Simulink. A comparative study of hysteresis and PWM control schemes associated with current controllers has been made in terms of harmonic spectrum and total harmonic distortion. Simulation results are given for two speeds of operation, one below rated and another above rated speed.

The PMSM is more suitable than induction motor, owing to the synchronous machine having interesting advantages, among which are:

(1) The overall weight and volume are significantly reduced for a given output power
(2) Better efficiency.
(3) Heat is efficiently dissipated, the Joule losses are smaller due to absence of rotor currents. However, the PMSM have a short constant-power region owing to their rather limited field weakening capability, resulting from the presence of the permanent magnet field. It is clear that with the recent technological advances it is now possible and attractive to implement robust and powerful nonlinear controllers to reduce energy consumption and to improve performance under a wide range of power-speed operating domains.

II.2 Description of the drive system

This chapter deals with the description of the different components such as permanent magnet motors, position sensors, inverters and current controllers of the drive system. A review of permanent magnet materials and classification of permanent magnet motors is also given

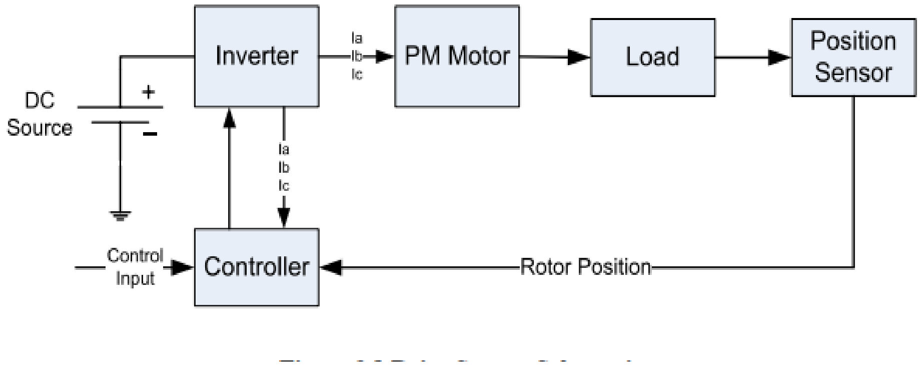

Fig II.1: Drive system schematic [18].

Descriptions of the different components are as follows:

II.2.1 Permanent magnet synchronous motor constructions and types:

II.2.1.1 constructions and types:

A permanent magnet synchronous motor, like any rotating electric motor, consists of a rotor and a stator. The stator is the fixed part. The rotor is the rotating part.

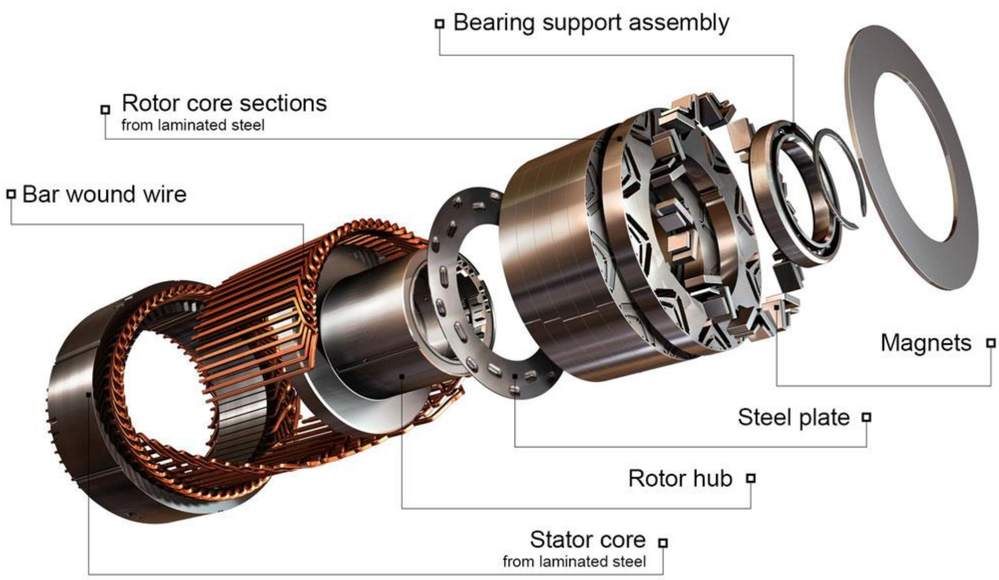

Fig II.2: constructions of PMSM [19].

Typically, the rotor is located inside the stator of the electric motor, there are also structures with an external rotor - inside out electric motors

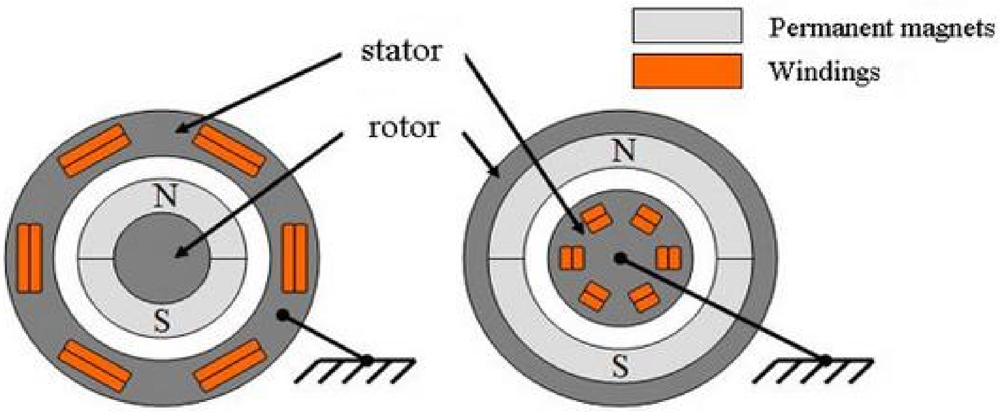

Fig II.3: Construction of a permanent magnet synchronous motor: on the left - standard, on the right - inside out

A. The **rotor** consists of permanent magnets. Materials with high coercive force are used as permanent magnets.

According to the rotor design, synchronous motors are divided into:

- electric motors with salient pole rotor
- electric motors with non-salient pole rotor.

An electric motor with non-salient pole rotor has an equal direct and quadrature inductances $L_d = L_q$, whereas for an electric motor with salient pole rotor the quadrature inductance is not equal to the direct $L_q \neq L_d$.

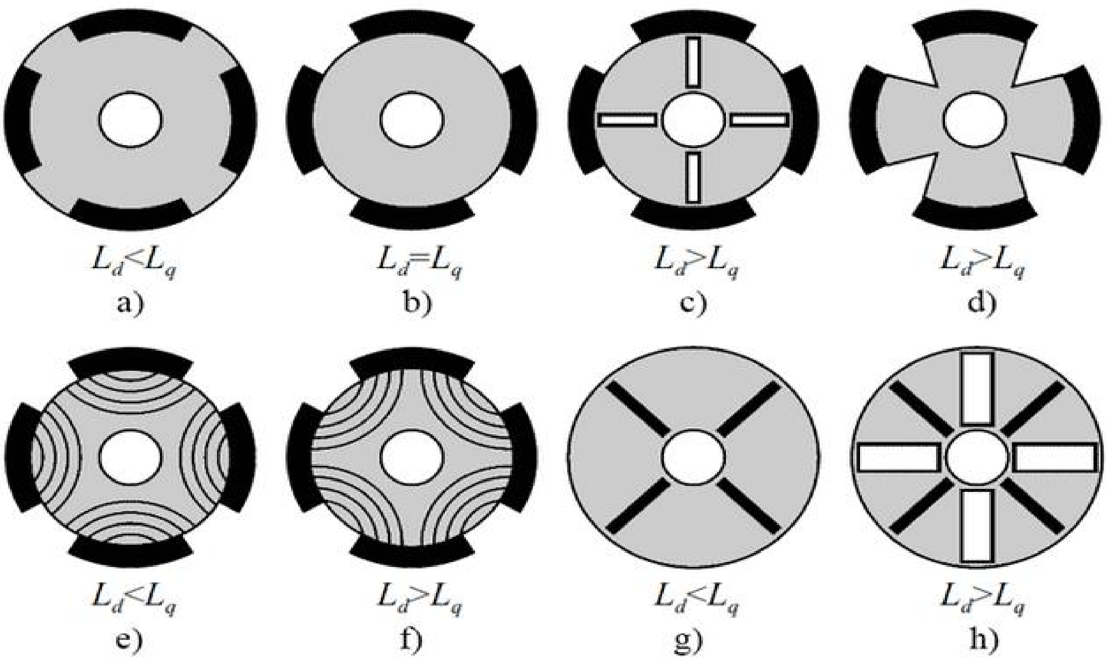

Fig II.4: Types of PMSM

The cross sections of the rotors with a different ratio of L_d/L_q. Magnets marked black. Figure e, f shows axially layered rotors, figure c, and h shows the rotors with barriers.

Also, according to the design of the rotor, the PMSM are divided into:

- surface permanent magnet synchronous motor;
- interior permanent magnet synchronous motor

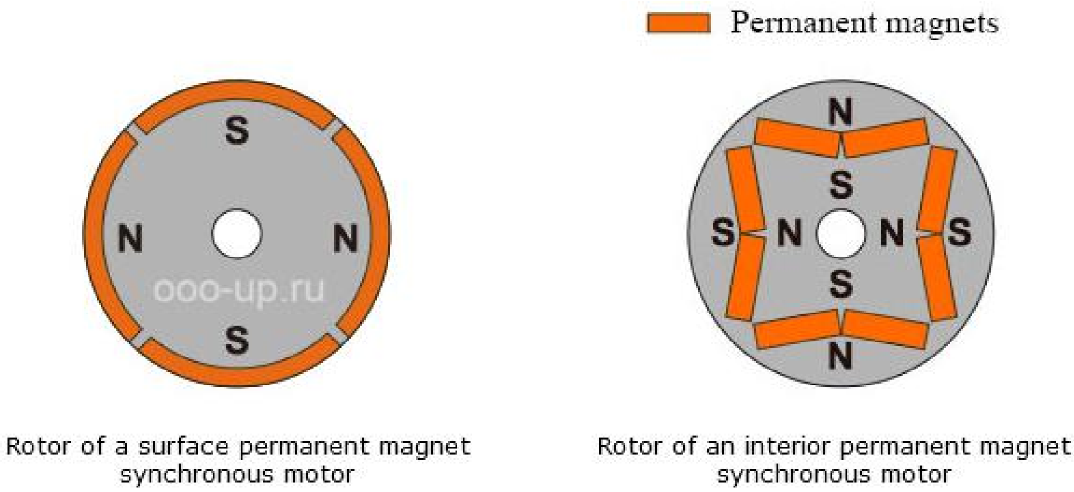

Fig II.5: Types of PMSM according to the design of the rotor

B. The **stator** consists of an outer frame and a core with windings. The most common design with two- and three-phase winding

Depending on the stator design, a permanent magnet synchronous motor can be:

- with distributed winding;
- with concentrated winding

Fig II.6: Types of PMSM according to the design of the stator

1. **Distributed** call such a winding, in which the number of slots per pole and phase Q = 2, 3,.k

2. **Concentrated** called such a winding, in which the number of slots per pole and phase Q = 1. In this case, the slots are evenly spaced around the circumference of the stator. The two coils forming the winding can be connected both in series and in parallel. The main disadvantage of such windings is the impossibility of influencing on the form of the EMF curve

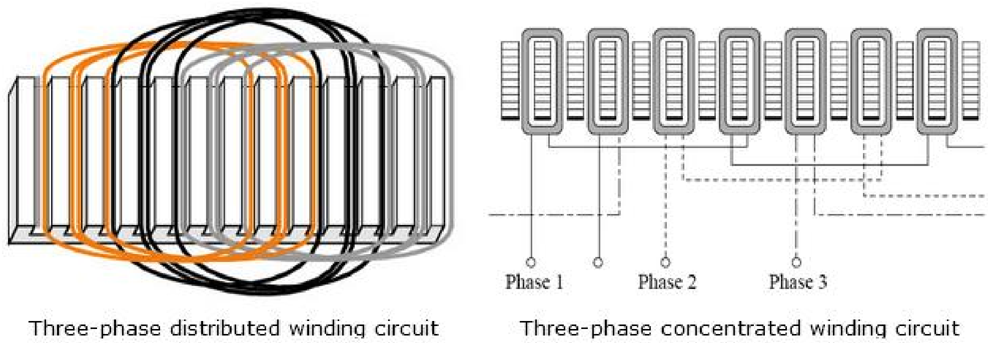

Fig II.7 the different types of stator winding

C. The **form of the back EMF** of the electric motor can be:

- Trapezoidal;
- Sinusoidal.

The form of the EMF curve in the conductor is determined by the distribution curve of the magnetic induction in the gap around the stator circumference.

It is known that the magnetic induction in the gap under the salient pole of the rotor has a trapezoidal shape. The EMF induced in the conductor has the same form. If it is necessary to create a sinusoidal EMF, then the pole tips are given such a shape that the induction distribution curve would be close to sinusoidal. This is facilitated by the bevels of the pole tips of the rotor

Model (year)	Power (kW)	Torque (Nm)	Max. speed (r/min)	CPSR	Slot/pole	Windings	Cooling	kW/L
Toyota Prius (2010)	60	207	13,500	4.87	48/8	Distributed	Water-jacket	4.8
Nissan Leaf (2012)	80	280	10,390	3.8	48/8	Distributed	Water-jacket	4.2
Tesla Model S 60 (2013)	225	430	14,800	2.96	—/4	Distributed	Water-jacket with shaft cooling	—
Honda Accord (2014)	124	—	14,000	—	12/8	Concentrated	—	2.9
BMW i3 (2016)	125	250	11,400	3.0	72/12	Distributed	Water-jacket	9.1
Chevy Volt (2016)	125	370	12,000	3.71	72/12	Distributed-Hairpin	Oil cooled	—
Tesla Model 3 (2017)	192	410	18,000	4.02	54/6	Distributed	—	—
Toyota Prius (2017)	53	163	17,000	5.4	48/8	Distributed-Hairpin	Water-jacket	5.7
Nissan Leaf (2017)	80	280	10,390	3.8	48/8	Distributed	Water-jacket	4.2
Chevy Bolt (2017)	150	360	8,810	2.20	48/8	Distributed-Hairpin	Oil cooled	—
BMW iX3 (2020)	210	400	15,000	3	48/6	Hairpin	—	—
Nissan Leaf (2020)	160	340	—	—	48/8	Distributed	Water-jacket	—
US DOE (2025)	100	144	20,000	≥ 3	—	—	—	50

Table II.1 Representative Set of Electric Machines Used in Commercially Available EVs/HEVs [20].

II.2.1.3 Detailed Modeling of PMSM:

A. Mathematical Model of Three-Phase PMSM:

The schematic representation of the permanent magnet synchronous machine in electric space is given in the figure:

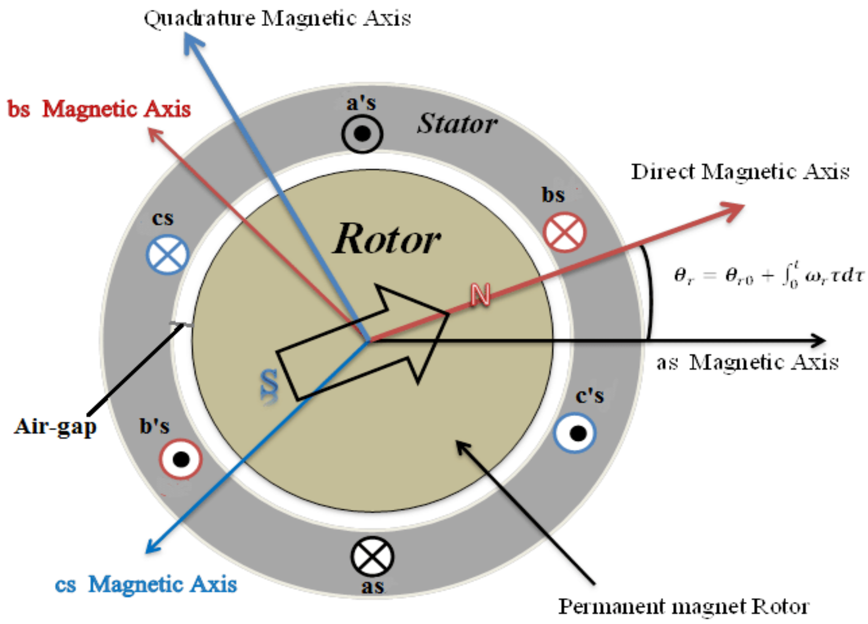

Fig II.8: PMSM in electric space

A.1 Electric Equations:

The three-phase stator voltage equations can be expressed as

$$[V_{sabc}] = \text{Rs}\ [I_{sabc}] + \frac{d[\varphi_{sabc}]}{dt} \qquad \text{(II.1)}$$

Where

$[\text{Vsabc}] = [\text{vsa}, \text{vsb}, \text{vsc}]^T$ are the voltages of each stator phase phase;

Rs is the stator resistance;

$[\text{I sabc}] = [\text{i sa}, \text{i sb}, \text{i sc}]^T$ are the phase stator currents

$[\Psi\text{sabc}] = [\Psi\text{sa}, \Psi\text{sb}, \Psi\text{sc}]^T$ are the stator fluxes,

A.2 Magnetic equations:

$$[\Psi\text{sabc}] = [\text{Lss}]\ [\text{I sabc}] + [\Psi\text{rabc}] \qquad \text{(II.2)}$$

Where

$$[\lambda_{m_{\text{abc}}}] = [\lambda_{m_a}, \lambda_{m_b}, \lambda_{m_c}]^T \qquad \text{(II.3)}$$

is given by

$$\begin{bmatrix} \lambda_{m_a} \\ \lambda_{m_b} \\ \lambda_{m_c} \end{bmatrix} = \varphi \begin{bmatrix} \cos(P\theta) \\ \cos\left(P\theta - \frac{2\pi}{3}\right) \\ \cos\left(P\theta + \frac{2\pi}{3}\right) \end{bmatrix} \tag{II.4}$$

$$\varphi_{sa} = L_{aa}\, I_{sa} + L_{ab}\, I_{sb} + L_{ac}\, I_{sc} + \lambda_{m_a} \tag{II.5}$$

$$\varphi_{sb} = L_{ab}\, I_{sa} + L_{bb}\, I_{sb} + L_{bc}\, I_{sc} + \lambda_{m_b} \tag{II.6}$$

$$\varphi_{sc} = L_{ac}\, I_{sa} + L_{bc}\, I_{sb} + L_{ac}\, I_{cc} + \lambda_{m_c} \tag{II.7}$$

B. The Concordia/Clark and Park Transformations:

The three-phase mathematical models of permanent magnet synchronous motors are developed. The classical models using the Concordia/Clarke and Park transformations are derived to define the two-phase equivalent models of AC machines. Using these transformations, many concepts, interpretations, and simplified models can be obtained to analyze the AC machine behavior.

An approach to study AC machines is to transform the variables (voltages, currents, and flux linkages) stated in a fixed reference frame to a rotating frame defined by the Concordia/Clarke and Park transformations. These transformations are used in the analysis of AC machines to reduce the complexity of the differential equation describing the behavior of the AC machines by eliminating time-varying terms in the inductances.

The transformation from a three-phase (stationary (a, b, c) frame) to a two-phase (rotatory direct-quadrature frame or (d, q) frame) transformation is referred as the Park transformation. However, this transformation can be decomposed in two transformations. A first transformation from a fixed three-phase system to a fixed two-phase system (Clarke's/Concordia's transformations). Next, by a transformation from a fixed two-phase frame to a rotating two-phase frame associated to a rotating variable (mechanical position and flux, for instance).

Before applying these transformations to PMSM machines, some assumptions are introduced:

B.1 Modeling Assumptions:

The study of an electric motor behavior is a hard task and requires, first of all, good knowledge of its model to properly predict its dynamic behavior under different operating conditions.

Modeling a permanent magnet synchronous motor is similar to a classical synchronous machine, except that the flux from the magnets is constant. Then, the model is derived from the classical synchronous machine. In the following study, the machine has a stator and a rotor with symmetric distribution with p pairs of poles (p = 2 on **Fig** II.9).

To simplify the modeling of the machine, the following assumptions are introduced:

Assumptions:

- The damping effect of the rotor is neglected.
- The magnetic circuit of the machine is not saturated.
- The distribution of the magnetomotive forces (MMF) is sinusoidal.
- The coupling capacitors between the windings are neglected.
- The hysteresis phenomena and the eddy's currents are neglected.
- The gap irregularities owing to the stator slots are neglected.

Under these assumptions and using basic concepts, the electrical and mechanical equations describing the dynamical behavior of the PMSM are obtained. The model will be essential to design and implement the controllers and the observers

B.2 Park Transformations:

A general representation of the Park transformation is given as

$$\begin{bmatrix} Xd \\ Xq \\ Xo \end{bmatrix} = \mathrm{P}(\theta) \begin{bmatrix} Xa \\ Xb \\ Xc \end{bmatrix} \qquad \text{(II.8)}$$

Where :

$$\mathrm{P}(\theta) = \frac{2}{3} \begin{bmatrix} cos\theta r & \cos(\theta r - 120) & \cos(\theta r + 120) \\ sin\theta r & \sin(\theta r - 120) & \sin(\theta r + 120) \\ \frac{1}{2} & \frac{1}{2} & \frac{1}{2} \end{bmatrix} \qquad \text{(II.9)}$$

with θ as the angle between the axis α of the stationary reference frame and the real axis-d of the rotating reference frame, and with $\frac{2}{3}$ as the ratio between the amplitude of the three-phase system variables Xa , Xb, Xc (voltages, currents, ...) with respect to the amplitude of the corresponding two-phase system variables Xd , Xq , Xo

C. Application of the Park transformation to the pmsm:

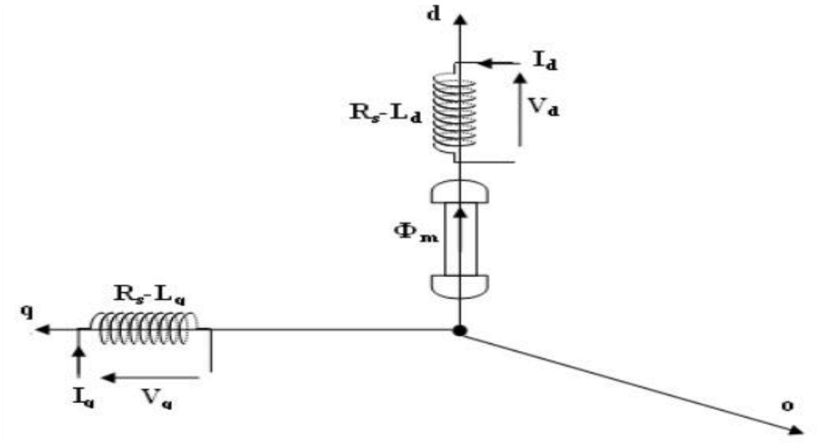

Fig II.9: PMSM in DQ space

C.1 Electrical equations of a three-phase winding in the d-q axis system:

$$[V_{dqo}] = [P(\theta)]\ [V_{sabc}] = [P(\theta)]\ \left([Rs]\ [I_{sabc}] + \frac{d[\varphi_{sabc}]}{dt}\right) \quad (II.10)$$

Applying the inverse Park transformation to the currents and fluxes we obtain

$$[I_{sabc}] = [P(\theta)]^{-1}\ [I_{dqo}] \quad (II.11)$$

$$[\varphi_{sabc}] = [P(\theta)]^{-1}\ [\varphi_{dqo}] \quad (II.12)$$

$$[V_{dqo}] = [P(\theta)]\ \left([Rs][P(\theta)]^{-1}[I_{dqo}] + \frac{d[P(\theta)]^{-1}[\varphi_{dqo}]}{dt}\right) \quad (II.13)$$

$$= [P(\theta)]\ [Rs][P(\theta)]^{-1}[I_{dqo}] + [P(\theta)]\ \frac{d[P(\theta)]^{-1}[\varphi_{dqo}]}{dt} \quad (II.14)$$

We have:

$$[P(\theta)]\ [Rs][P(\theta)]^{-1}[I_{dqo}] = [Rs][I_{dqo}] \quad (II.15)$$

$$[P(\theta)]\ \frac{d([P(\theta)]^{-1}[\varphi_{dqo}])}{dt} = [P(\theta)]\left\{\left(\frac{d([P(\theta)]^{-1}}{dt}\right)[\varphi_{dqo}] + [P(\theta)]^{-1}\left(\frac{d[\varphi_{dqo}]}{dt}\right)\right\} \quad (II.16)$$

$$= [P(\theta)]\left(\frac{d([P(\theta)]^{-1}}{dt}\right)[\varphi_{dqo}] + [P(\theta)]\ [P(\theta)]^{-1}\left(\frac{d[\varphi_{dqo}]}{dt}\right) \quad (II.17)$$

$$[P(\theta)]\ \frac{d([P(\theta)]^{-1}[\varphi_{dqo}])}{dt} = [P(\theta)]\left(\frac{d([P(\theta)]^{-1}}{dt}\right)[\varphi_{dqo}] + \left(\frac{d[\varphi_{dqo}]}{dt}\right) \quad (II.18)$$

$$\left(\frac{d([P(\theta)]^{-1}}{dt}\right) = \omega \begin{bmatrix} -sin\theta & -\ cos\theta & 0 \\ -sin\left(\theta - \frac{2\pi}{3}\right) & -\ cos\left(\theta - \frac{2\pi}{3}\right) & 0 \\ -sin\left(\theta - \frac{4\pi}{3}\right) & -\ cos\left(\theta - \frac{4\pi}{3}\right) & 0 \end{bmatrix} \quad (II.19)$$

We multiply the PARK equations and the derivative of PARK we get

$$[P(\theta)]\left(\frac{d([P(\theta)]^{-1})}{dt}\right) = \omega \begin{bmatrix} 0 & -1 & 0 \\ 1 & 0 & 0 \\ 0 & 0 & 0 \end{bmatrix} \quad (II.20)$$

$$[P(\theta)]\frac{d([P(\theta)]^{-1}[\varphi_{dqo}])}{dt} = \omega \begin{bmatrix} 0 & -1 & 0 \\ 1 & 0 & 0 \\ 0 & 0 & 0 \end{bmatrix} + \left(\frac{d[\varphi_{dqo}]}{dt}\right) \quad (II.21)$$

We replace the equations of resistances and derivative of PARK in the equation

$$\begin{bmatrix} V_d \\ V_q \\ V_0 \end{bmatrix} = \begin{bmatrix} R_s & 0 & 0 \\ 0 & R_s & 0 \\ 0 & 0 & R_s \end{bmatrix}\begin{bmatrix} I_d \\ I_q \\ I_0 \end{bmatrix} + \omega \begin{bmatrix} 0 & -1 & 0 \\ 1 & 0 & 0 \\ 0 & 0 & 0 \end{bmatrix}\begin{bmatrix} \varphi_d \\ \varphi_q \\ \varphi_0 \end{bmatrix} + \frac{d}{dt}\begin{bmatrix} \varphi_d \\ \varphi_q \\ \varphi_0 \end{bmatrix} \quad (II.22)$$

Since the system is balanced Vo =0, we finally obtain the dynamic electrical model for the equivalent two-phase stator winding

$$V_d = R_s I_d + \frac{d\varphi_d}{dt} - \omega\,\varphi_q \quad (II.23)$$
$$V_q = R_s I_q + \frac{d\varphi_q}{dt} - \omega\,\varphi_d \quad (II.24)$$
$$\varphi_d = L_d I_d + \lambda_m \quad (II.25)$$
$$\varphi_q = L_q I_q \quad (II.26)$$

The equivalent circuit of the PMSM in the d-q axis system:

$$V_d = R_s I_d + L_d \frac{dI_d}{dt} - \omega\, L_q I_q \quad (II.27)$$
$$V_q = R_s I_q + L_q \frac{dI_q}{dt} + \omega\, L_d I_d + \omega\lambda_m \quad (II.28)$$

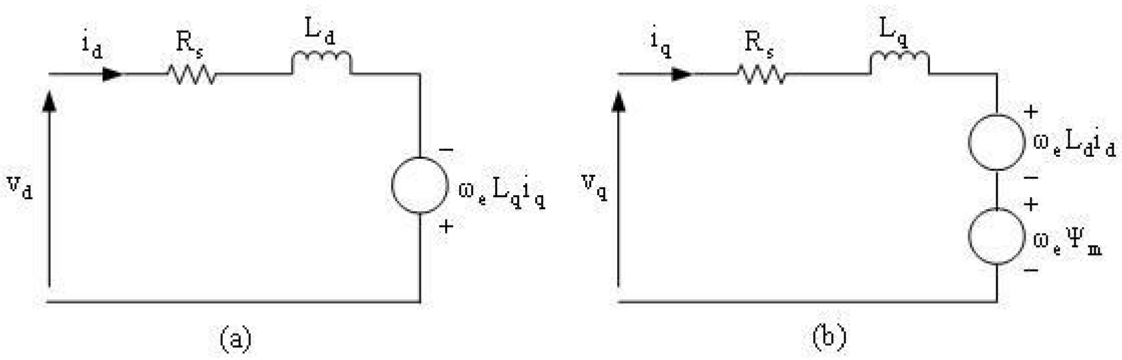

Fig II.10: PMSM equivalent circuit from dynamic equations

C.2 Instantaneous power equation:

$$P(t) = V_{sa}I_{sa} + V_{sb}I_{sb} + V_{sc}I_{sc} = \frac{3}{2}\left(V_q I_q + V_d I_d\right) \quad (II.29)$$

$$P(t) = \frac{3}{2}\left(\left(R_s I_d + \frac{d\varphi_d}{dt} - \omega\,\varphi_q\right) I_d + \left(R_s I_q + \frac{d\varphi_q}{dt} - \omega\,\varphi_d\right) I_q\right) \quad (II.30)$$

$$= \frac{3}{2} R_s\left(I_d^{\,2} + I_q^{\,2}\right) + \frac{3}{2}\left(\frac{d\varphi_d}{dt} I_d + \frac{d\varphi_q}{dt} I_q\right) + \frac{3}{2}\,\omega\left(\varphi_d I_q - \varphi_q I_d\right) \quad (II.31)$$

$P_j = \frac{3}{2} R_s\left({I_d}^2 + {I_q}^2\right)$ → represents the losses by Joules effect in the stator windings

$P_{mag} = \frac{3}{2}\left(\frac{d\varphi_d}{dt}\, I_d + \frac{d\varphi_q}{dt}\, I_q\right)$ → represents the energy variations magnetic stored in stator windings

$P_{mec} = \frac{3}{2}\, \omega\, \left(\varphi_d I_q - \varphi_q I_d\right)$ → represents the electrical power transformed into mechanical power inside the machine or electromagnetic power

C.3 Electromagnetic torque equation:

$$C_e = \frac{P_{mec}}{\Omega} = \frac{3}{2} P \left(\varphi_d I_q - \varphi_q I_d\right) \qquad \text{(II.32)}$$

$$C_e = \frac{3}{2} P\left[\left(L_d - L_q\right) I_d I_q + \lambda_m I_q\right] \qquad \text{(II.33)}$$

The electromagnetic torque breaks down into two terms:

$C_{ep} = \frac{3}{2} P \varphi_f I_q$ → Présente le couple principal

$C_e = \frac{3}{2} P \left(L_d - L_q\right) I_d I_q$ → Introduces the reluctance couple variable

D. State representation of the PMSM model in the d-q frame:

$$\begin{cases} V_d = R_s I_d + L_d \frac{dI_d}{dt} - \omega\, L_q I_q \\ V_q = R_s I_q + L_q \frac{dI_q}{dt} + \omega\, L_d I_d + \omega \lambda_m \end{cases}$$

$$\begin{cases} \frac{dI_d}{dt} = \frac{R_s}{L_d} I_d + \frac{L_q}{L_d} \mathrm{P}\, \Omega I_q + \frac{1}{L_d} V_d \\ \frac{dI_q}{dt} = \frac{R_s}{L_q} I_q - \frac{L_d}{L_q} \mathrm{P}\, \Omega I_q - \frac{\varphi_f}{L_q} \mathrm{P}\, \Omega + \frac{1}{L_q} V_q \end{cases}$$

II .2.2 Inverter:

Voltage Source Inverters are devices that convert a DC voltage to AC voltage of variable frequency and magnitude. They are very commonly used in adjustable speed drives and are characterized by a well-defined switched voltage wave form in the terminals. Fig **II.11** shows a voltage source inverter. The AC voltage frequency can be variable or constant depending on the application

Three phase inverters consist of six power switches connected as shown in Fig **II.11** to a DC voltage source. The inverter switches must be carefully selected based on the requirements of operation, ratings and the application. There are several devices available

Today and these are thyristors, bipolar junction transistors (BJTs), MOS field effect transistors (MOSFETs), insulated gate bipolar transistors (IGBTs) and gate turn off thyristors (GTOs). The devices list with their respective power switching capabilities are shown in **Table II.2** MOSFETs and IGBTs are preferred by industry because of the MOS gating permits high power gain and control advantages. While MOSFET is considered a universal power device for low power and low voltage applications, IGBT has wide acceptance for motor drives and other application in the low and medium power range. The power devices when used in motor drives applications require an inductive motor current path provided by antiparallel diodes when the switch is turned off. Inverters with antiparallel diodes

Device	Power Capability	Switching Speed
BJT	Medium	Medium
GTO	High	Low
IGBT	Medium	Medium
MOSFET	Low	High
THYRISTOR	High	Low

Table II.2. Devices Power and Switching Capabilities

II.2.2.1 Modeling of the Voltage source Inverter with PWM Control:

A. Inverter Modeling:

The voltage inverter is the essential part of the power supply system, it ensures the transformation of energy from a continuous source into an alternative energy, which can be at fixed or variable frequency. Each star of the MSDEAP is connected to a three-phase inverter. The latter consists of three arms, two switches for each. Each switch is mounted in reverse parallel with a recovery diode.

To ensure the continuity of the alternating currents and avoid the short circuit of the source, the switches Ti and Ti' (assumed to be ideal switches), must be controlled in such a way additional. To model the voltage inverter, we consider its power supply as a perfect source, supposed to consist of two generators of emf equal to U0 /2 connected to each other by a point noted n_0.

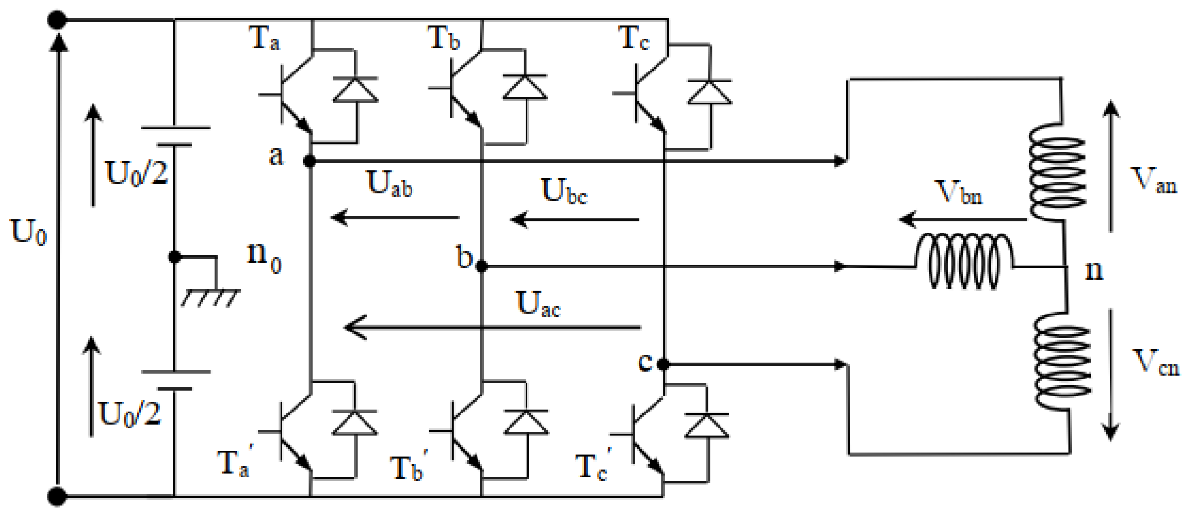

Fig II.11.Three-Phase Two-Level Inverter Schematic

To simplify the study and the complexity of the structure of the two-level inverter, we will assume that:

✓ The switching of the switches is instantaneous.

✓ The voltage drop across the terminals of the switches is negligible.

✓ The three-phase load is balanced and star-coupled with an isolated neutral [22].

The diodes (D = 1, 2,..) are transistor protection diodes providing freewheeling or recovery. Hence each pair (transistor-diode) is presented by a single bidirectional switch. The machine was modeled from simple voltages that we note Van, Vbn and Vcn and the inverter is controlled from the logical quantities Si. We have:

- if Si = 1, then T_i i is conducting and $T_{i'}$ is open,
- if Si = 0, then T_i is open and $T_{i'}$ is conducting.

with : $S_i + S_{i'} = 1$ and i = a, b, c.

Line-to-line voltages are obtained from the inverter outputs:

$$V_{ab} = V_{an0} - V_{bn0} \quad \text{(II.34)}$$

$$V_{bc} = V_{bn0} - V_{cn0} \quad \text{(II.35)}$$

$$V_{ca} = V_{cn0} - V_{an0} \quad \text{(II.36)}$$

The phase-to-neutral voltages of the load phases resulting from the phase-to-phase voltages have a zero sum, so:

$$V_{an} = \frac{1}{3}[U_{ab} - U_{ca}] \quad \text{(II.37)}$$

$$V_{bn} = \frac{1}{3}[U_{bc} - U_{ab}] \quad \text{(II.38)}$$

$$V_{cn} = \frac{1}{3}[U_{ca} - U_{bc}] \quad \text{(II.39)}$$

They can be written from the output voltages of the inverter by introducing the load neutral voltage with respect to the n_0 reference point.

$$V_{an} + V_{nn} = V_{an0} \quad \text{(II.40)}$$

$$V_{bn} + V_{nn} = V_{bn0} \quad \text{(II.41)}$$

$$V_{cn} + V_{nn} = V_{cn0} \quad \text{(II.42)}$$

So, we can deduce that:

$$V_{nn} = \frac{1}{3}[V_{an0} + V_{bn0} + V_{cn0}] \quad \text{(II.43)}$$

The state of switches supposedly perfect: S_{ij} (i=a, b, c et j= 1.2) we have:

$$V_{ijno} = S_{ij}\, U_0 - \frac{U_0}{2} \qquad \text{(II.44)}$$

So we have:

$$V_{ajno} = (S_{aj}\text{-}0.5)\, U_0 \qquad \text{(II.45)}$$

$$V_{bjno} = (S_{bj}\text{-}0.5)\, U_0 \qquad \text{(II.46)}$$

$$V_{jno} = (S_{cj}\text{-}0.5)\, U_0 \qquad \text{(II.47)}$$

By replacing (1.39) in (1.37), we get:

$$V_{ajn} = \frac{2}{3} V_{ajno} - \frac{1}{3} V_{bjno} - \frac{1}{3} V_{cjno} \qquad \text{(II.48)}$$

$$V_{bjn} = -\frac{1}{3} V_{ajno} + \frac{2}{3} V_{bjno} - \frac{1}{3} V_{cjno} \qquad \text{(II.49)}$$

$$V_{cjn} = -\frac{1}{3} V_{ajno} - \frac{1}{3} V_{bjno} + \frac{2}{3} V_{cjno} \qquad \text{(II.50)}$$

By replacing (1.39) in (1.40), we get:

$$\begin{bmatrix} V_{ajn} \\ V_{bjn} \\ V_{cjn} \end{bmatrix} = \frac{1}{3} \begin{pmatrix} 2 & -1 & -1 \\ -1 & 2 & -1 \\ -1 & -1 & 2 \end{pmatrix} \begin{pmatrix} S_{aj} \\ S_{bj} \\ S_{cj} \end{pmatrix} U_0 \qquad \text{(II.51)}$$

II.3 Control of PMSM:

A permanent magnet synchronous motor requires a control system, for example, a variable frequency drive or a servo drive. There are a large number of control techniques implemented control systems. The choice of the optimal control method mainly depends on the task that is put in front of the electric drive. The main methods for controlling a permanent magnet synchronous motor are shown in the table below.

Control			Advantages	Disadvantages
Scalar			Simple control scheme	Control is not optimal, not suitable for tasks where the variable load, loss of control is possible
Vector	Field oriented control	With position sensor	Smooth and precise setting of the rotor position and motor rotation speed, large control range	Requires rotor position sensor and powerful microcontroller inside the control system
		Without position sensor	No rotor position sensor required. Smooth and precise setting of the rotor position and motor rotation speed, large control range, but less than with position sensor	Sensorless field oriented control over **full speed range** is possible only for PMSM with salient pole rotor, a powerful control system is required
	Direct torque control		Simple control circuit, good dynamic performance, wide control range, no rotor position sensor required	High torque and current ripple

Table II.3 different methods for pmsm control [19].

Field Oriented Control (FOC):

II .3.1 Introduction

In order to achieve better dynamic performance, a more complex control scheme needs to be applied to control the PM motor. With the mathematical processing power offered by the microcontrollers, advanced control strategies can be implemented, which use mathematical transformations to control AC machines like DC machines, providing independent control of flux and torque producing currents. Such de-coupled torque and magnetization control is commonly called FOC.

II.3.2 The Main Philosophy Behind the FOC:

In order to understand the spirit of the FOC technique, start with an overview of the separately excited direct current (DC) motor. Torque is defined as the cross product of armature current and stator flux. Electrical study of the DC motor shows that the armature current and the stator flux can be independently tuned. The strength of the field excitation (the magnitude of the field excitation current) sets the value of the stator flux. If the flux is held constant, then the current through the rotor windings determines how much torque is produced.

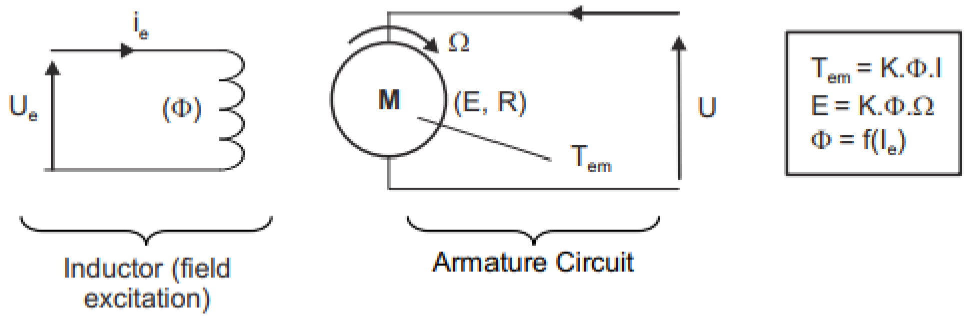

Fig II.12. Separated Excitation DC Motor Model (Flux and Torque are Independently Controlled and the Current Through the stator Windings Determines How Much Torque is Produced) [21].

AC machines do not have the same key features as the DC motor. The flux and torque producing current are not necessarily orthogonal.

The goal of the FOC (also called vector control) on synchronous and asynchronous machine is to be able to control those like a separately excited DC machine wherein the flux producing and torque producing currents are separately controlled. In other words, the control technique goal is, in a sense, to imitate the control of a DC motor. FOC control will allow us to decouple the flux and torque producing currents enabling them to be controlled independently. To decouple the torque and flux producing currents, it is necessary to engage several mathematical transforms, and this is where the microcontrollers add the most value. The processing capability provided by the microcontrollers enables these mathematical transformations to be carried out very quickly. This in turn implies that the entire algorithm controlling the motor can be executed at a fast rate, enabling higher dynamic performance. In addition to the decoupling, a dynamic model of the motor is now used for the computation of many quantities such as rotor flux angle and rotor speed. This means that their effect is accounted for, and the overall quality of control is better

II.3.4 Field oriented control types

Field-oriented control (FOC) allows you to smoothly, accurately and independently control the speed and torque of a PMSM motor. For the operation of the field oriented control algorithm, it is necessary to know the position of the rotor of the brushless motor.

There are two ways to determine the rotor position:

- by the position sensor;
- sensorless - by calculating the angle by the real-time control system based on the information available.

PMSM field oriented control by position sensor:

The following types of sensors are used as angle sensors:

- inductive: resolver, inductosyn, etc .;
- optical;
- magnetic: magnetoresistive sensors.

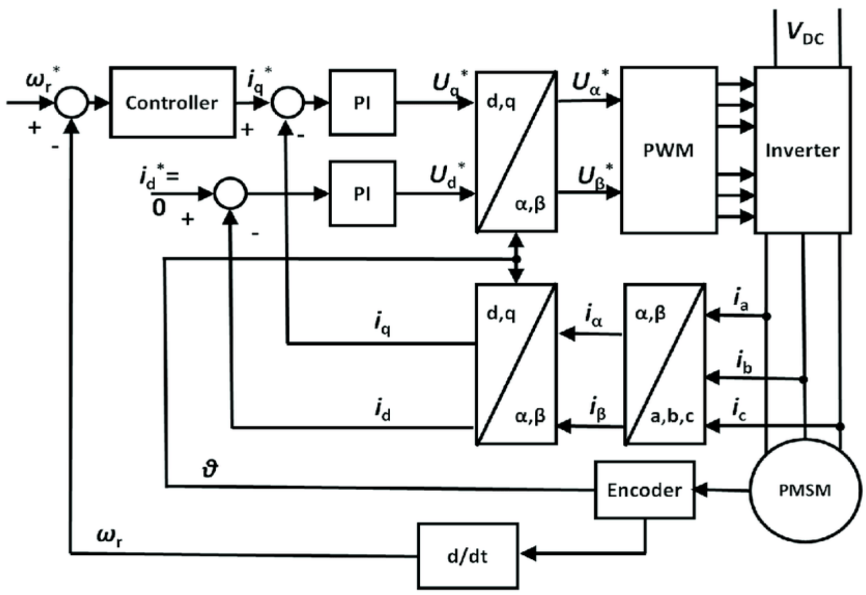

Fig II.13: Field Oriented Control of Permanent Magnet Synchronous Motor using a rotor position sensor

II.3.5 Block Diagram of Sensored FOC of PMSM:

The control can be summarized as follows:

• The three-phase stator currents are measured. For a motor with balanced three-phase windings, only two currents are sufficient to be measured. The third current can be calculated by the following equation: Ia+Ib+Ic = 0

• The three-phase currents are converted to a stationary two-axis system. This conversion provides the variables iα and iβ from the measured ia, ib, ic values. The values iα, iβ are time-varying quadrature current values as viewed from the perspective of the stator.

• The stationary two-axis coordinate system is rotated to align with the rotor flux using a transformation angle measured at the last iteration of the control loop. This conversion provides the id, iq variables from iα and iβ. The values id and iq are the quadrature currents transformed to the rotating coordinate system. For steady state conditions, id, iq are constant.

• Reference values of currents are explained below:

– id reference: controls rotor magnetizing flux

– iq reference: controls the torque output of the motor

• The error signals are fed to PI controllers. The output of the controllers provide vd, vq, which are voltage vectors that will be applied to the motor.

• A new transformation angle is measured from the encoder pulses input. This new angle guides the FOC algorithm as to where to place the next voltage vector.

• The vd, vq output values from the PI controllers are rotated back to the stationary reference frame using the new angle. This calculation provides the next quadrature voltage values vα,vβ.

• The vα,vβ values are used to calculate the new PWM duty cycle v[illegible] which will generate the desired voltage vector

• Mechanical speed (Ω) is calculated after every discrete PWM cycle

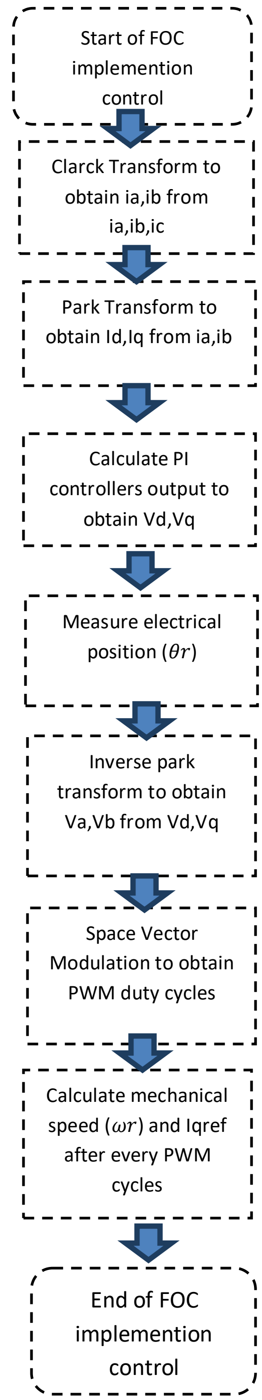

Flow chart of sensored FOC implementation

II.3.6 Field-oriented control of PMSM without a position sensor:

Since the 1970s sensorless vector control methods for PMSM AC motors began to be developed, thanks to the rapid development of microprocessors. The first sensorless methods for estimating the angle were based on the property of the electric motor to generate back EMF during rotation. The motor back EMF contains information about the position of the rotor, therefore, by calculating the value of the back EMF in the stationary coordinate system, you can calculate the position of the rotor. But when the rotor is not rotating, the back EMF is absent, and at low speed the back EMF has a small amplitude, which is difficult to distinguish from noise, therefore this method is not suitable for determining the position of the motor rotor at low speed.

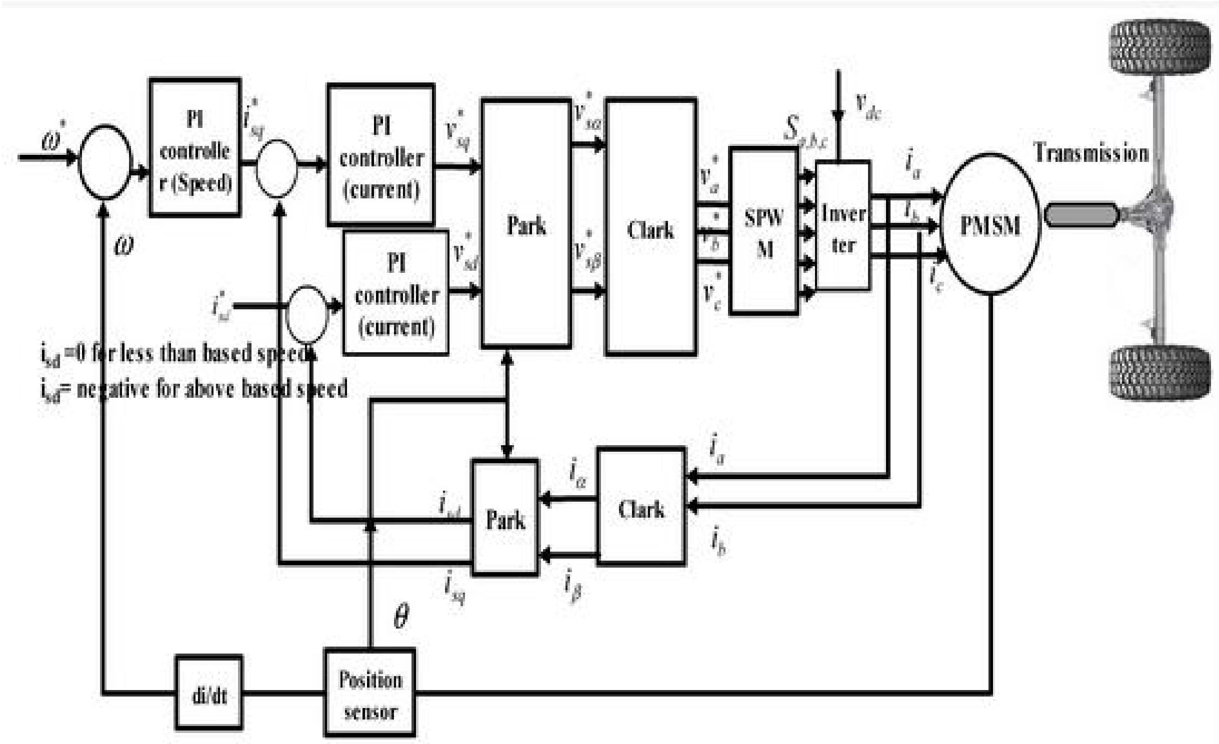

Fig II.14: Field Oriented Control of Permanent Magnet Synchronous Motor using a rotor position sensor [30].

The problem of sensorless control of a permanent magnet electric motor can be divided into 3 stages:

1 determining the initial position of the rotor for starting the electric motor;

2 control of the electric motor at low speeds, i.e. acceleration of the electric motor to speed (usually 10% of the nominal), where the generated back-EMF becomes sufficient to determine the position of the rotor;

3 acceleration of the electric motor to the rated (preset) rotation speed, control of the motor rotation speed during operation, maintaining the maximum torque.

II.4 Observability Property of PMSM Machine:

It will be shown by the following observability study that an interesting field of research is related to the high-performance sensorless position control of synchronous machines. It involves zero speed control at a determined rotor position. An additional problem is the observer structure is strongly dependent on [23].

II.4.1 Observability

First of all, what is observability? The answer to this question is: Observability is the possibility to reconstruct the full trajectory of the system from the data obtained from the input and output measurements.

II.4.2 Observation Objective:

Consider that in the (α, β) frame, the stator currents isα and isβ are the measurable outputs, the stator voltages vsα and vsβ are the control inputs of the motor. The objective is to reconstruct the rotor mechanical speed Ω and the position θ_m assuming that they are not available by measurement and moreover under the fact that the stator-winding resistance Rs and the stator-winding inductance Ls are inaccurately known

II.5 Conclusion:

In the first part of this chapter, a state of the art has been presented, where we have briefly describes multi-phase machines, their classifications (type of machine according to stators and rotors), their respective characteristics, their advantages and disadvantages as well as their uses.

The second part was devoted to the mathematical modeling of the machine permanent magnet synchronous motor PMSM in different bases. Use of a certain number of assumptions allowed us to reduce the complexity of the model of this machine. Then, we presented, the structure of the power supply system (Two-level voltage rectifier-filter-inverter controlled by the sine-triangle PWM strategy), and we give a brief introduce to observation method to control the PMSM. The next chapter will be devoted to the observers and the sensorless control of PMSM The real drive system is simulated using Simulink with block by block explanation. Chapter 3 deals with the simulation results.

Chapter III

Speed Sensorless Vector Control of PMSM

III.1 Introduction

The field oriented control (FOC), developed for permanent magnet synchrons motor (PMSM), requires the measurement of the speed to perform the coordinate transformations. Physically, this measurement is performed using a mechanical speed sensor mounted on the rotor shaft, which unfortunately increases the complexity and cost of installation (additional wiring and maintenance).

Moreover, the mechanical speed sensors are usually expensive, fragile and affect the reliability of the control. In this context, our study focuses mainly the speed estimation the observers are very attractive and give good performance in a wide range of speeds. The observation algorithms are using an analytical model of the machine to produce the speed and the rotor flux estimations from the stators' currents and voltages.

Among the observational methods we have deterministic observers (sliding mode observer), the Kalman filter, and the Model Reference Adaptive System (MRAS). These observers are used to observe the flux and speed estimation in a closed loop. Although such approaches lead to different performance in relation to the degree of algorithmic and computational complexity, they generally offer good performance in a wide range of speed but cannot estimate very low speeds in a stable manner.

III.2 Sensorless Control Scheme for Rotor Initial and Low Speed Position Detection:

As a major difficulty facing the sensorless control technology, the position detection of the motor rotor at zero and low speed is a significant influencing factor in the starting torque and stability of the motor [24]. In sensorless control strategy, the rotor position is determined by using the salient pole characteristic of the motor, saturation characteristic of the magnetic circuit or polarity of the magnetic circuit. These methods are summarized in Fig III.1.

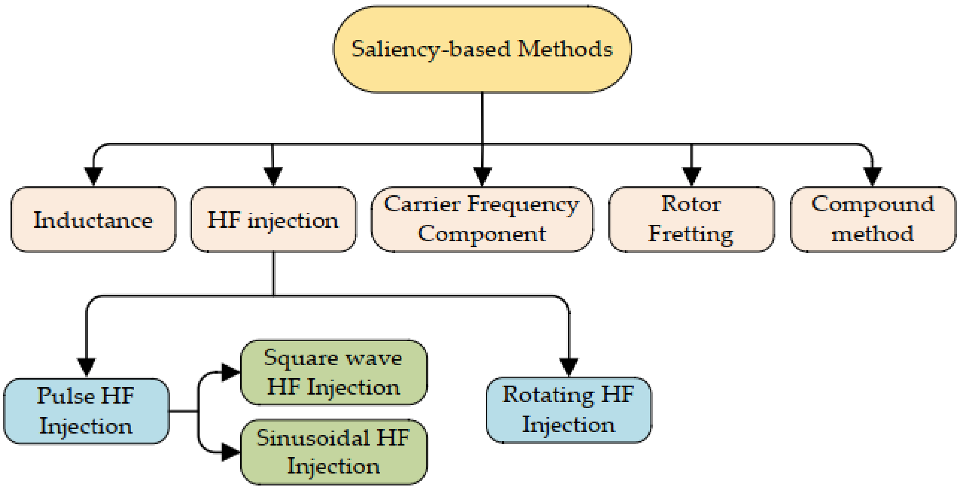

Fig III.1 Sensorless strategies for initial and low speed.

III.3 Sensorless Control Scheme for Medium-High Speed Operation:

In addition to the aforementioned method based on salient pole tracking, the sensorless control technology of PMSM includes the method of fundamental wave model, which relies on the back electromotive force related to the rotational speed of the motor in the fundamental wave excitation model for the estimate of rotor position and speed. As the motor runs at zero speed and very low speeds, while the signal-to-noise ratio of useful signals is extremely low, it is usually difficult to conduct extraction.

At present, there are several types of sensorless control technologies applicable for medium-high speed operation, including back EMF method, third harmonic, flux estimation method, model referencing adaptive system (MRAS), state observer method and so on, as shown in next figures. A brief introduction of each estimation method follows.

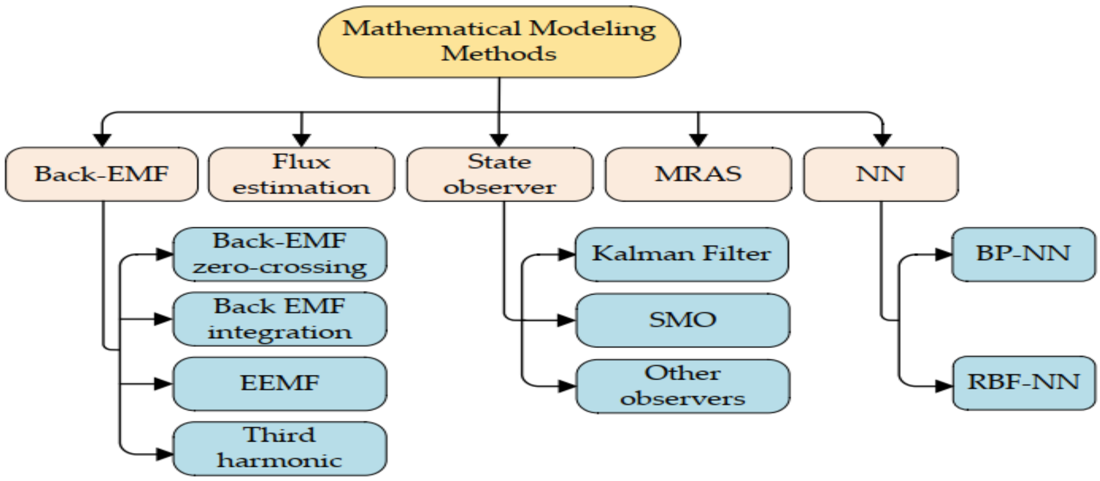

Fig III.2 Sensorless strategies for medium-high speed.

- The rotor position can be softly measured through a sensorless technique, which can realize high-performance control of the permanent magnet traction motor. The sensorless control has a broad application prospect in the field of electric vehicle traction systems. At present, the basic principle and control strategy of permanent magnet drive motor without position sensor for electric vehicle have got a certain application. However, in general, the position sensorless control strategy of permanent magnet traction motor and its application are still in the primary stage.
- It is a significant research direction to investigate the speed and position estimation approach considering the motor parameters identification techniques, which can realize the stable and reliable operation of the traction motor for EV.
- The traction motor for electric vehicle faces complex operation conditions, such as frequent start/stop, rapid acceleration/deceleration, overload and uphill/downhill, which is supposed to operate in a wide speed range. The rotor position estimation methods should be switched frequently, especially while the EV is operating in the urban setting. That means the hybrid rotor position estimation methods for sensorless control should be investigated to improve the reliability and the dynamic performance of the traction motor in the wide speed range [1].

III.4 Estimation Vector

In analyzing real motor and model behaviors, some variables should be specifically considered. From the observer's point of view, some variables should be estimated because they are an important part of the state space model. Based on the analysis, complex mechanical structures of supplied electric drives are noted; such generalized load torque T_L can be helpful during control. The problem of this extended observation has often been noted in the literature [23]. The state space vector of the proposed observer is:

$$\hat{X} = \begin{bmatrix} I_d & I_q & \omega_r & \theta \end{bmatrix}^T \qquad \text{(III.a)}$$

Where *id* and *iq* are the *dq* axis currents, *wr* is the rotor speed, θ is the mechanical shaft position.

$$\frac{dI_d}{dt} = \frac{R_s}{L_d} I_d + \frac{L_q}{L_d} \omega_r I_q + \frac{1}{L_d} V_d \qquad \text{(III.b)}$$

$$\frac{dI_q}{dt} = \frac{R_s}{L_q} I_q - \frac{L_d}{L_q} \omega_r I_q - \frac{\lambda_m}{L_q} \omega_r + \frac{1}{L_q} V_q \qquad \text{(III.c)}$$

$$J\frac{d\,\omega_r}{dt} = PT_e - PT_L - B\,\omega_r \qquad \text{(III.d)}$$

III.5 Sensorless Vector Control of Permanent Magnet Synchronous Motor Based on Model Reference Adaptive System (MRAS):

Firstly the MRAS algorithm is used to identify the rotor speed and position of the permanent magnet synchronous motor. Based on the algorithm, the sensorless vector control model of the permanent magnet synchronous motor is built. Based on this algorithm, the vector control experiment platform is built, simulation and experimental results show that the MRAS algorithm can accurately estimate the motor rotor speed and position, it is suitable for permanent magnet synchronous motor sensorless vector control.

The model reference adaptive system, developed using Popov's stability criterion, is one of many promising techniques employed in adaptive control for estimating the speed and stator resistance.

Among various types of adaptive system configuration, MRAS is important since it leads to a relatively easy-to-implement system with a fast adaptation for a wide range of applications. The basic principle is illustrated in **Fig** III.3, called *parallel MRAS*. The dynamic models are represented by the block "Reference Model", which is the actual system (for example, the motor, containing all unknown parameters, *i.e.*, motor speed, stator and rotor resistances) and the block "Adjustable Model", which has the same structure as the reference one (*i.e.*, motor, but with the adjustable or estimated parameters, instead of the unknown ones). An error vector ϵ is derived using the difference between the outputs of two dynamic models and is driven to zero through an adaptation law. As a result, the estimated parameter vector will converge to its true value *X*. One of the most noted advantages of this type of adaptive system is its high speed of adaptation. This is due to the fact that a measurement of the difference between the outputs of the reference model and adjustable model is obtained directly by comparison of the states (or outputs) of the reference model with those of the adjustable model system. It is remarkable that the error signal may be formulated with flux (F-MRAS), back-EMF (E-MRAS), reactive power (Q-MRAS) and active power (P-MRAS)

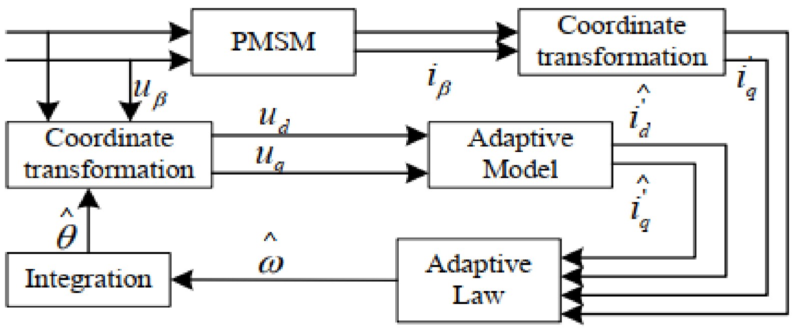

Fig III.3 Block diagram of speed estimation for sensorless vector control model based on MRAS.

A. Determination of the Reference Model and the Adjustable Model:

The stator current mathematical model of permanent magnet synchronous motor in *d q* axis coordinate system are [25]

$$\frac{dI_d}{dt} = \frac{R_s}{L_d} I_d + \frac{L_q}{L_d} \omega_r I_q + \frac{1}{L_d} V_d \qquad \text{(III.1)}$$

$$\frac{dI_q}{dt} = \frac{R_s}{L_q} I_q - \frac{L_d}{L_q} \omega_r I_q - \frac{\lambda_m}{L_q} \omega_r + \frac{1}{L_q} V_q \qquad \text{(III.2)}$$

According to the above two equations, the stator current model of the permanent magnet synchronous motor in the *d.q* axis system is only related to its speed, so choose the current model as the adjustable model, the permanent magnet synchronous motor itself as the reference model and use the parallel structure for speed identification. In order to analyze the stability of the system, the speed is limited to the system state matrix, do some corresponding changes in the control variables and state variables of the two equations, we can obtain:

$$\frac{d}{dt}\begin{bmatrix} I_d + \frac{\lambda_m}{L_q} \\ I_q \end{bmatrix} = \begin{bmatrix} -\frac{R_s}{L_d} & \omega_r \\ -\omega_r & -\frac{R_s}{L_q} \end{bmatrix} \begin{bmatrix} I_d + \frac{\lambda_m}{L_q} \\ I_q \end{bmatrix} + \frac{1}{L_q} \begin{bmatrix} V_d + \frac{R_s \lambda_m}{L_d} \\ V_q \end{bmatrix} \qquad \text{(III.3)}$$

Let: $I'_d = I_d + \frac{\lambda_m}{L_q}$ $\quad I'_q = I_q$ $\quad V'_d = V_d + \frac{R_s \lambda_m}{L_d}$ $\quad V'_q = V_q$

Then:

$$\frac{d}{dt}\begin{bmatrix} I'_d \\ I'_q \end{bmatrix} = \begin{bmatrix} -\frac{R_s}{L_d} & \omega_r \\ -\omega_r & -\frac{R_s}{L_q} \end{bmatrix} \begin{bmatrix} I'_d \\ I'_q \end{bmatrix} + \frac{1}{L} \begin{bmatrix} V'_d \\ V'_q \end{bmatrix} \qquad \text{(III.4)}$$

Simplified form is as follows:

$$\frac{dI'}{dt} = Ai' + Bu' \qquad \text{(III.5)}$$

i'= $\begin{bmatrix} I'_d \\ I'_q \end{bmatrix}$, u'= $\begin{bmatrix} V'_d \\ V'_q \end{bmatrix}$,A= $\begin{bmatrix} -\frac{R_s}{L_d} & \omega_r \\ -\omega_r & -\frac{R_s}{L_q} \end{bmatrix}$ B= $\frac{1}{L}$

The state matrix of equation (III.4) contains the information of rotor speed, so this equation is used as an adjustable model, and the permanent magnet synchronous motor itself is used as a reference model. Imitate equation (III.4). express the current and voltage in equation (III.4) by the estimated value, then the equation (III.6) can be obtained:

$$\frac{d}{dt}\begin{bmatrix} \widehat{I'_d} \\ \widehat{I'_q} \end{bmatrix} = \begin{bmatrix} -\frac{R_s}{L_d} & \widehat{\omega_r} \\ -\widehat{\omega_r} & -\frac{R_s}{L_q} \end{bmatrix}\begin{bmatrix} \widehat{I'_d} \\ \widehat{I'_q} \end{bmatrix} + \frac{1}{L}\begin{bmatrix} V'_d \\ V'_q \end{bmatrix} \qquad \text{(III.6)}$$

With the same principle, the simplified form is as follows:

$$\frac{d\widehat{\imath'}}{dt} = \hat{A}\text{i'} + \text{Bu'} \qquad \text{(III.7)}$$

Use equation (III.4) minus equation (III.6), we can obtain:

$$\begin{bmatrix} \frac{de_d}{dt} \\ \frac{de_q}{dt} \end{bmatrix} = \begin{bmatrix} -\frac{R_s}{L_d} & \omega_r \\ -\omega_r & -\frac{R_s}{L_q} \end{bmatrix}\begin{bmatrix} e_d \\ e_q \end{bmatrix} - \text{J}(\omega_r - \widehat{\omega_r})\begin{bmatrix} \widehat{I'_d} \\ \widehat{I'_q} \end{bmatrix} \qquad \text{(III.8)}$$

In the above equation:

$e_d = I'_d - \widehat{I'_d}$, $e_q = I'_q - \widehat{I'_q}$, J= $\begin{bmatrix} 0 & -1 \\ 1 & 0 \end{bmatrix}$

Equation (III.8) can be simplified as follows:

$$\frac{de}{dt} = A_e \, \text{e} - \omega \qquad \text{(III.9)}$$

In the above equation, A_e =A = $\begin{bmatrix} -\frac{R_s}{L_d} & \omega_r \\ -\omega_r & -\frac{R_s}{L_q} \end{bmatrix}$

$$\text{e}=\begin{bmatrix} e_d \\ e_q \end{bmatrix} \quad \omega = (\omega_r - \widehat{\omega_r})\begin{bmatrix} \widehat{-I'_q} \\ \widehat{I'_d} \end{bmatrix}$$

B. ***Determination of the Adaptive Law*****:**

In order to construct a well-behaved MRAS algorithm, it is necessary to determine the appropriate adaptive law, and the adaptive law generally selects the form of proportional plus integral. Designing the appropriate adaptive law requires finding the relationship between the amount of fitness and the amount of feedback. Here a non-linear time varying feedback system is used to express its relationship. According to the Popov hyper stability theory. The model reference adaptive system is designed. It can not only make the adjustable model approach the reference model, but also can guarantee the system's stability. Therefore, this study uses Popov super stability theory to design adaptive law. Nonlinear variable part satisfies Popov integral inequality:

$$\eta\ (0,t_0) = \int_0^{t_0} v^T\ \ \omega_r\ dt \geq \gamma_0^2 \qquad \text{(III.10)}$$

$\forall t_0 \geq 0$, γ_0^2 is any finite positive number.

Substitute *v* and Z into the Popov integral inequality (III.10):

$$\eta\ (0,t_0) = \int_0^{t_0} e^T\ (\widehat{\omega_r} - \omega_r\ )\ \mathrm{J}\ \widehat{\imath'}\mathrm{dt} \geq \gamma_0^2 \qquad \text{(III.11)}$$

According to the general structure of the model reference adaptive parameter, take $\widehat{\omega_r}$ into the proportional integral form of the following equation (III.12):

$$\widehat{\omega_r} = \int_0^{t} F_1\ (v,t,\tau)\mathrm{d}\tau + F_2(\mathrm{v,t}) + \widehat{\omega_r}(0) \qquad \text{(III.12)}$$

In the above equation $\widehat{\omega_r}(0)$ is original value. Equation (III.12) shows a proportional integral structure with universal significance. Substitute equation (III.12) into equation (III.11):

$$\eta\ (0,t_0) = \int_0^{t_0} e^T \left[\int_0^{t} F_1\ (v,t,\tau)\mathrm{d}\tau\ +\ F_2(\mathrm{v,t}) +\ \widehat{\omega_r}(0)\right] \mathrm{J}\ \widehat{\imath'}\mathrm{dt}$$

$$= \int_0^{t_0} e^T \left[\int_0^{t} F_1\ (v,t,\tau)\mathrm{d}\tau\ +\ \ \widehat{\omega_r} +\ \widehat{\omega_r}(0)\right] \mathrm{J}\ \widehat{\imath'}\mathrm{dt} + \int_0^{t_0} e^T\ F_2(\mathrm{v,t})\ \mathrm{J}\ \widehat{\imath'}\mathrm{dt}$$

$$= \eta_1\ (0,t_0) + \eta_2\ (0,t_0)$$

To make $\eta\ (0,t_0) \geq \gamma_0^2$ we can let

$$\eta_1\ (0,t_0) = \int_0^{t_0} e^T \left[\int_0^{t} F_1\ (v,t,\tau)\mathrm{d}\tau\ +\ \ \widehat{\omega_r} +\ \widehat{\omega_r}(0)\right] \mathrm{J}\ \widehat{\imath'}\mathrm{dt} \geq \gamma_1^2 \qquad \text{(III.13)}$$

$$\eta_2\ (0,t_0) = \int_0^{t_0} e^T\ \ \int_0^{t_0} e^T\ F_2(\mathrm{v,t})\ \mathrm{J}\ \widehat{\imath'}\mathrm{dt} \geq \gamma_2^2 \qquad \text{(III.14)}$$

In the above equation, $\gamma_1^2$and$\gamma_2^2$are finite positive numbers. Equation (III.15) is as follows:

$$\int_0^{t_0} \frac{df(t)}{dt}\mathrm{kf\ (t)\ dt} = \frac{2}{k}\ [f^2(t_0) - f^2(0)\ ] \geq \frac{1}{2}\ \mathrm{k}f^2(0) \qquad \text{(III.15)}$$

Here:

$$\frac{df(t)}{dt} = e^T\ \mathrm{J}\ \widehat{\imath'}$$

$$\mathrm{k}\ f(t) = \int_0^{t} F_1\ (v,t,\tau)\mathrm{d}\tau\ +\ \ \widehat{\omega_r} +\ \widehat{\omega_r}(0) \qquad \text{(III.16)}$$

Differentiate the equation (III.17), get:

$$F_1(v,t,\tau) = k_i e^T\ \mathrm{J}\ \widehat{\imath'} \qquad \text{(III.17)}$$

Substitute equation (III.17) into: $\eta_1\ (0,t_0)$ then $\eta_1\ (0,t_0)\ \geq \gamma_1^2$ can be guaranteed. If the left part of the inequality is positive, the inequality must be correct. So let:

$$F_2(\mathrm{v},\mathrm{t}) = K_p e^T \, \mathrm{J} \, \hat{i'} \qquad \text{(III.18)}$$

Obviously, substitute equation (III.18) and equation (III.17) into equation (III.12), Popov integral inequality must be satisfied, that means

$$\eta\,(0,t_0) = \int_0^{t_0} e^T \left[\int_0^t k_i e^T \, \mathrm{J} \, \hat{i'} \, \mathrm{d}\tau + K_p e^T \, \mathrm{J} \, \hat{i'} - \widehat{\omega_r} + \widehat{\omega_r}(0)\right] \mathrm{J} \, \hat{i'} \mathrm{d}t \geq \gamma_0^2 \qquad \text{(III.19)}$$

On the contrary, to improve equation (III.12):

$$\widehat{\omega_r} = \int_0^t k_i e^T \, \mathrm{J} \, \hat{i'} \, \mathrm{d}\tau + K_p e^T \, \mathrm{J} \, \hat{i'} + \widehat{\omega_r}(0) \qquad \text{(III.20)}$$

If take $\widehat{\omega_r}$ into the form of equation (22), the feedback from the stator current vector error must be asymptotic stable.

Substitute $e^T = \begin{bmatrix} I'_d & -\widehat{I'_d} \\ I'_q & -\widehat{I'_q} \end{bmatrix}$ J=$\begin{bmatrix} 0 & -1 \\ 1 & 0 \end{bmatrix}$ $\hat{i'} = \begin{bmatrix} \widehat{I'_d} \\ \widehat{I'_q} \end{bmatrix}$

Into equation (III.20), get

$$\widehat{\omega_r} = \int_0^t k_i\left(I'_d\widehat{I'_q} - I'_q\widehat{I'_d}\right)\mathrm{d}\tau + K_p\left(I'_d\widehat{I'_q} - I'_q\widehat{I'_d}\right) + \widehat{\omega_r}(0) \qquad \text{(III.21)}$$

Let : $I'_d = I_d + \frac{\lambda_m}{L_q}$ $\quad I'_q = I_q$ $\quad V'_d = V_d + \frac{R_s\lambda_m}{L_d}$ $\quad V'_q = V_q$

into equation (III.21), obtain the adaptive law:

$$\widehat{\omega_r} = \int_0^t k_i\left(I_d\widehat{I_q} - I_q\widehat{I_d} - \frac{\lambda_m}{L_q}(I_q - \widehat{I_q})\right)\mathrm{d}\tau + K_p\left(I_d\widehat{I_q} - I_q\widehat{I_d} - \frac{\lambda_m}{L_q}(I_q - \widehat{I_q})\right) + \widehat{\omega_r}(0)$$

In the above equation, $\widehat{I_d}$ and $\widehat{I_q}$ can be calculated from adjustable model equation (III.6), I_d and I_q will be calculated after the motor detection

C- Sensorless Vector Control Based on MRAS simulation:

Instead of traditional mechanical sensor, the MRAS algorithm is used to estimate the rotor speed $\widehat{\omega_r}$ and position $\hat{\theta}$ of the permanent magnet synchronous motor, then sent $\widehat{\omega_r}$ and $\hat{\theta}$ into the whole vector control system of the permanent magnet synchronous motor to help the system run normally

The block diagram of MRAS speed identification algorithm is shown in **Fig** III.4. In the adjustable model, the speed ($\widehat{\omega_r}$) is an adjustable parameter, but also a parameter need to be identified, recorded as $\widehat{\omega_r}$ If the stator current estimated by the model is the same as that determined by the reference model, that is, the error between the two is zero, then the speed estimate value ($\widehat{\omega_r}$) should also be consistent with the actual value (ω_r) In **Fig** III.4, use the stator current vector error between the adjustable model and the reference model, Construct a suitable adaptive law with the above-mentioned adaptive law generation theory, to make the $\widehat{\omega_r}$ of the adjustable model close to ω_r

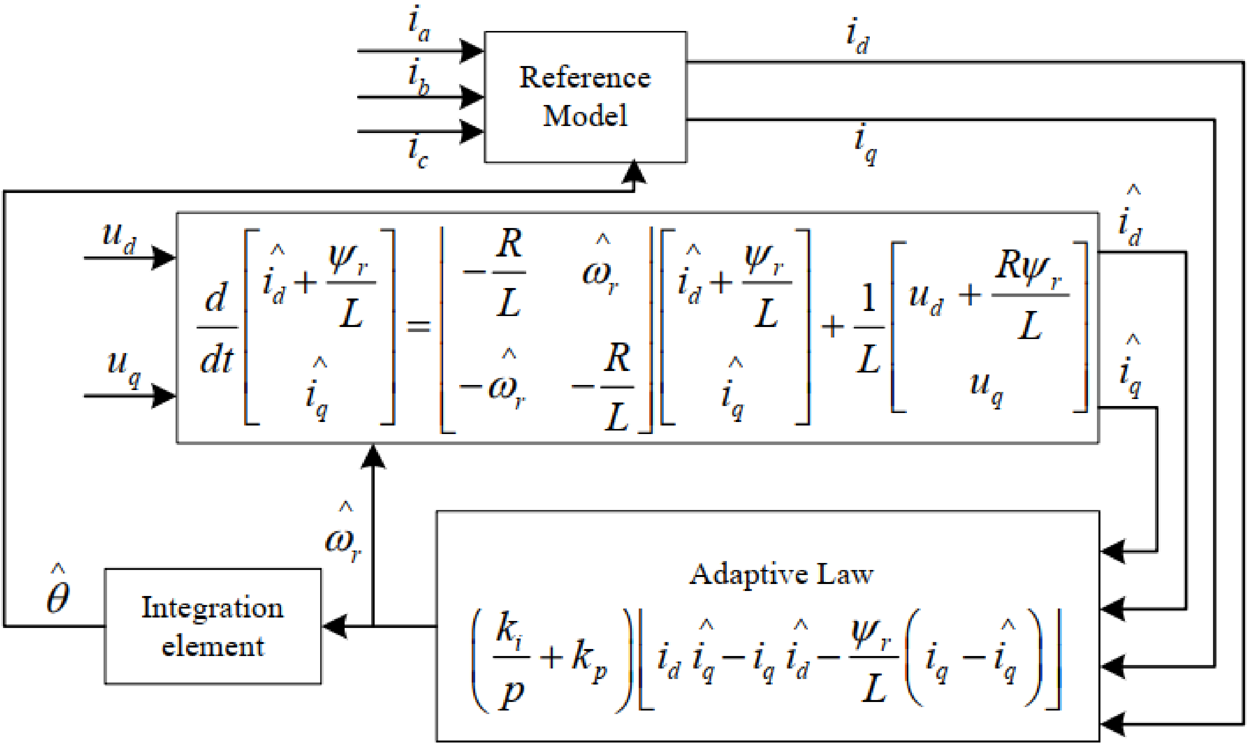

Fig III.4 Speed identification diagram of MRAS

Results and analysis

The computer simulation and experiment have been performed for the verification of the proposed control algorithm. Simulations have been carried out in MATLAB/Simlink environment to verify the effectiveness of the suggested control strategy, **Fig** III.5 shows the whole system based on MATLAB/SIMULINK software:

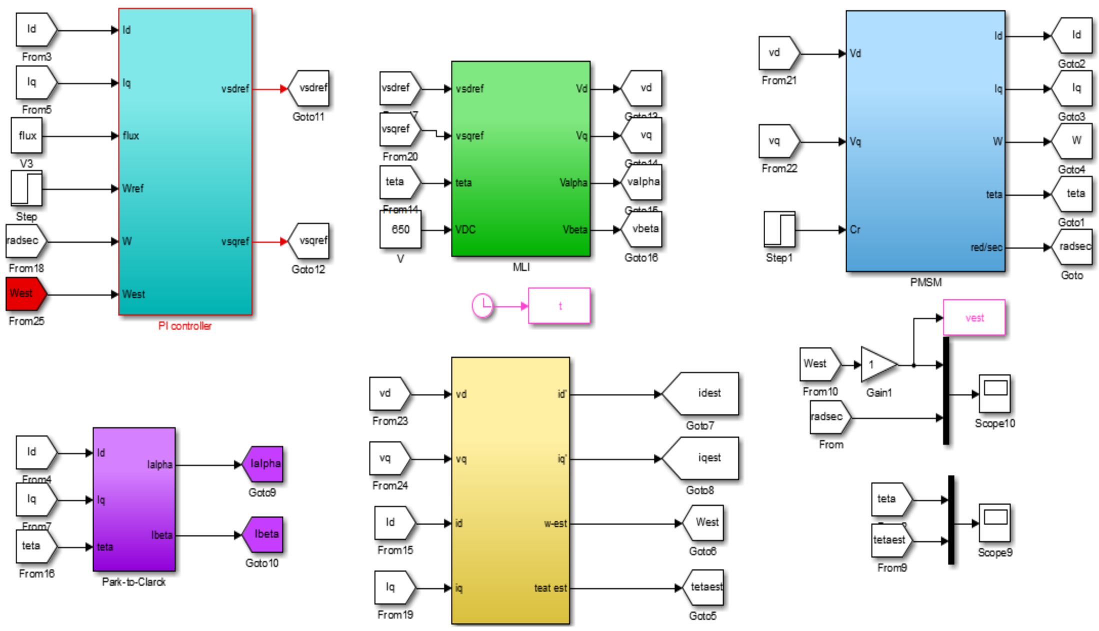

Fig III.5 the whole system based on Simulink software

The main parts of the simulation model based on PMSM algorithm of MRAS sensorless vector control system include: coordinate transformation module, PI module,PMSM motor, SVPWM module and MRAS speed estimation module and so on. The block diagram of sensorless vector control for permanent magnet synchronous motor is shown in Fig III.5

parameters	*values*
Power (KW)	60
Rs (Ω)	0.153
Ld (mH)	1.8
Lq (mH)	1.8
P	2
Flux (Wb)	0.2778
J ($Kg.m^2$)	0.008
F (N..m.s)	0.0015

Table III.A1:PMSM parameters

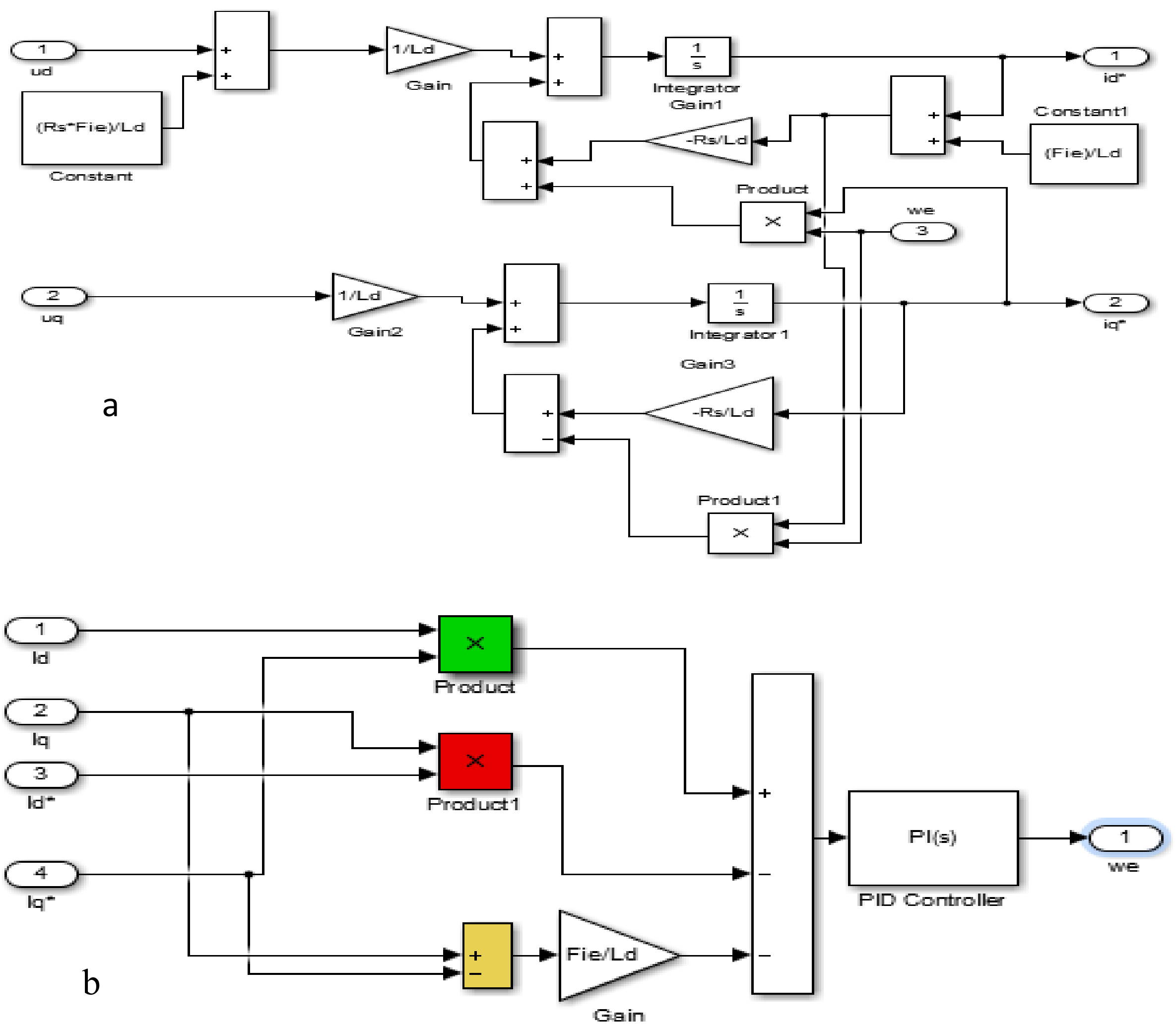

Fig III.6. SIMULATION MODEL OF MRAS SYSTEM a) **Adjustable Model**, b) ***the Adaptive Law***

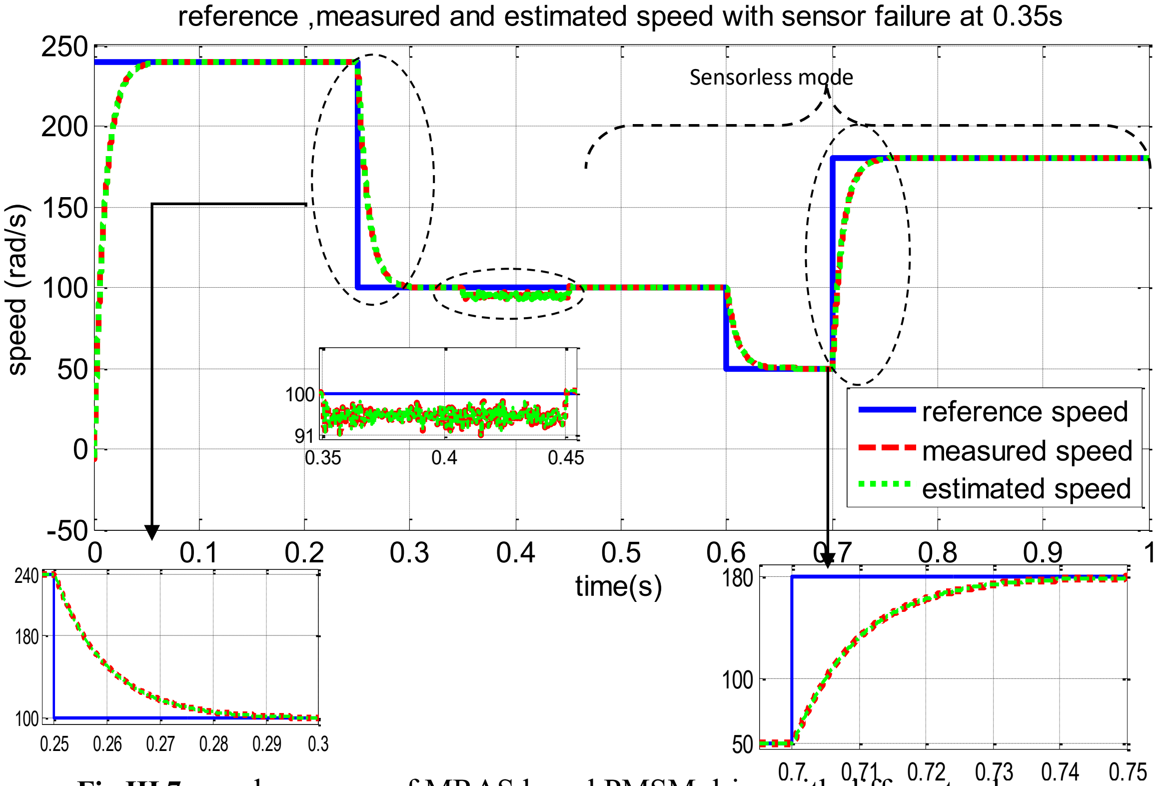

Fig III.7 speed response of MRAS based PMSM drive with different values

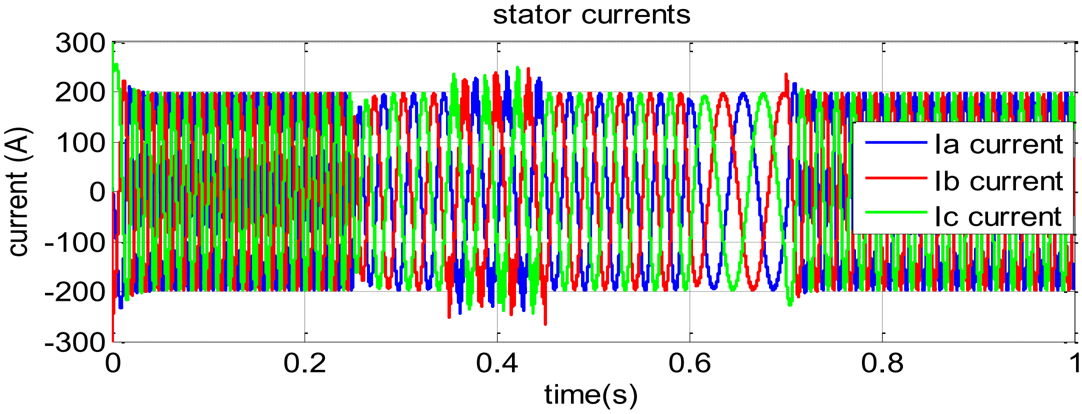

Fig III.8 currents response of MRAS based PMSM drive

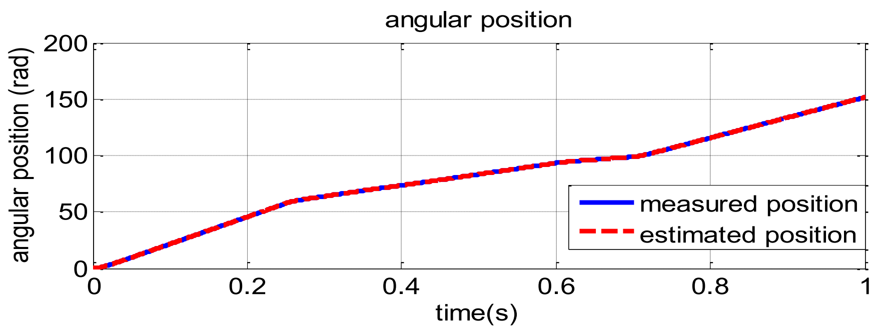

Fig III.9 compared between measured and estimated position

Fig III.7 shows the speed response in the reference rotor speed of 2290rpm in full load, the proposed sensorless control algorithm has good response.

During the analysis, the PMSM motor is made to run in four phases two of them in sensor mode and the other in sensorless mode when it start at 0.45s after sensor failure at 0.35s. That is in first phase the speed is increased [0 to 240rad/s]; in second, speed is decreased [240 to 100rad/s], in third speed is reduced [100 to 50rad/s] and in fourth phase it rises [50 to 180rad/s]

Fig III.7 shows the estimated rotor angle and the rotor angle estimation error for speed of 200rpm. From these experimiiental results, it shows this MRAS approachi is effective and feasible.

In the phase of motor starting, the estimated speed of the motor and the actual speed curve are shown in Fig III.7. Compared with the two curves, it can be seen that the MRAS algorithm can estimate the motor speed well in the phase of motor starting. The estimated speed can track the actual speed of the motor well. The system will need 0.04s time to reach steady state.

At 0.25s, the given speed is changed from (240tr/s) 2292rpm to (100tr/s) 955rpm. it can be seen that the estimated rotational speed can track the actual speed of the motor well and the accuracy of the estimation can meet the requirements of the vector control system. In the phase of motor starting and the phase of speed mutation, the estimation error of the speed is small, but the error under the MRAS algorithm is quickly converged, and the large speed fluctuation does not occur. The system can quickly reach the new stable state. The simulated effect is good

it can be seen that current in all the phases are balanced during the steady state condition. The phase current are different at the sudden change in the speed but these values are small

III.6 PMSM AND BACK-EMF SLIDING MODE OBSERVER:

The SMO is widely studied in the field of a motion control, and it can be applied to nonlinear systems, such as PMSM motors. This technique applied to control systems encounters restrictions in practice, due to the high voltage values of the power supply needed and severe stress given to the static power converters. On the other hand, the sliding mode has been shown very efficient in the state estimation due to its salient features, *i.e.*, robustness to parameter variations and disturbances including the measurement noise. The use of sliding mode in state observer does not present physical restrictions relative to the convergence condition (the estimation error moves toward zero) and does not subject the system to undesirable chattering [26]:

$$U = RI + \frac{d\varphi}{dt} \qquad \text{(III.22)}$$

$$\varphi = LI + \lambda_m \qquad \text{(III.23)}$$

We substitute the equation (III.23) in (III.22)

$$\frac{di_a}{dt} = -\frac{R}{L} i_a - \frac{1}{L} e_a + \frac{1}{L} u_a \qquad \text{(III.a)}$$

$$\frac{di_b}{dt} = -\frac{R}{L} i_b - \frac{1}{L} e_b + \frac{1}{L} u_b \qquad \text{(III.b)}$$

$$\frac{di_c}{dt} = -\frac{R}{L} i_c - \frac{1}{L} e_c + \frac{1}{L} u_c \qquad \text{(III.c)}$$

$$e_a = \frac{d\varphi_{ma}}{dt} = -\lambda_m \omega_r \sin(\theta_e) \qquad \text{(III.24)}$$

$$e_b = \frac{d\varphi_{mb}}{dt} = -\lambda_m \omega_r \sin(\theta_e - \frac{2\pi}{3}) \qquad \text{(III.25)}$$

$$e_b = \frac{d\varphi_{mc}}{dt} = -\lambda_m \omega_r \sin(\theta_e + \frac{2\pi}{3}) \qquad \text{(III.26)}$$

By using the usual Clarke transform, the current equations are obtained in α, β frame:

$$\frac{di_\alpha}{dt} = -\frac{R}{L} i_\alpha - \frac{1}{L} e_\alpha + \frac{1}{L} u_\alpha \qquad \text{(III.27)}$$

$$\frac{di_\beta}{dt} = -\frac{R}{L} i_\beta - \frac{1}{L} e_\beta + \frac{1}{L} u_\beta \qquad \text{(III.28)}$$

The back-EMF from (III.27), (III.28) becomes:

$$e_\alpha = \frac{d\varphi_{m\alpha}}{dt} = -\lambda_m \omega_r \sin(\theta_e) \qquad \text{(III.29)}$$

$$e_\beta = \frac{d\varphi_{m\beta}}{dt} = -\lambda_m \omega_r \cos(\theta_e) \qquad \text{(III.30)}$$

To estimate the rotor speed, it is necessary to estimate the back-EMF $e\alpha$ and $e\beta$ first. For this purpose, a sliding mode observer will be used, which is given by:

$$\frac{d\widehat{\iota_\alpha}}{dt} = -\frac{R}{L}\widehat{\iota_\alpha} + \frac{1}{L}u_\alpha - \frac{l1}{L}\text{sign}(\widehat{\iota_\alpha} - i_\alpha) \qquad \text{(III.31)}$$

$$\frac{d\widehat{\iota_\beta}}{dt} = -\frac{R}{L}\widehat{\iota_\beta} + \frac{1}{L}u_\alpha - \frac{l1}{L}\text{sign}(\widehat{\iota_\beta} - i_\beta) \qquad \text{(III.32)}$$

A sliding mode is enforced after a limited time if l_1 > max (|eα |, |eβ|) By using the equations (III.31) and (III.32), defining errors as

$\widetilde{\iota_\alpha} = \widehat{\iota_\alpha} - i_\alpha$, $\widetilde{\iota_\beta} = \widehat{\iota_\beta} - i_\beta$ the following relations are obtained:

$$\frac{d\widetilde{\iota_\alpha}}{dt} = -\frac{R}{L}\widetilde{\iota_\alpha} + \frac{1}{L}u_\alpha - \frac{l1}{L}\textbf{sign}(\widetilde{\iota_\alpha}) \qquad \text{(III.33)}$$

$$\frac{d\widetilde{\iota_\beta}}{dt} = -\frac{R}{L}\widetilde{\iota_\beta} + \frac{1}{L}u_\alpha - \frac{l1}{L}\textbf{sign}(\widetilde{\iota_\beta}) \qquad \text{(III.34)}$$

When sliding mode occurs, the error is null thus $\widetilde{\iota_\alpha}$=0 and $\widetilde{\iota_\beta}$=0 and also $\frac{d\widetilde{\iota_\alpha}}{dt} = \mathbf{0}$ $\frac{d\widetilde{\iota_\beta}}{dt} = \mathbf{0}$ The desired back-EMF quantities eα and eβ are obtained by using the equivalent values of the switching quantities:

$$(l_1 \text{sign}(\widetilde{\iota_\alpha}))_{eq} = \boldsymbol{e_\alpha} \qquad \text{(III.35)}$$

$$(l_1 \text{sign}(\widetilde{\iota_\beta}))_{eq} = \boldsymbol{e_\beta} \qquad \text{(III.36)}$$

However, they could not be used as is due to the high frequency residual, and to the delay from the low pass filter. Consider their low pass filtered result *za* and *zb*:

$$Z_\alpha(t) + \Delta_\alpha(t) = e_\alpha \qquad (III.37)$$

$$Z_\beta(t) + \Delta_\beta(t) = e_\beta \qquad (III.38)$$

Where $\boldsymbol{\Delta_\alpha}$ and $\boldsymbol{\Delta_\beta}$ are the errors

Although the use of such a filter can reduce the chattering, following an observer is presented for smoothing the $\boldsymbol{e_\alpha}$ and $\boldsymbol{e_\beta}$ for estimation of ω_r

We assume that ω_r= 0 (the variations of the rotor speed ω_r are slow in comparison to other quantities involved in the observer). With this assumption, the equation (III.29), (III.30), becomes:

$$\dot{e}_\alpha = \lambda_m \omega_r^2 \cos(\boldsymbol{\theta_e}) \qquad (III.39)$$

$$\dot{e}_\beta = -\lambda_m \omega_r^2 \sin(\boldsymbol{\theta_e}) \qquad (III.40)$$

Which can be rewritten as:

$$\dot{e}_\alpha = -\omega_r e_\beta \qquad (III.41)$$

$$\dot{e}_\beta = \omega_r e_\beta \qquad (III.42)$$

To obtain *eα*, *eβ* equations ((III.31) (III.32)) - ((III.41) (III.42)) are integrated, while obtaining an important low pass filter action. The observer equations are:

$$\dot{\widehat{e_\alpha}} = -\widehat{\omega_r}\widehat{e_\beta} - l_2(\widehat{e_\alpha} - Z_\alpha) \qquad (III.43)$$

$$\dot{\widehat{e_\beta}} = \widehat{\omega_r}\widehat{e_\alpha} - l_2(\widehat{e_\beta} - Z_\beta) \qquad (III.44)$$

$$\dot{\widehat{\omega_r}} = (\widehat{e_\alpha} - Z_\alpha)\widehat{e_\beta} - (\widehat{e_\beta} - Z_\beta)\widehat{e_\alpha} \qquad (III45)$$

Parameters $\boldsymbol{l_1}$ and $\boldsymbol{l_2}$ are the design parameters that ensure the flexibility of the observer implementation, but which must be above max ($|\boldsymbol{e_\alpha}|$, $|\boldsymbol{e_\beta}|$). Defining errors quantities

$\overline{\boldsymbol{e_\alpha}} = \widehat{\boldsymbol{e_\alpha}} - \boldsymbol{e_\alpha}$, $\overline{\boldsymbol{e_\beta}} = \widehat{\boldsymbol{e_\beta}} - \boldsymbol{e_\beta}$ and $\overline{\omega_r} = \widehat{\omega_r} - \omega_r$, considering zα(t) → eα(t) and zβ(t) → eβ(t), the equation (III.43), (III.44), (III45) can be rewritten as:

$$\dot{\overline{\boldsymbol{e_\alpha}}} = -\widehat{\omega_r}\widehat{\boldsymbol{e_\beta}} + \omega_r \boldsymbol{e_\beta} - \boldsymbol{l_2}(\widehat{\boldsymbol{e_\alpha}} - \boldsymbol{e_\alpha}) \qquad \textbf{(III.46)}$$

$$\dot{\overline{\boldsymbol{e_\beta}}} = \widehat{\omega_r}\widehat{\boldsymbol{e_\alpha}} - \omega_r \boldsymbol{e_\alpha} - \boldsymbol{l_2}(\widehat{\boldsymbol{e_\beta}} - \boldsymbol{e_\beta}) \qquad \textbf{(III.47)}$$

$$\dot{\overline{\omega_r}} = (\widehat{\boldsymbol{e_\alpha}} - \boldsymbol{e_\alpha})\widehat{\boldsymbol{e_\beta}} - (\widehat{\boldsymbol{e_\beta}} - \boldsymbol{e_\beta})\widehat{\boldsymbol{e_\alpha}} \qquad \textbf{(III.48)}$$

To prove the observer convergence, a Lyapunov function candidate V is used, which is given by:

$$\dot{\boldsymbol{V}} = \frac{1}{2}(\overline{\boldsymbol{e_\alpha}}^2 + \overline{\boldsymbol{e_\beta}}^2 - \overline{\omega_r}^2) \qquad (III.49)$$

The derivative of V is given by:

$$\dot{V} = \dot{\overline{e_\alpha}}\ \overline{e_\alpha} + \dot{\overline{e_\beta}}\ \overline{e_\beta} + \dot{\overline{\omega_r}}\ \overline{\omega_r}$$

$$= -\widehat{\omega_r}\widehat{e_\beta}\overline{e_\alpha} + \omega_r e_\beta \overline{e_\alpha} - l_2(\widehat{e_\alpha} - e_\alpha)\overline{e_\alpha} + \widehat{\omega_r}\widehat{e_\alpha}\overline{e_\beta} - \omega_r e_\alpha \overline{e_\beta} - l_2(\widehat{e_\beta} - e_\beta)\overline{e_\beta} + \dot{\overline{\omega_r}}\ \overline{\omega_r} \qquad \text{(III.50)}$$

and after some calculus equation (III.50) become:

$$\dot{V} = -l_2\left(\overline{e_\alpha}^2 + \overline{e_\beta}^2\right)\overline{e_\alpha} \qquad \text{(III.51)}$$

From this are obtained that $\overline{e_\alpha}$and $\overline{e_\beta}$ tend to 0 and $\overline{e_\alpha}$ and $\overline{e_\beta}$ converge respectively to e_α and e_β

By rewriting the equation **(III.46), (III.47), (III.48)**in the form:

$$\dot{\overline{e_\alpha}} = -\overline{\omega_r}\widehat{e_\beta} - \omega_r\ \overline{e_\beta} - l_2\overline{e_\alpha} \qquad \text{(III.52)}$$

$$\dot{\overline{e_\beta}} = \overline{\omega_r}\widehat{e_\alpha} + \omega_r\ \overline{e_\alpha} - l_2\overline{e_\beta} \qquad \text{(III.53)}$$

$$\dot{\overline{\omega_r}} = \overline{e_\alpha}\ \widehat{e_\beta} - \overline{e_\beta}\ \widehat{e_\alpha} \qquad \text{(III.54)}$$

and considering $\overline{e_\alpha}$=0 and $\overline{e_\beta}$=0 , it results that:

$$-\overline{\omega_r}\widehat{e_\beta} = 0 \qquad \text{(III.55)}$$

$$-\overline{\omega_r}\widehat{e_\alpha} = 0 \qquad \text{(III.56)}$$

The equations **(III.55), (III.56),** imply that $\overline{\omega_r}$ tends to 0 and $\widehat{\omega_r}$ converge to ω_r

The block diagram of the back-EMF sliding mode observer described above is implemented in Matlab/Simulink like in Fig III.10. Equations (III.31), (III.32), to (III.37), (III.38), are implemented on the upper side of the intermediate filtering block in Fig III.10 and equations (III.39), (III.40) to (III.46)**,** (III.47), (III.48), on the down side of the intermediate filtering block.

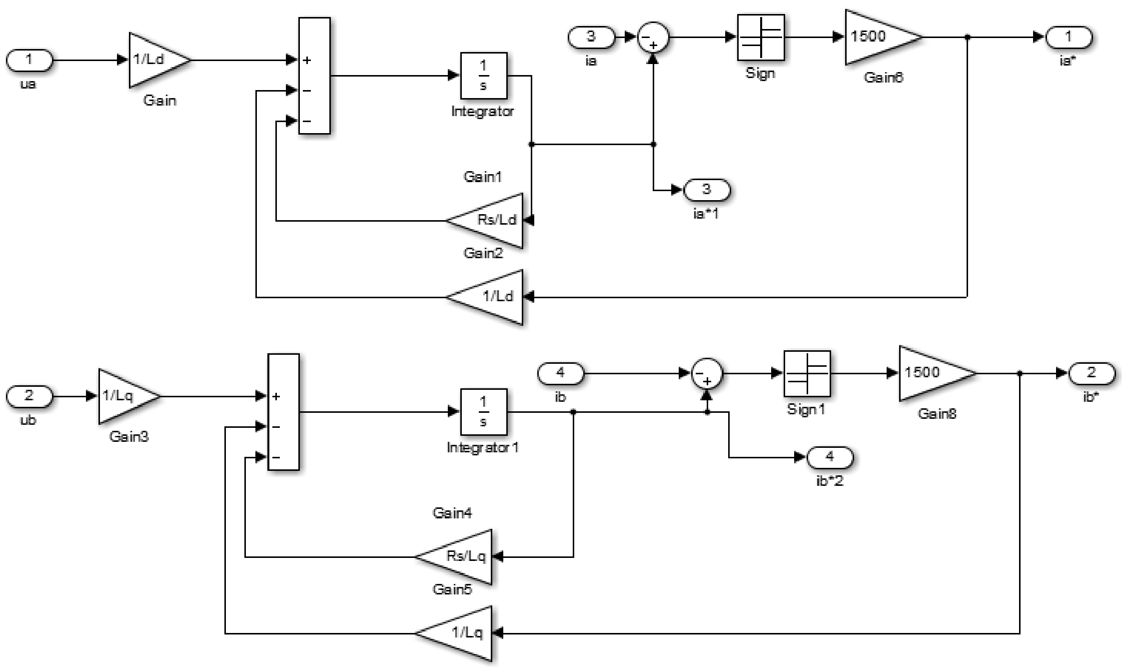

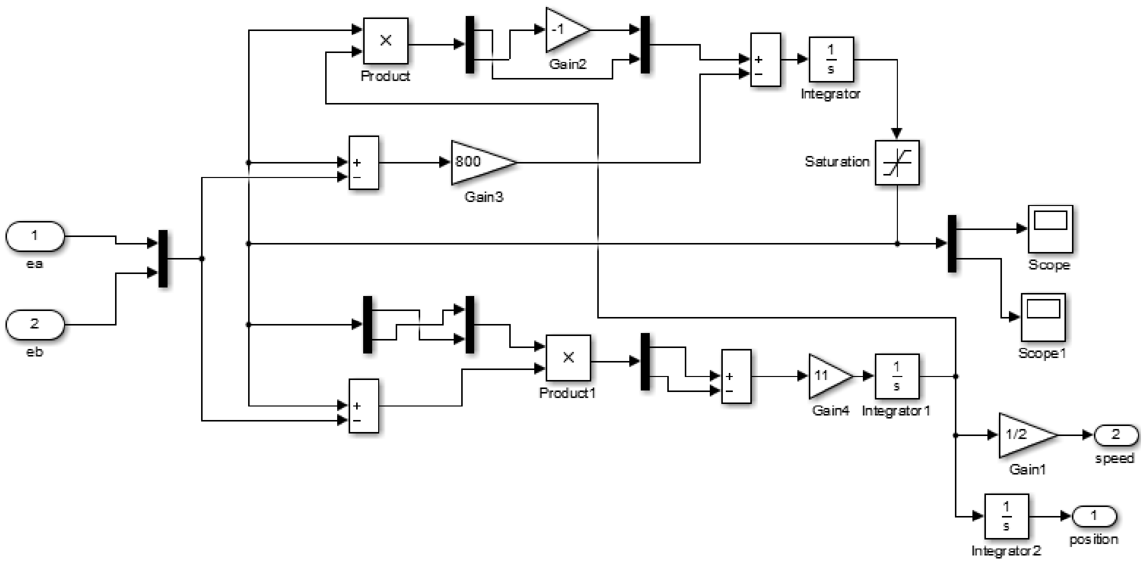

Fig III.10 the SMO observer for sensorless FOC control of PM synchronous motor

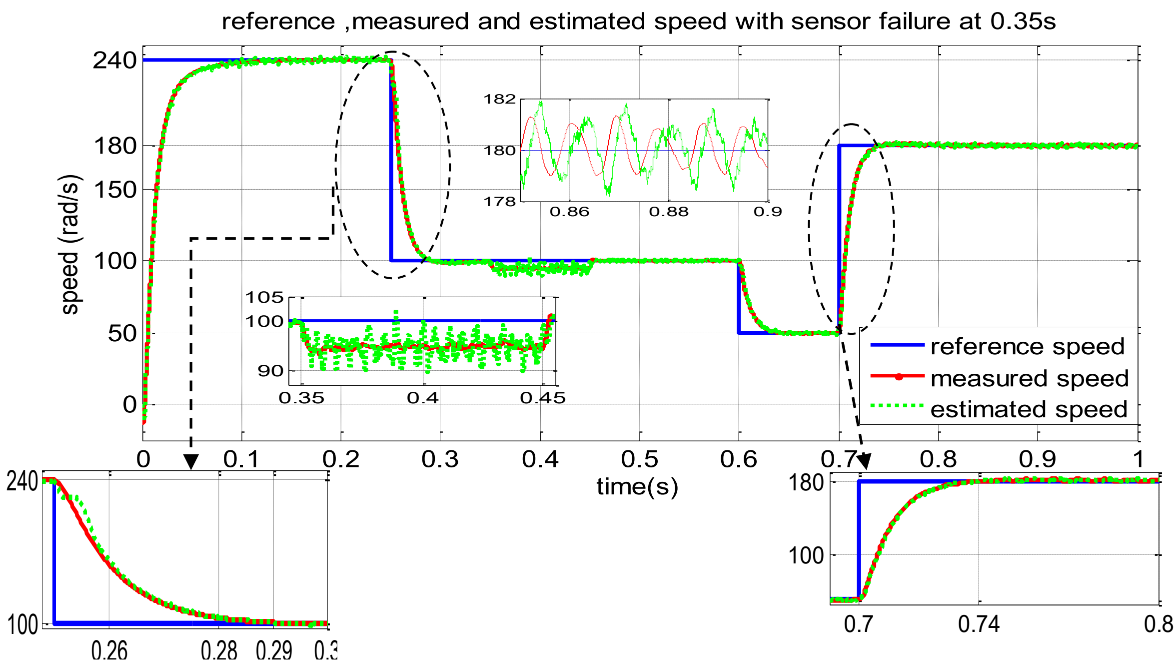

Fig III.11: speed response of SMO based PMSM drive with different values

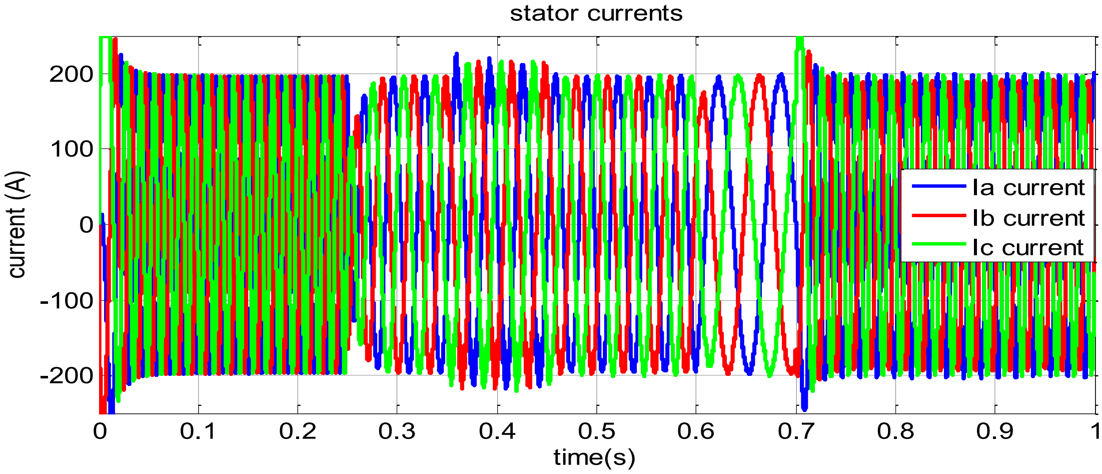

Fig III.12 currents response of SMO based PMSM drive

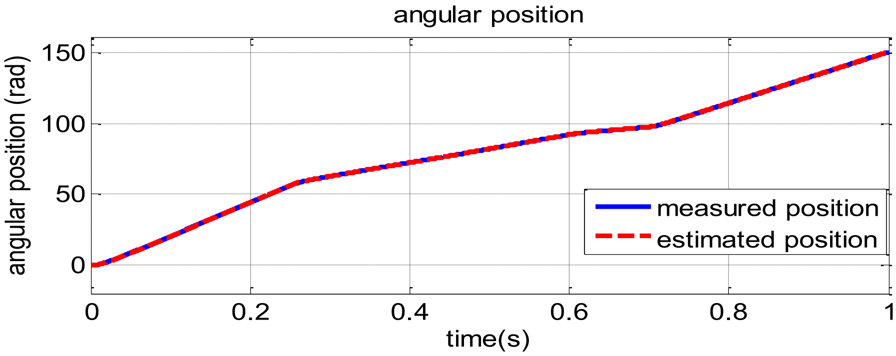

Fig III.13 compared between measured and estimated position

In Fig III.11 is presented the time evolution simulation of sensorless control of PMSM motors with back-EMF sliding mode observer for a speed reference sequence the speed is increased [0 to 240rad/s]; decreased [240 to 100rad/s], reduced [100 to 50rad/s] and rises [50 to 180rad/s].

The simulation results are shown in Fig III.11. According to the simulation results obtained, we can see that to the time to reach steady state in both modes is same 0.04s, the use of sliding mode control method is also effective with some fluctuation 2% , It can be observed that the estimated velocity and position show high accuracy and good tracking ability

The rotor position by encoder and the estimated value of the rotor position. As can be seen at the beginning the control output reached the sliding surface, it is estimated that the larger deviation angle. With the steady-state operation, the sliding surface is to reach the estimated value. Estimates and the actual value of the sample encode are in good agreement, which can be used to vector control measurement of rotor position.

In Fig III.11, when the green curve tracks the red curve, there are obvious burr and chatter in the green curve. This shows that traditional SMO has a large high frequency chattering phenomenon in the high-speed operation of the system due to the traditional SMO applying the sign function as the control function of the system. Because of the sudden change of the sign function at the zero point, the system appears as high-frequency chattering. Note that the chattering exists in the velocity estimation in both cases

In Fig III.13, the above represent the actual position angle and estimated position angle of rotor, and the below is estimated speed simulation curve obtained through differential of estimated position angle. The accuracy of rotor position angle plays a decisive role for the quality of estimated speed waveform, for the speed is obtained from estimated rotor position angle. From the figure one can see that there exists fluctuation of estimated rotor position angle, and so estimated speed is fluctuant, not stable when it is steady-state. So it is very important for final estimation of speed how to get good linear rotor position angle from estimated EMF waveform or how to get more accurate EMF.

III.7 Sensorless Control of PMSM Drive Based on Extended Kalman Filter:

The extended Kalman filter algorithm is an optimal recursive estimation algorithm for nonlinear systems. It processes all available measurements regardless of their precision, to provide a quick and accurate estimate of the variables of interest, and also achieves a rapid convergence. This is done using the following factors: the knowledge of the system dynamics, statistical description of the system errors (noises, disturbances, *etc.*), and information about the initial conditions of the variables

This method can be used to estimate the rotor position and speed. Motor state variables are estimated by means of measurements of stator line voltages and currents, and applying EKF next. During this process, voltage and current measuring signals are not filtered, and rotor position and speed can be estimated with sufficient accuracy in both steady state and dynamic operations. Unlike the deterministic base of other studies, the model uncertainties and nonlinearities in motors are well suited to the stochastic nature of EKFs,as well as the persistency of excitation due to the system and measurement noises. This is the reason why the EKF has found wide application in speed-sensorless control, in spite of its computational complexity. However, with the developments in high performance processor technology, the computational burden and speed of EKF has ceased to be a problem

The block diagram of the system for speed and rotor position estimation of a PMSM motor is shown in Figure 18. The system can be functionally divided in two basic parts: the speed control system and the estimation system. The first one consists of a power circuit (DC supply, inverter and motor) and control circuits, which perform three functions: current commutation, current control and speed control. The measured speed ($\omega_r k$) and phase currents (ik) as well as the estimated rotor position ($\hat{\theta} k/k$) are used as feedback signals. The main blocks of the estimation algorithm are the EKF and the block for calculating average motor line voltages during sampling time

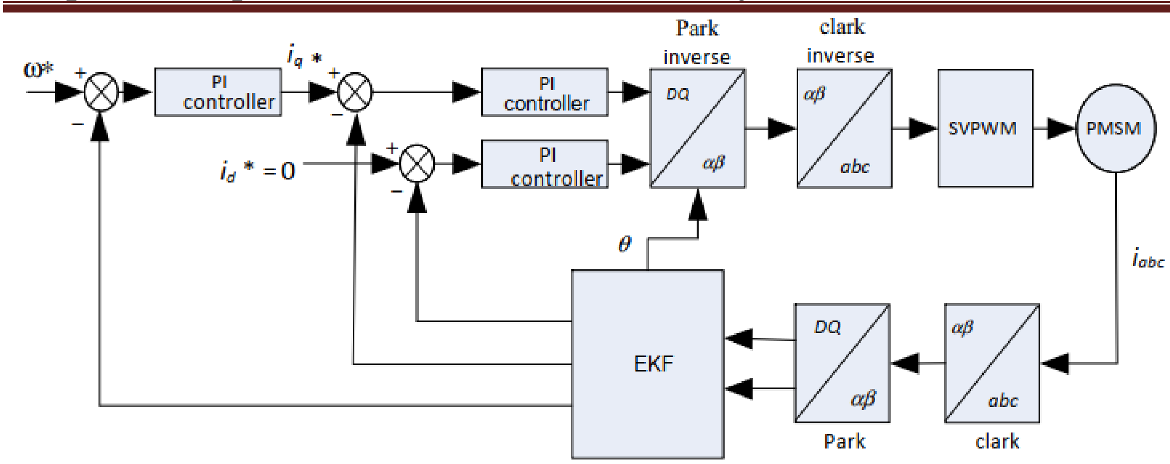

Fig III.14. System configuration for speed and rotor position estimation of a PMSM

III.7.1 Brief EKF Theory:

The EKF represents two-step recursive algorithm. The first step of EKF is calculation of the machine model (prediction step) - this step is in detail discussed in the next paragraph [27]. In the second step, the result of the machine model calculation is corrected using the weighted difference between the calculated and measured quantities (in this case, the stator currents). In consequence of this feedback correction derived from the error between the real (measured) and calculated (predicted) stator currents, the EKF (and generally the state observers) provides quite exact estimation of the non-measurable machine parameters (e.g. rotor speed and position) in the wide operating region. The second step of EKF is often called "correction step" or sometimes called "filtering

The EKF algorithm is summarized in the **Fig III.15**:

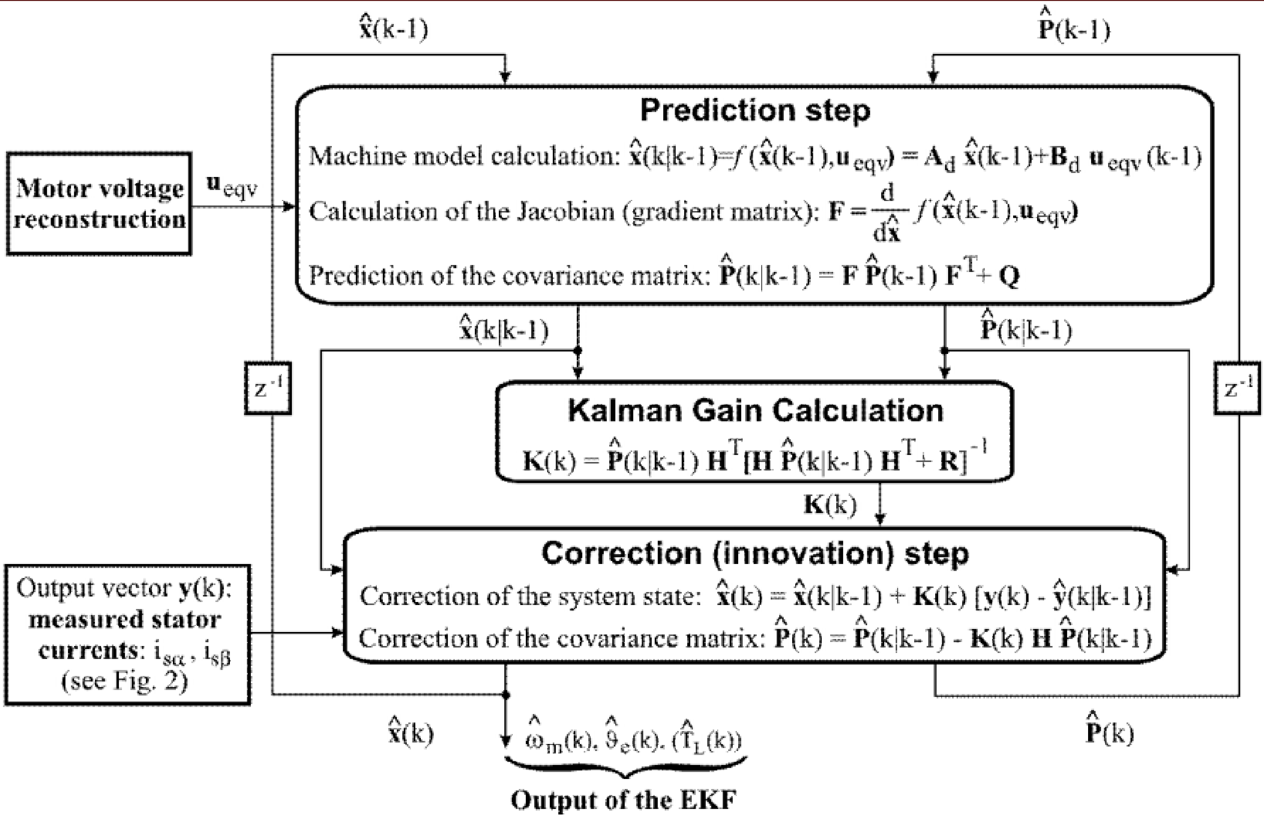

Fig III.15: Algorithm of the Extended Kalman Filter

X: the real system state,

$\hat{X}$: The system state estimated by EKF,

$\hat{X}$(K↓K-1): the result of the machine model calculation prediction of the system state in time t = k. T (index (k-1) highlights that the machine model is calculated from the previous system state),

$\hat{X}$(K↓K) =$\hat{X}(K)$: the estimation of the system state in the time t = k. T,

T: sampling period,

y: the system output vector,

H: the system output matrix,

$\hat{P}$, Q, R: the covariance matrices

III.7.2 Selection of the Machine Model for Prediction Step of EKF:

The machine model employed in the first step of EKF can be designed in either stationary or revolving reference frame. The equations of the machine model in revolving reference frame (d, q) are simpler than the equations in the stationary reference frame (α, β), however, the measured stator currents required for the proper function of the EKF correction term must be transformed from the natural stationary frame into the revolving frame. This transformation is performed via the system output matrix H. The matrix H includes, in case of the revolving reference frame model, the goniometric functions required for Park's transform. Thus, the terms of the matrix H are dependent on the system state and, therefore, the matrix H is time-variant.

In consequence of the above briefly described drawbacks (both the theoretical and computational) of the machine model in the revolving reference frame, the machine model in the stationary reference frame is preferred. Generally, two basic machine models in the stationary frame can be used:

$$\hat{X}(K|K\text{-}1) = \begin{bmatrix} \dot{I_d} \\ I_q \\ \omega_r \\ \theta \end{bmatrix} = \begin{bmatrix} \frac{R_s}{L_d} & \frac{L_q}{L_d}\,\omega_r & 0 & 0 \\ \frac{L_d}{L_q}\,\omega_r & \frac{R_s}{L_q} & -\frac{\varphi_f}{L_q} & 0 \\ 0 & 0 & 1 & 0 \\ 0 & 0 & 0 & 1 \end{bmatrix} \begin{bmatrix} I_d \\ I_q \\ \omega_r \\ \theta \end{bmatrix} + \begin{bmatrix} \frac{1}{L_d} & 0 \\ 0 & \frac{1}{L_q} \\ 0 & 0 \\ 0 & 0 \end{bmatrix} \begin{bmatrix} V_d \\ V_q \end{bmatrix} \qquad \text{(III.57)}$$

$$f(K\text{-}1) = \begin{Bmatrix} I_d(k) + \left(\frac{V_d}{L_d} - \frac{R_s}{L_d} I_d + \omega_r \frac{L_q}{L_d} I_q\right) * T_s \\ I_q(k) + \left(\frac{V_q}{L_q} - \frac{R_s}{L_q} I_q - \omega_r \frac{L_d}{L_q} I_d - \frac{\varphi_f}{L_q}\,\omega_r\right) * T_s \\ \omega_r(k) \\ \theta(k) + \omega_r * T_s \end{Bmatrix} \qquad \text{(III.58)}$$

Define matrix F:

$$F = \frac{df}{dx} = \begin{bmatrix} 1 - \frac{T_s * R_s}{L_d} & \frac{T_s * L_q}{L_d}\,\omega_r & \frac{T_s * L_q}{L_d} I_q & 0 \\ -\frac{T_s * L_d}{L_q}\,\omega_r & 1 - \frac{T_s * R_s}{L_d} & T_s * \left(-\frac{L_d}{L_q} I_d - \frac{\varphi_f}{L_q}\right) & 0 \\ 0 & 0 & 1 & 0 \\ 0 & 0 & T_s & 1 \end{bmatrix} \qquad \text{(III.59)}$$

The following recommendations can help in the filter tuning:

* Initial values of the terms of the system covariance matrix P (0) can often be selected equal zero. If the initial values must be tuned (in order to improve the filter performance at the filter start up), only the diagonal terms are usually taken into account. The initial values of the matrix P do not affect the transient durations as well as the filter steady-state behaviour.

* In consequence of lacking statistical information about the drive system and especially in order to simplify the tuning process, the covariance matrices Q and R are considered to be diagonal and, moreover, invariant. It means that all the terms out of the main diagonal are considered to be zero.

* The EKF works with the square errors. Exactly, the covariance matrices represent mean square error of corresponding quantities. This knowledge helps to define the initial values of the tuned covariance matrices (Q, R). Of course, the final values have to be found by the iterative simulation

process.

* The filter convergence and stability is much more sensitive to the terms of the covariance matrix Q than R.
* Increasing values of the terms of the matrix Q correspond to the less exact machine model. In such case, the measured values are more accented via Kalman gain K.
* Increasing values of the terms of the matrix R correspond to the less exact measurement results. In such case, the machine model is more accented.
* Big differences between the terms of the matrices Q and R can lead to the filter divergence.

III.7.3 Designed Sensorless Control System Configuration of EKF

The Fig III.16 shows the investigated control system that will be used for description of properties of different EKF structures and for presentation of developed simulation technique for fixed-point implementation. The control system employs the vector control together with pulse width modulation (PWM). Selected type of the vector control with two current controllers (separate control of the flux and torque current component) is eligible for PMSM drives. The dynamic properties of the control structure are improved by the decoupling. The most important part of the decoupling circuit is the calculation of the back EMF that is added to the torque (quadrature) component as is evident from Fig III.16. The rotor speed, which is required for the speed controller, and the rotor position, required for the transform of the measured stator currents from the stationary frame into the revolving frame and for the transform of required voltage vector from the revolving frame into the stationary frame, are estimated using EKF as has been described in the previous paragraph

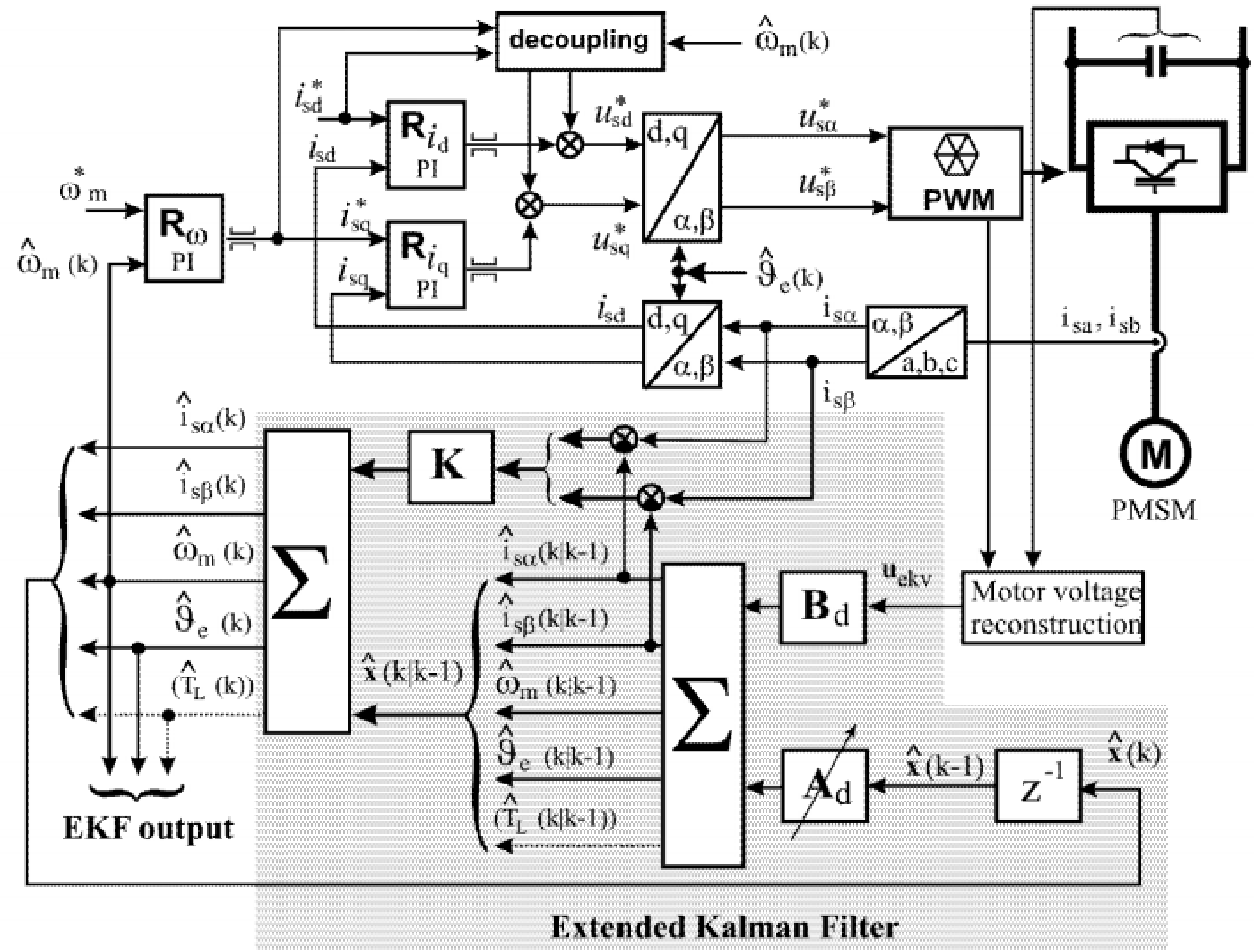

Fig III.16: Investigated sensorless control system to drive with PMSM

The mechanical equation respects both the drive mechanical parameters (inertia, friction) and the load torque, which is considered as the term of the system state vector and, therefore, is also estimated (joint estimation of the system state variables and parameters):

The approach (1) (equation (III.57)) without Torque equation is more frequently applied. There are generally three reasons, why this approach is preferred:

* It is not required to know the mechanical parameters (inertia, friction; load torque is also avoided and is considered as perturbance).
* In this case, only 4 terms of covariance matrices Q and R must be tuned. Thus, the filter tuning is easier in this case. (In the case (2), the 5 terms must be tuned).
* The order of the matrices is reduced and, therefore, the computation is faster and the memory requirements are reduced too.

SIMULATION AND ANALYSIS:

Fig III.17 displays the result simulation of the control system employing EKF. The simulation has been performed under the same conditions as previous observers, sampling period of the EKF and the control system 0.00001. From the Fig III.17 is clear that the EKF is properly tuned. The filter is stable also during speed changing. In spite of the rotor speed and position, we observe don't occur fluctuation, It presents that the estimated rotor flux position can follows the actual rotor flux position with some delay time. The delay time at 0.25s, in the sensor speed control we continue the simulation work in sensorless control architecture (0.45s). The estimated rotor position will be feed-backed to the current loop for vector control and to the speed loop for speed control. The simulation work of the step speed response is more accurate and without delay

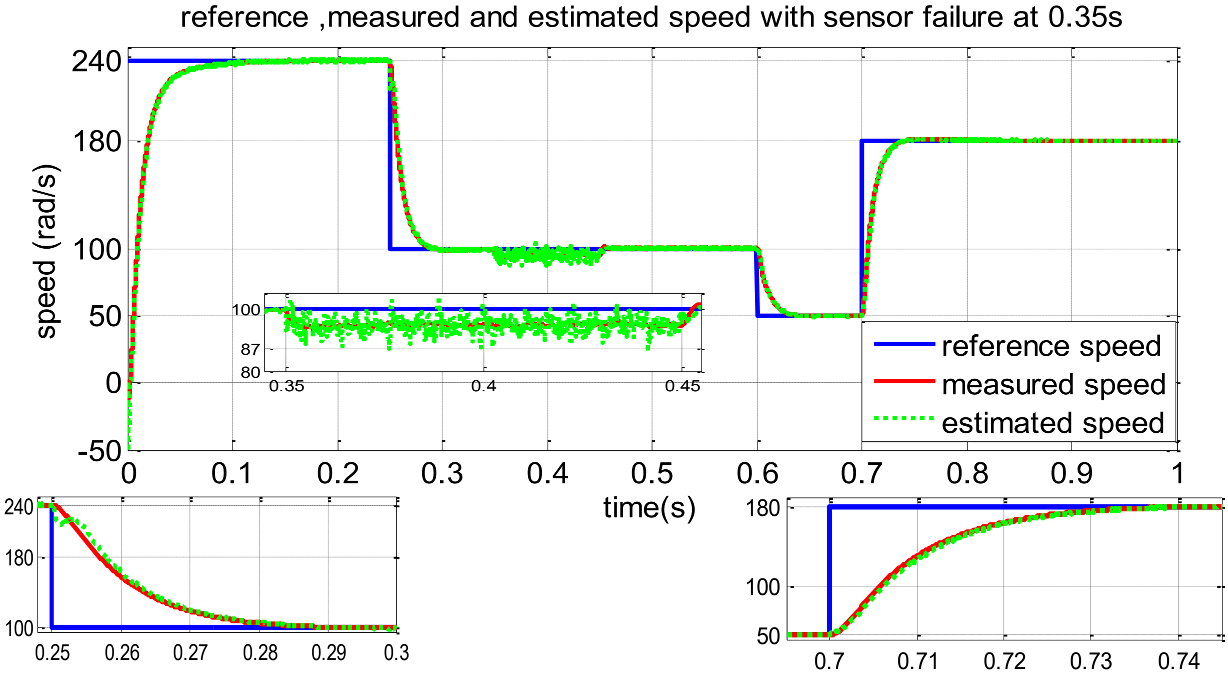

Fig III.17: speed response of EKF based PMSM drive with different values

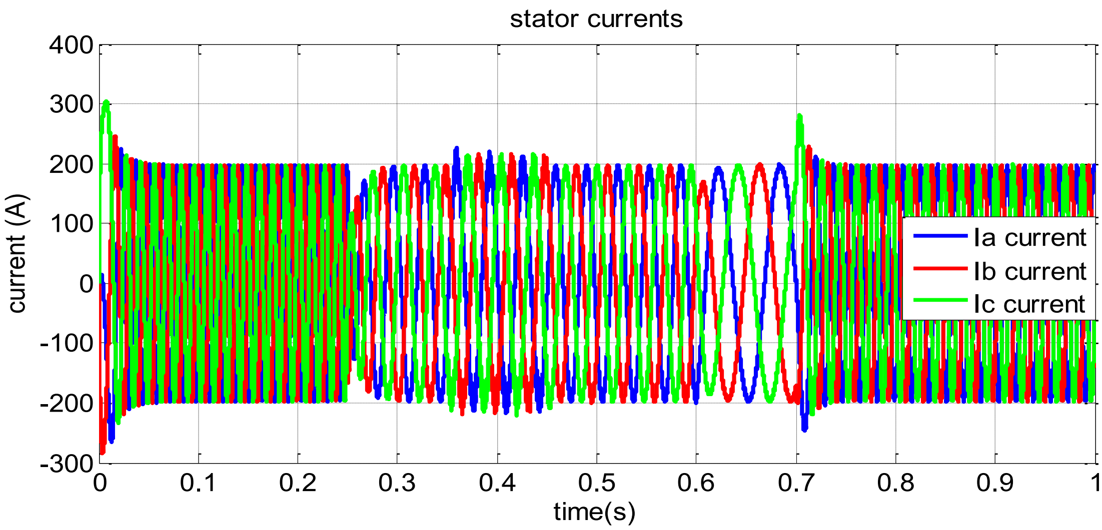

Fig III.18 currents response of EKF based PMSM drive

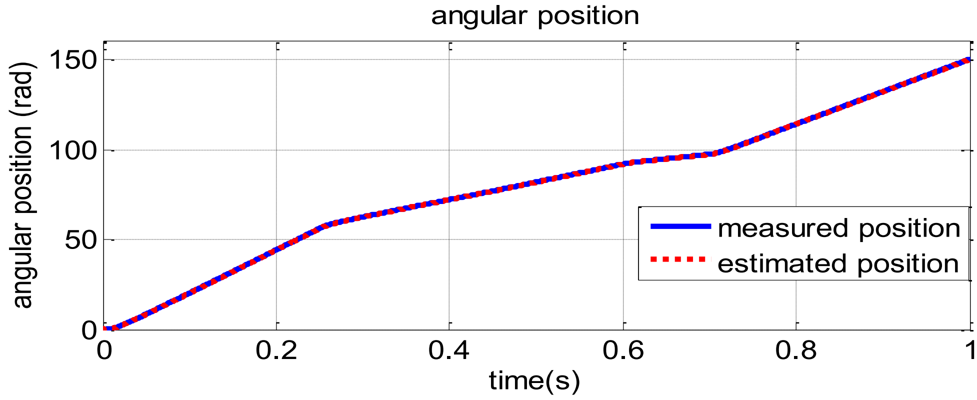

Fig III.19 compared between measured and estimated position

III.8 A Comparative study between MRAS, SMO .and EKF :

Computer simulation is used to verify the estimation performance of the PMSM vector control observer. Matlab/Simulink is the simulation platform. The Simulink model of the PMSM vector control system has been constructed including the proposed sliding mode observer, MRAS and the EKF observer. And the three algorithm simulations are conducted in the same condition so that the proposed algorithm performance can be evaluated objectively

We observe that the speed of each one well tracking the reference speed, but the results show that the MRAC response is more rapid compared to the others, and the speed is stable. When failure happens, we notice slight fluctuations for MRAC, then SMO, and for EKF, Its fluctuations are quite large

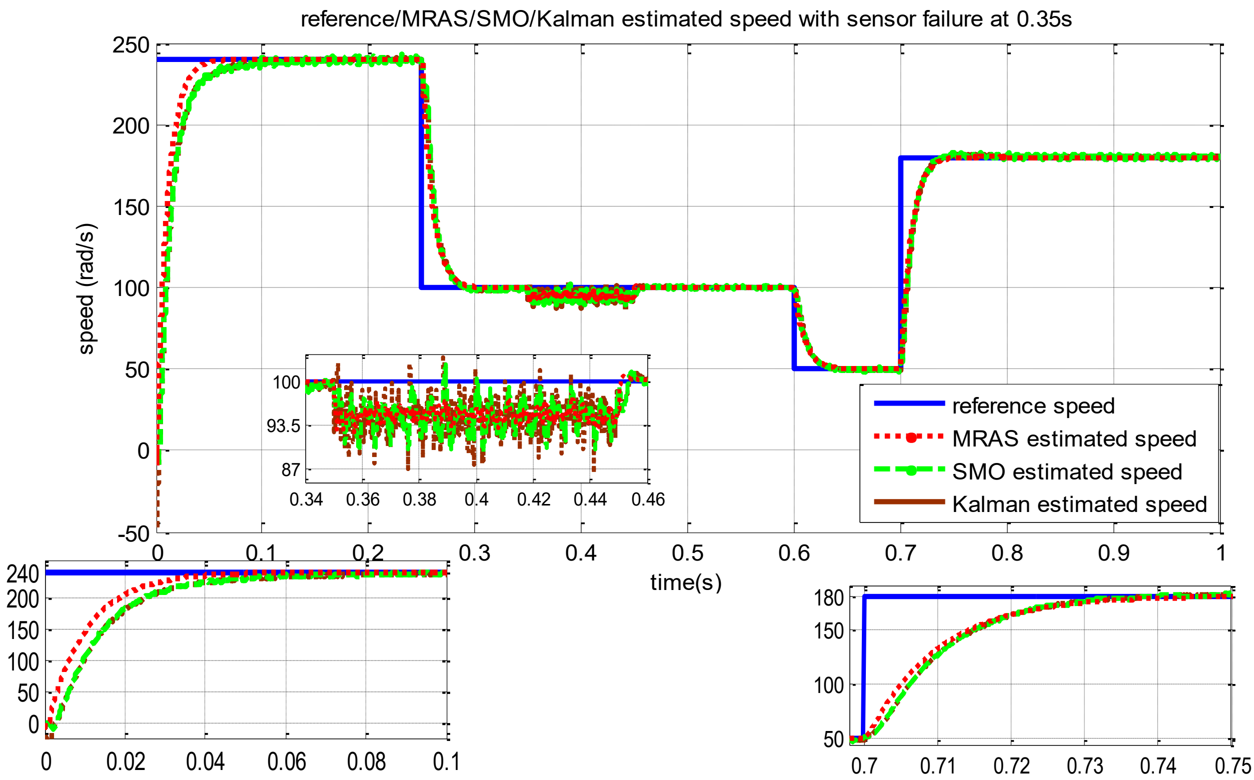

Fig III.20 Comparative between MRAS , SMO .and EKF speed esyimated

	MRAS		SMO		EKF	
steady state time	sensor	sensorless	sensor	sensorless	sensor	sensorless
	0.045	0.04	0.06	0.038	0.06	0.04
Fluctuation ratio during sensor failure $\frac{\widehat{\omega_{max}} - \widehat{\omega_{min}}}{\widehat{\omega_{average}}}$	5%		11.9%		14.12%	

Table III.1: Comparative between MRAS , SMO .and EKF

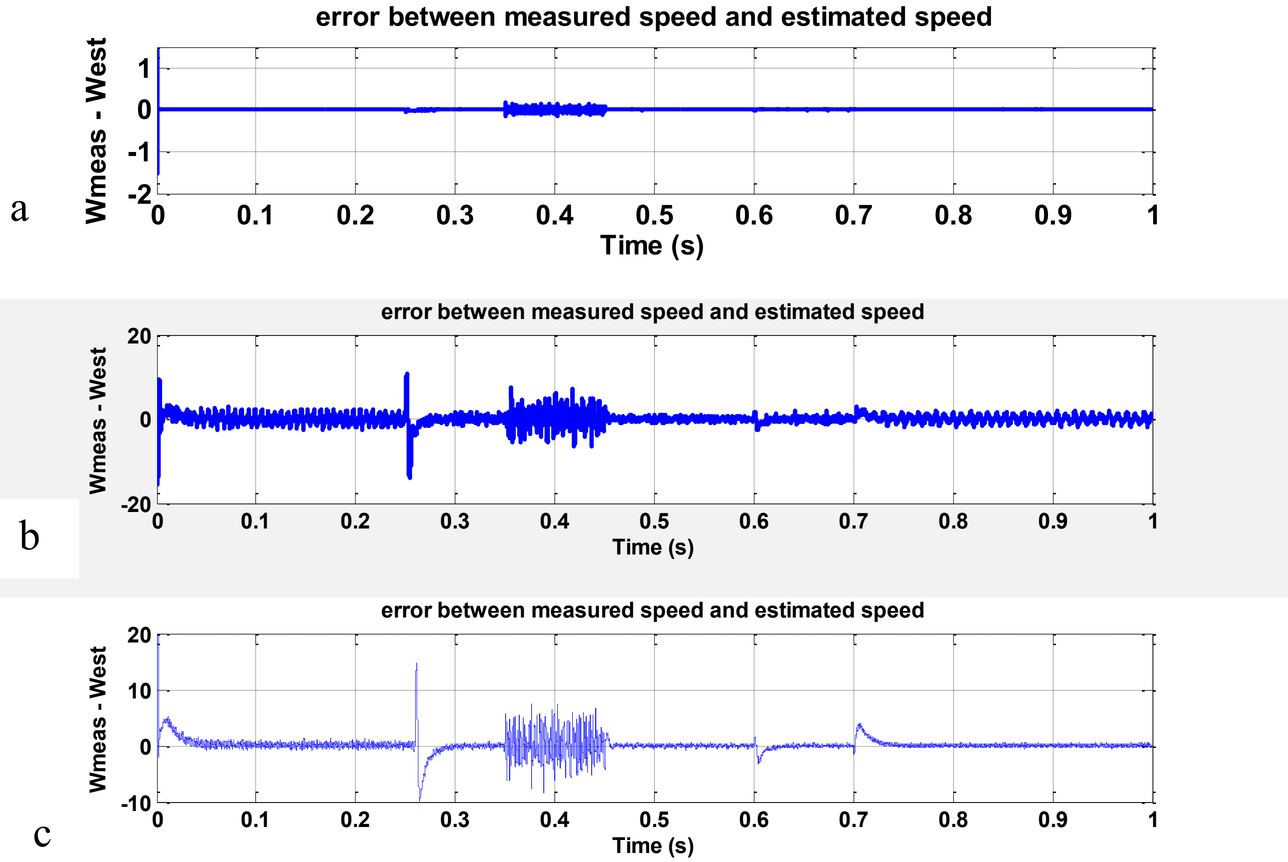

Fig III.21 error between measured speed and estimated speed a)MRAS b)SMO c)EKF

III.9 PARAMETER PERTURBATION ROBUSTNESS ANALYSIS OF VECTOR FIELD-ORIENTED CONTROL:

Robustness is an important criterion to evaluate speed controller performance. In the process of PMSM operation, motor parameters are always changing. If speed response still keeps good dynamics against parameter variations, the speed controller will has well robustness. Under the case that inertia and phase resistance all occur variation, this part simulates the response speed of the sensorless filed oriented control of PMSM.

For the purpose of inspection of the robustness of the observer of its value nominal load

Tr =240N.m, change the parameters of the motor in the observer to a half of the resistance and inductance and inertia moment of the actual motor. and again chanded the resistance and inductance and inertia moment to a double of the actual motor values (Fig III.22,23,24) shows comparison of the actually measured value to the observing value of the revolution under the conditions changed. According to the figure, the estimated revolution can still follow up the actual revolution well and the error of the revolution is smaller. Both can still be kept identical.the zoom Figures shows the wave form of the actual rotor speed on sensor mode driving and sensorless mode driving. Therefore, the observer can still estimate the rotor position well.

Robustness test of MRAS filter estimated speed:

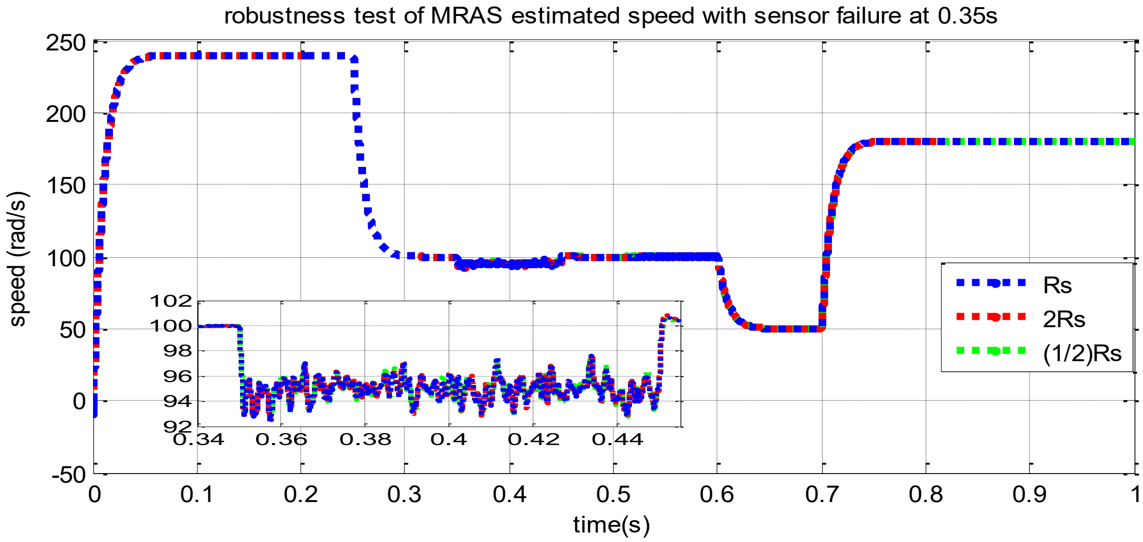

a

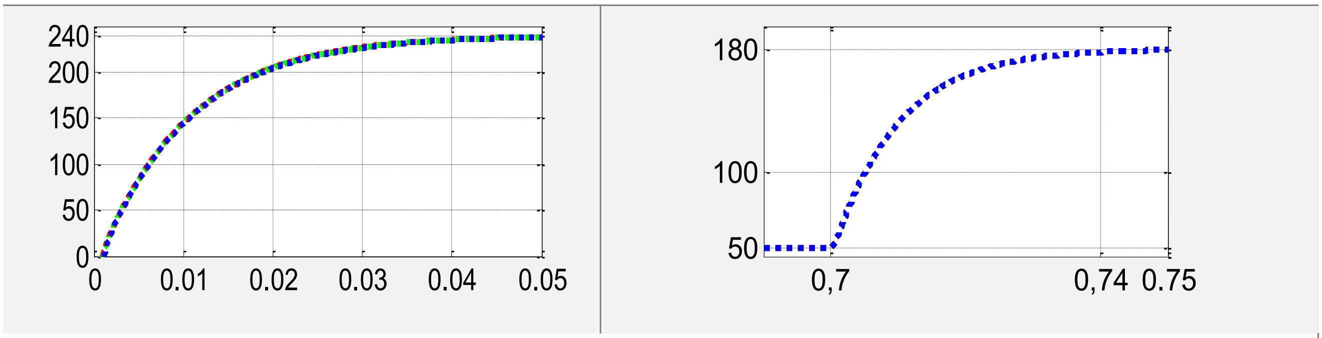

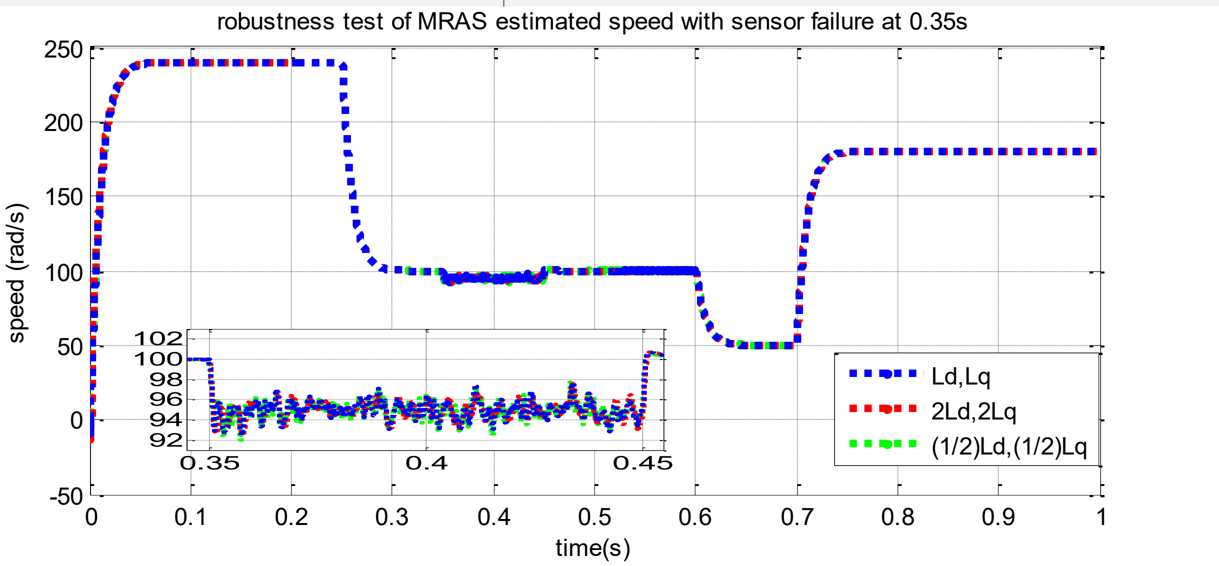

b

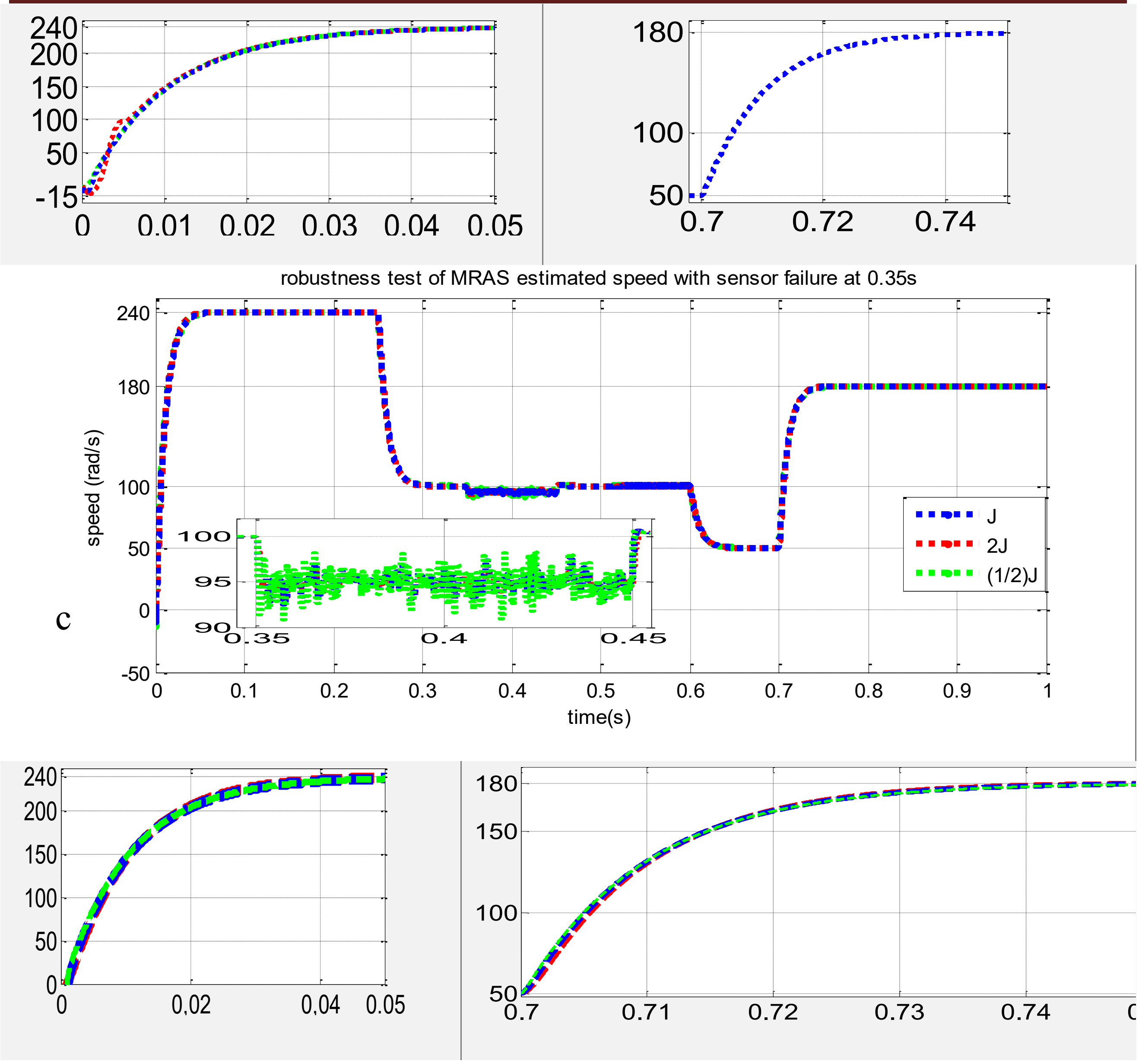

Fig III.22 shows the simulation under the case that (a) Stator resistance changes. (b) Stator inductance changes. (c) moment inertia changes

Robustness test of SMO filter estimated speed:

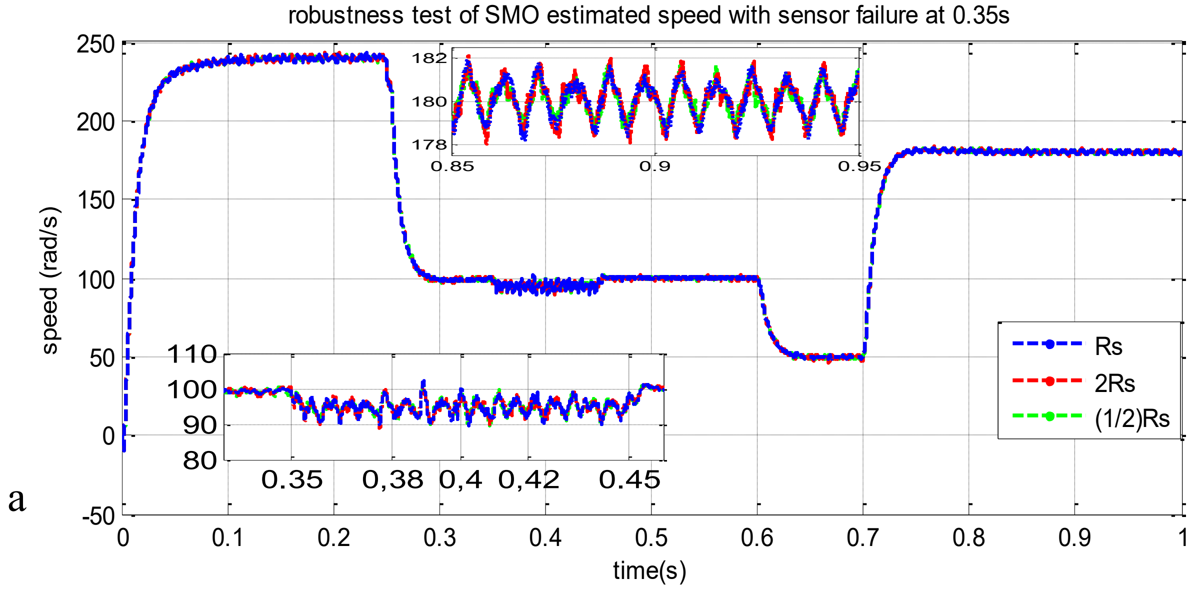

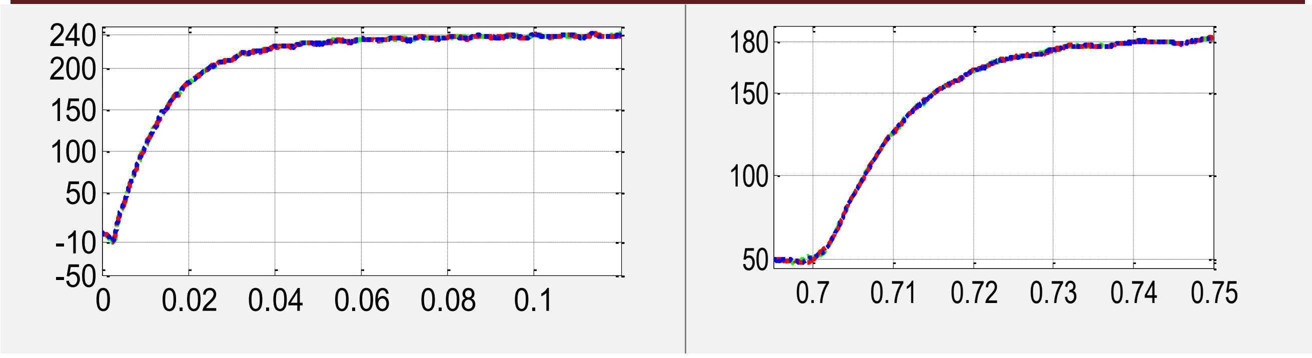
240
200
150
100
50
-10
-50
0 0.02 0.04 0.06 0.08 0.1
180
150
100
50
0.7 0.71 0.72 0.73 0.74 0.75

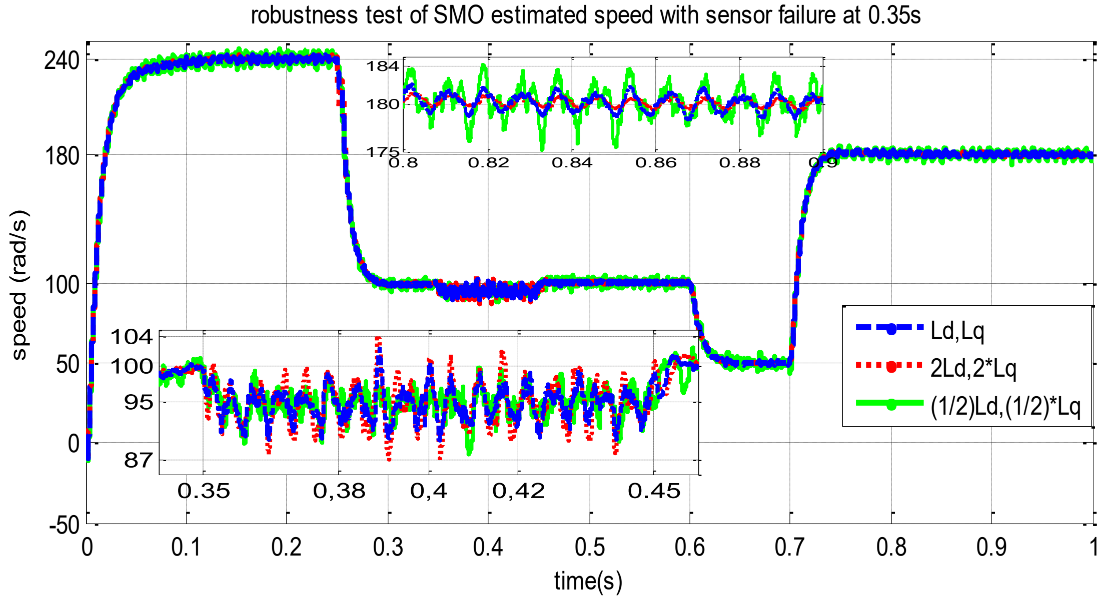
robustness test of SMO estimated speed with sensor failure at 0.35s
speed (rad/s)
time(s)
Ld,Lq
2Ld,2*Lq
(1/2)Ld,(1/2)*Lq
0 0.1 0.2 0.3 0.4 0.5 0.6 0.7 0.8 0.9 1
0.35 0,38 0,4 0,42 0.45
0.8 0.82 0.84 0.86 0.88 0.9

b

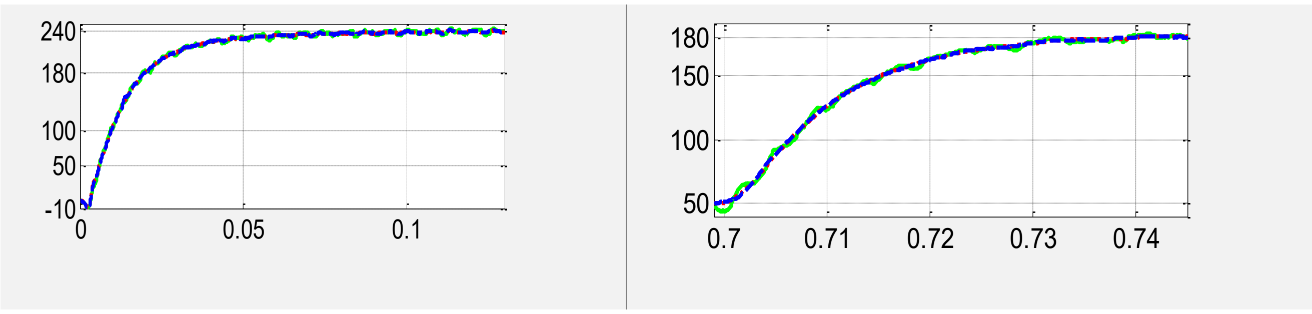
240
180
100
50
-10
0 0.05 0.1
180
150
100
50
0.7 0.71 0.72 0.73 0.74

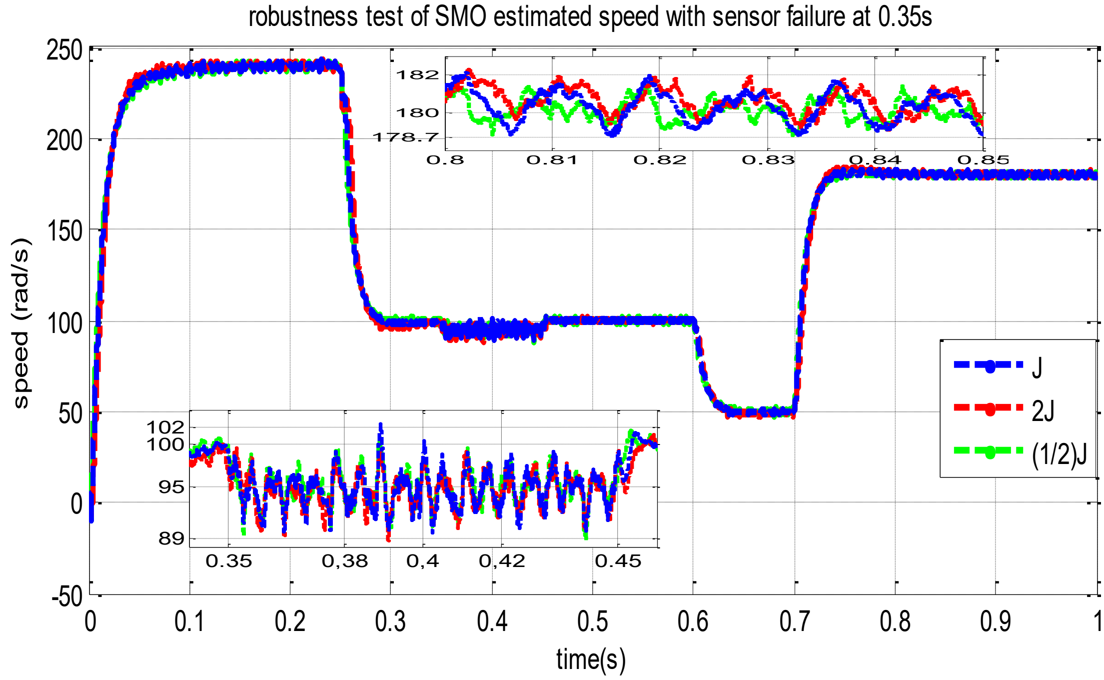
robustness test of SMO estimated speed with sensor failure at 0.35s
speed (rad/s)
time(s)
J
2J
(1/2)J
0 0.1 0.2 0.3 0.4 0.5 0.6 0.7 0.8 0.9 1
0.35 0,38 0,4 0,42 0.45
0.8 0.81 0.82 0.83 0.84 0.85

c

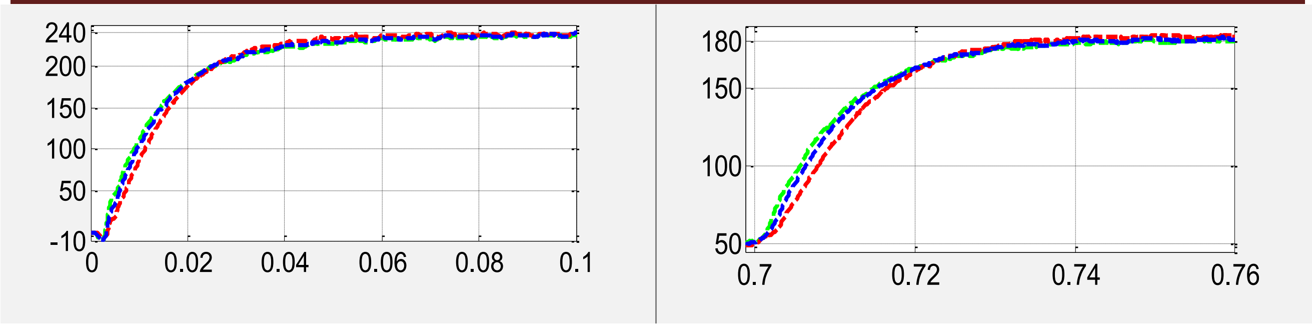

Fig III.23 shows the simulation under the case that (a) Stator resistance changes. (b) Stator inductance changes. (c) Moment inertia changes

Robustness test of EKF filter estimated speed:

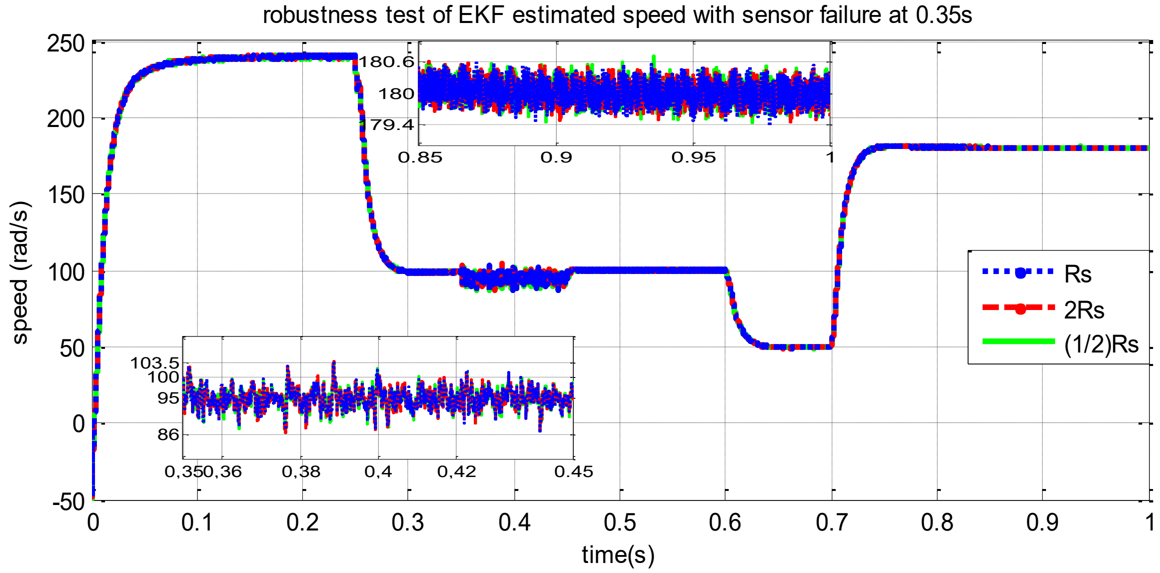

a

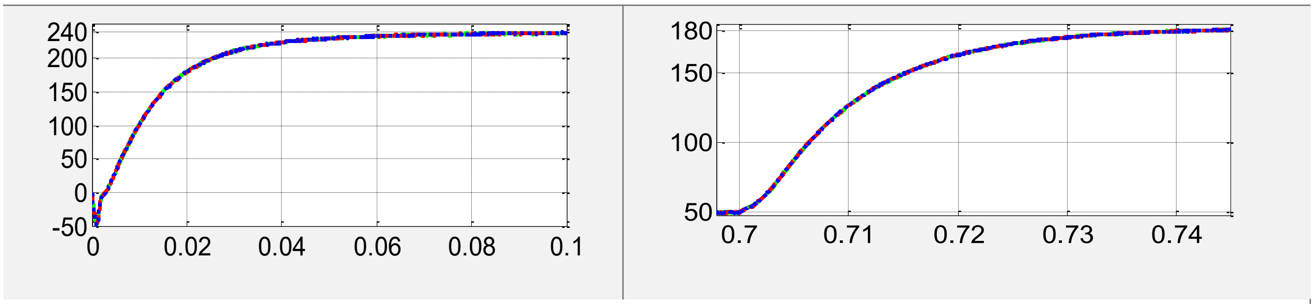

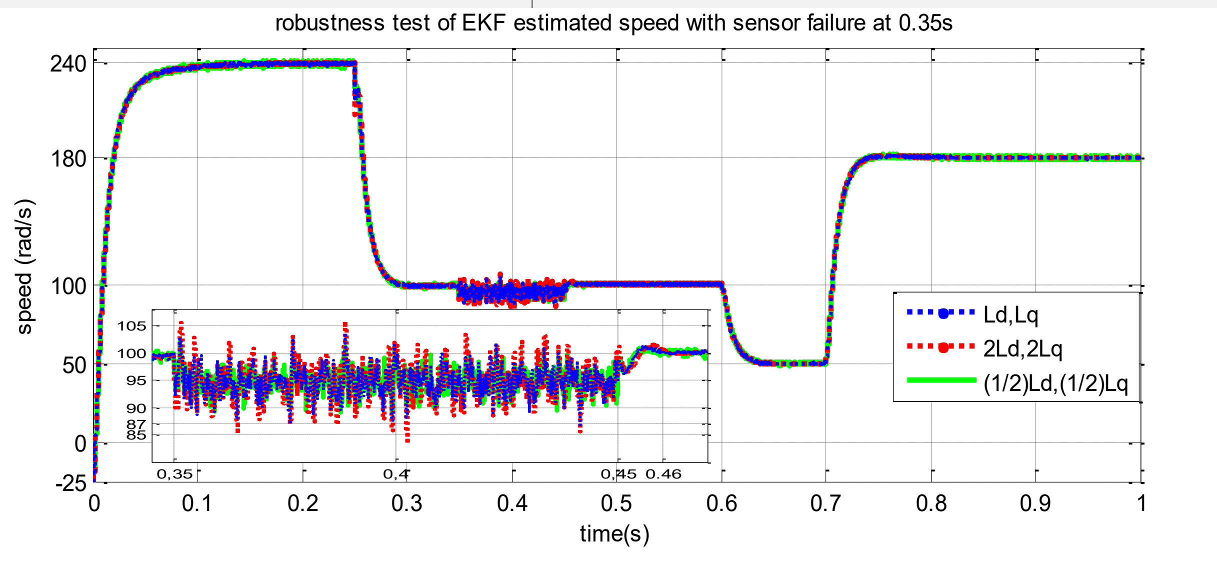

b

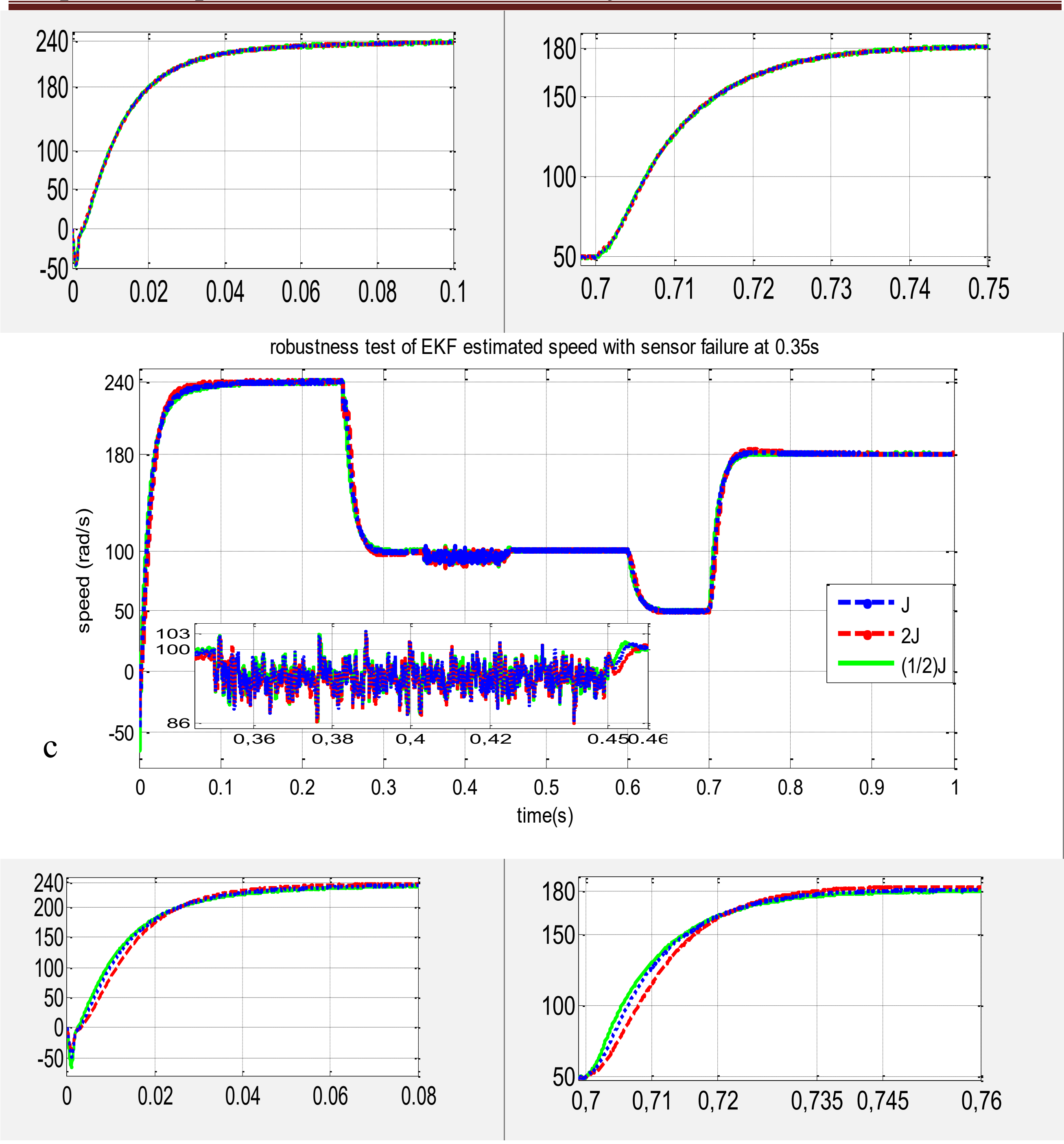

Fig III.24 shows the simulation under the case that (a) Stator resistance changes. (b) Stator inductance changes. (c) moment inertia changes

1) Stator resistance variation:

Fig III. (22 (a), 23 (a), 24 (a)) shows speed variation in healthy case until 0.35s, and with parametric variation. The estimated speed follow track rapidly its reference. Considering the resistance variation at around +100%, -50% show that an error of +100% of the stator resistance rating slightly affects the dynamic and static performance of the MRAS, EKF .SMO during the transient regime in case of speed variation, with an average error less than 1.1%, At 0.45s When the PMSM is fully loaded and sensorless driving at 180 rad/s (1719 rpm), the estimated and measured rotor speed are compared and with very close agreement. The vector controller, therefore, is working properly so that both track their reference value quite well. It should be noted that 1719 rpm is closer to rated speed 2290rpm

2) Stator inductance variation:

Considering the inductance variation at around +100%,-50% Fig III. (22 (b), 23 (b), 24 (b)) illustrate the low parametric sensitivity of the MRAS, EKF observers especially at start with the variation of the stator inductance. Indeed, this low sensitivity can result in a sufficient robustness of the observer compared to a possible saturation of the magnetic circuit. It's clear that the estimated parameters coincide with the reference values in both of transient and steady state, which is making the error converge to zero. Hence the SMO preserved its good performances and high robustness against the parametric variation

3) Moment inertia variation:

In **Fig** III. (22 (c), 23 (c), 24 (c)) a robustness test due to the variation of the moment of inertia is treated. So we reduced the moment of inertia by 50%J and raised it by 100% with application of the rated torque of 240N.m. we note that for the SMO and the EKF the speed response presents a delay in 2J and advancement in 0.5J with a rise time of 0.04s in the case of sensor and without sensor and also on the other hand for the Adaptive command these responses are robust to variations and the speed responds with the same rise time

III.10 Torque PERTURBATION ROBUSTNESS ANALYSIS OF VECTOR FIELD-ORIENTED CONTROL:

The previous experiment checked only the speed performance of the sensorless control system. Therefore, to check the robustness of the MRAS, SMO and EKF against disturbances while the motor is running, the disturbance rejection properties of the control system are checked. That is, while the motor is running at 2290 and 955 rpm, a sudden load is applied to the motor axis and the recovery characteristics are checked. These recovery characteristics are used to verify the robustness of the sensorless control system against unknown disturbances. **Fig** III.25 illustrates the experimental results of the disturbance responses for the observers MRAS SMO and the EKF

The torque step response are at (100rad/s) 955rpm, and in t=1s change to (240rad/s) 2290rpm are shown in **Fig** III.25. The PMSM output torque is changing from 100Nm (0.4s) to 240Nm (0.65s) at 955rpm, 100Nm (1.3s) and 240Nm (1.7s) at 1000rpm. The output torque of PMSM is so fast and the maximum time step is only about 0.13s, but also control the torque ripple is small.

Robustness test of MRAS filter estimated speed:

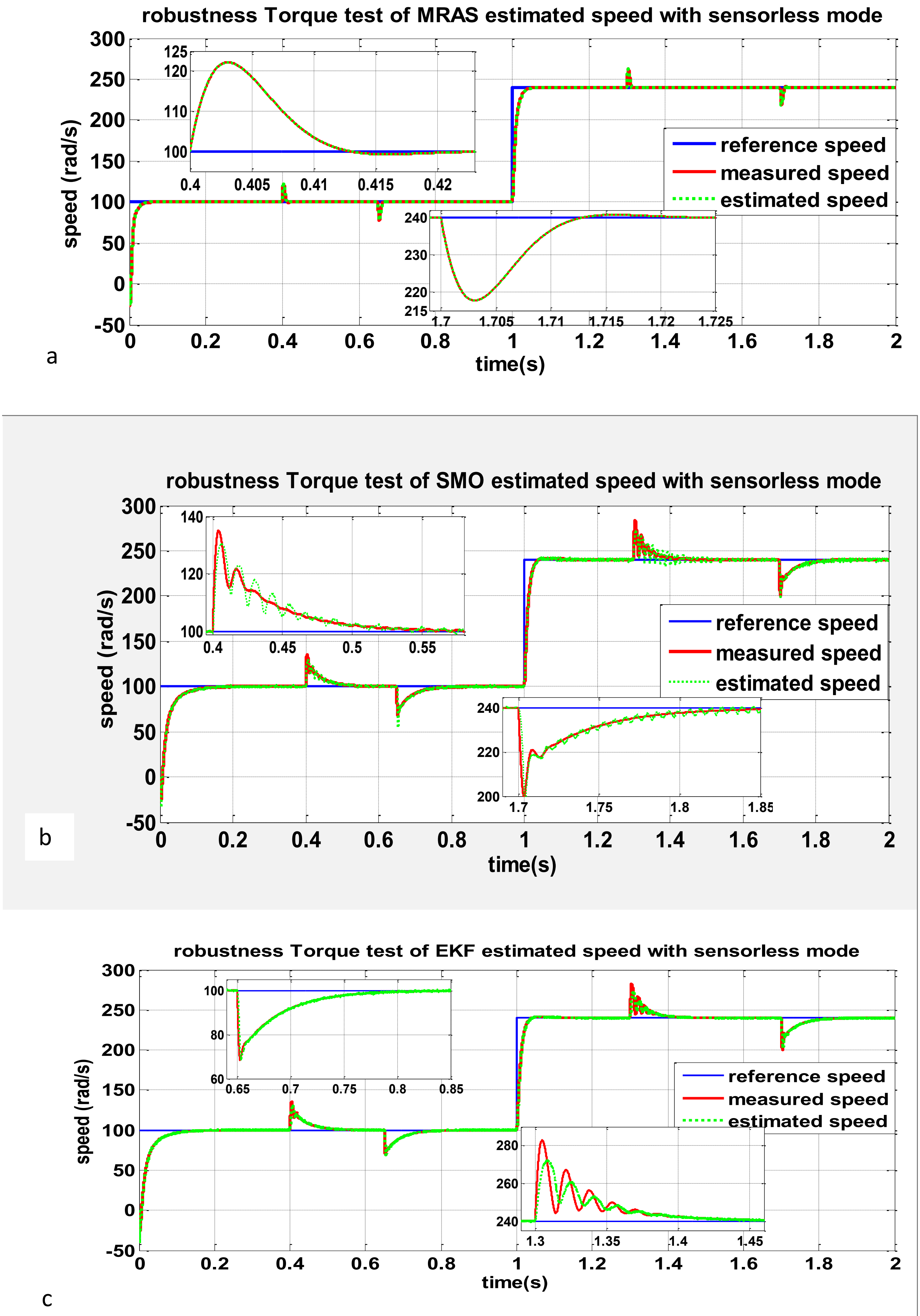

Fig III.25 shows the simulation under the Torque variation conditions (a) MRAS. (b) SMO. (c) EKF

	MRAS	SMO	EKF
Response time(s)	**0.04**	**0.04**	**0.04**
Disturbance rejection time (s)	**0.07**	**0.12**	**0.12**
Overshoot (%)	**9 to 22.5**	**16 to 45**	**13 to 30**

Table III.2 characteristics comparative between the three observers

Fig III.25 shows local enlargement of speed decrease when the load torque increases suddenly. After the increment of load torque, the speed can return to stable value a period of time later. It reflects that the control system based on VSS speed sensor-less has good robustness to load disturbance

load impacts with a speed reference creating a surpass of 42 rad/s are shown in Figure III.25. The test validates the good behavior of the estimated speed with smooth transients but when huge load variations are applied to the mechanical shaft suddenly maybe it will make it surpass undesirably.

III.11 Conclusion :

This study proposed a new speed sensorless control algorithms of a PMSM. The proposed control algorithms are based on the MRAS, sliding mode and extended Kalman filter. In this study, it is applied to the rotor speed estimation and position estimation, which are under the sensorless vector control of permanent magnet synchronous motor. The results are analyzed from two aspects: theory and simulation .The results show that:

1. MARS algorithm has a better adaptability for the start, the speed mutation and the variation speed scenario of permanent magnet synchronous motor;

2.MRAS-based sensorless vector control system designed in this study can accurately observe the rotational speed and rotor position of the permanent magnet synchronous motor, have better control performance, and realize the sensorless control of the permanent magnet synchronous motor successfully;

3. Permanent magnet synchronous motor sensorless control system based on the model reference adaptive algorithm can be a good substitute for photoelectric encoder**,** greatly improve systems reliability and reduce the costs, which is the ultimate goal of this study

The EKF has been preferred than others sensorless control method because it has quite a lot of advantages such as it can estimate the exact rotor speed and position without the information of initial position and mechanic parameters and also works fine at medium and high speed

Compared to the observers sensorless techniques, the proposed SMO method are simple, so the proposed technique is easy to be implemented in the real system.

However, since the sensorless control technique is designed based on machine model, its observability is lost at ultra-low speed and zero speed. Thus, ultra-low speed and zero speed sensorless operation still needs further investigation.

During operation of PMSM, its parameters are subject to variations that may be due to saturation or heating. For example, the stator resistance varies when the temperature of the winding increases following an application of the load. With the aim of verifying the performance of developed observer, it’s important to study the influence of parameter variation on the machine operation; we thus carried out tests of robustness in order to analyze the different transient and permanent performances, as well as that of the observer.

The robustness of an observer (or estimator) is its ability to ensure the stability of the system in the face of a type of disturbance. Several types of disturbances are possible, either at the level of the measured signals or at the level of the mathematical model considered. In this work, we We are particularly interested in the cheeked of the robustness with respect to the load variation and inaccuracy of the mathematical model of the process taking into account the variations parametric.

CHAPTERIV

ELECTRIC VEHICLE APPLICATION WITH A DRIVING CYCLE

IV.1 Introduction:

Vehicle driving cycles has been developed and utilized extensively in automotive industry to assess and evaluate a vehicle's capability. Initially served as the measurements of emissions and fuel consumptions, it is also used as testing platform for vehicle simulations and performance and reliability testing. As there arise needs to standardizing the procedure of each vehicle's testing, it is desirable to create a reproducible condition, by means of speed-time curve. A vehicle driving cycle allows a tested vehicle be placed at fixed schedule of vehicle's operations with its mechanical power requirements measured.

However, these give rise to many driving cycles. Different cycles are developed and practiced regionally that serves different purpose and measurements. Traditionally, the driving cycles relied on statistical data-collection from microtraps, which duration are long enough to be representative of actual driving behavior, but short enough to feasibly facilitate vehicle testing in laboratory. The driving activity are then further assessed and derived in its construction to form a driving cycle. Besides there also exists method of derivation of driving cycles based on random process theory, mainly the Markov theory. The data is further extrapolated with selected driving events into a more detailed and representative of a driving cycle

In this chapter, we discuss the application of control techniques on a vehicle. urban. We start with the definition of the specifications which contain information on the standardized driving cycle created by automobile designers and industry associations. the environment, and the dynamic model of the vehicle. The driving cycle (NEDC we will used) with the model dynamics of the vehicle generates us the load torque and the reference speed necessary for the mission. These two instructions will be used to test the control techniques to assess dynamic and static vehicle performance.

IV.2 Driving Cycles:

The European Driving Cycles, US Driving Cycles and Japanese Driving Cycles are popularly practiced and serves as the main benchmark on the performance of the vehicle in various countries. Mainly, these cycles also can be subcategorized into emissions test cycles and also specialized condition testing cycles. The specialized condition cycles include test cases for no-road use vehicles, engine bench tests and inspection and maintenance cycles, which are more focused on vehicle and drivetrain functions and durability instead of vehicle emissions. Meanwhile, vehicle emissions cycles are also subjected to different vehicle factors and operational factors, hence few different testing needs, they are generally differentiated by urban and highway driving cycles for light duty vehicles, and on engine dynamometer or chassis dynamometers for heavy-duty vehicles.

A. North European Driving Cycles (NEDC)

Being the shortest distance and quickest drive cycle, the NEDC drive cycle consists of four repetitions of UDC driving cycle and a segment of EUDC driving cycle, as shown in Fig IV.1, the repetitions are devised to represent urban driving conditions, which maximum speed up to 120Km/h this transient driving cycle has been criticized for bearing little relation to actual driving patterns and behaviors on the road. It's highly stylized cycle, with periods of constant acceleration, deceleration and speed, combined with may result in unrealistically low emission levels, besides the test procedure which also calls for vehicle to be placed at temperature of 20°C to 30°C prior testing is also much higher-than-average European outdoor temperature of 10°C, contrariwise it is also considered impractical to place the vehicle in high ambient temperature, which may induce heavier loading of air conditioning use.

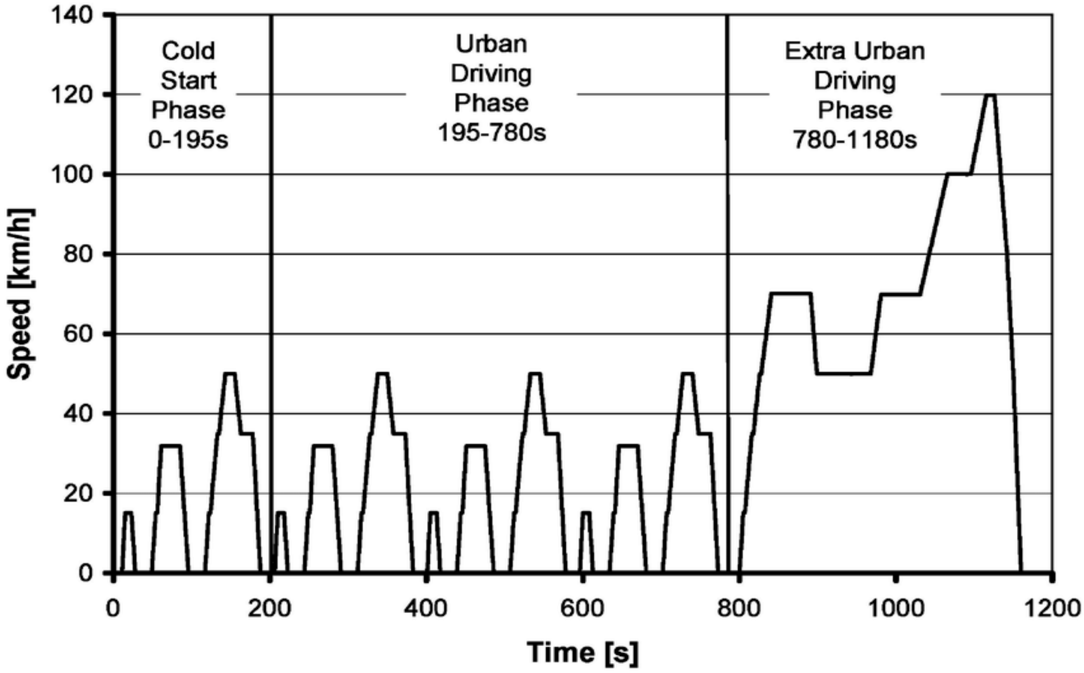

Fig IV.1. Velocity-time graph for the NEDC Driving Cycle [28].

B. FTP-75

For the United States, FTP-75 is a standard drive cycle for emissions certification and fuel economy testing. Also based on transient drive cycle, this cycle covers the longest distance of 17.77 Km and yet has the most stops out of the three certification cycles, as shown in Fig IV.2, the cycle has three distinctive phases, which is the cold start transient phase of 0 second to 505 seconds and hot soak with engine stopped for 10 minutes. The fourth phase is the repeat of the transient phase, however, with the engine started prior and warm, which this phase considered as hot start transient phase Nonetheless since year 2000,the United States has included mandatory additional testing cycle to be carried out for on the road vehicle emissions certifications, The cycles are Supplemental Federal Test Procedures (SFTP) which provide better coverage of both aggressive highway driving and simulate use of air-conditioning units at higher ambient temperature.

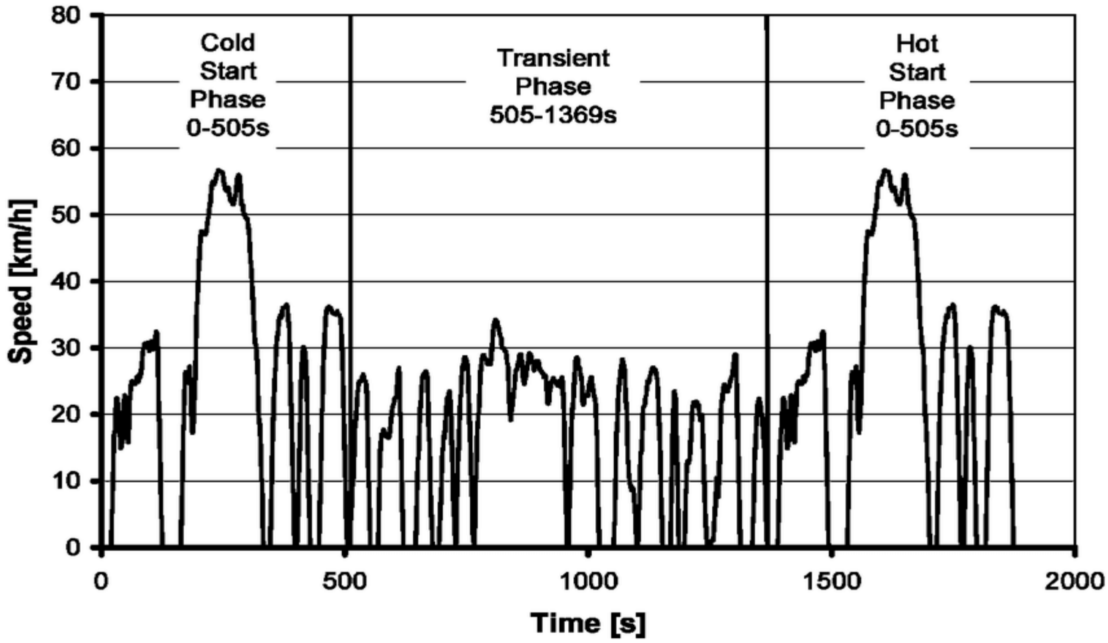

Fig IV.2: Velocity-time graph for the US FTP Driving Cycle

C. JE 05 Driving Cycle

As shown in Fig IV.3, the JE 05 Cycle is pretty demanding cycle for a vehicle test. Based on congested urban traffic condition, this cycle travels the shortest distance, yet has the hardest acceleration and idle considerably long for its cycle length, This test cycle requires running the vehicle on both cold start and warm start, this model cycle has been last cycle, which is largely similar to NEDC cycle, has also been criticized for similar reasons. Mainly lack of speed variation and only holding constant acceleration, which bears little relation to actual driving patterns. The JE 05 cycle initially expects a 15% variation as compared with 10-15 mode, however, is expected to reflect more realistic figures.

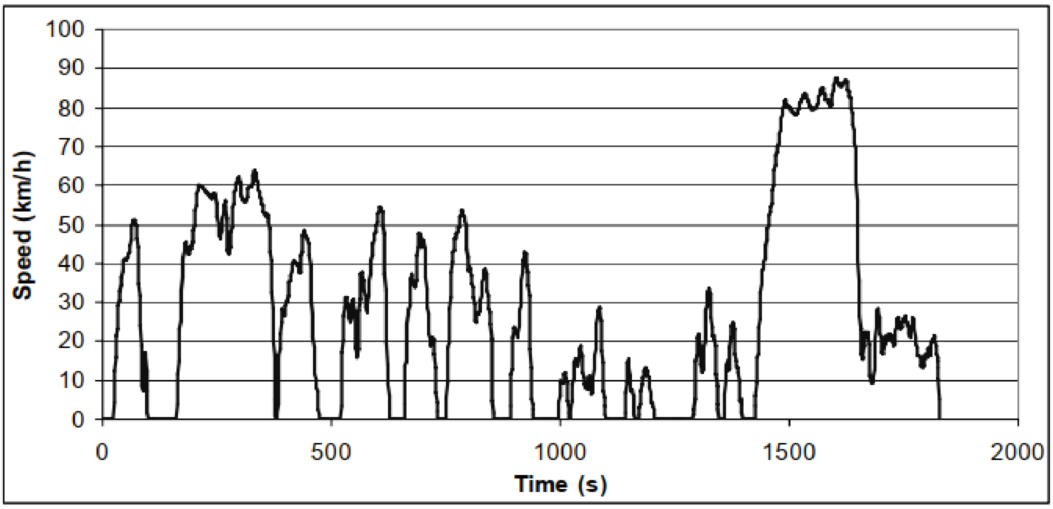

Fig IV.3: Velocity-time graph for the JE 05 Driving Cycle

To get an idea of these driving cycles, we show in the following table (IV.1) shows the cycles with these characteristics

Table.IV.1. the characteristics of driving cycles

Characteristics	NEDC	FTP-75	JE05
Total distance (m)	*11016.63*	*17786.59*	*13897.4*
Total time (s)	*1180*	*1874*	*1829*
Maximum speed (Km/h)	*120.09*	*91.09*	*87.49*
Average driving speed (Km/h)	*42.24*	*39.21*	*34.74*
Drive time (s)	*458*	*376*	*294*
Drive time spent accelerating (s)	*278*	*683*	*601*
Drive time spent decelerating (s)	*204*	*574*	*545*
Standing time (s)	*241*	*241*	*389*

IV.3 Vehicle dynamic model:

The vehicle considered in our work is the urban type, it is the Bluecar vehicle, it represents in fig (IV.4), and the parameters of this car are summarized in the table.VI.1

Fig.IV.4. the Bluecar vehicle

Table IV. 2 Parameters of Bluecar type urban electric vehicle

VE Parameters	Value
Vehicle mass (*MVE*)	820 kg
gravity force (*g*)	9.81 m/s^2
radius of a wheel (*r*)	0.33 m
Air density (ρ)	1.2 kg/m^3
Front area (*S*)	2.75
Air penetration coefficient (*Cx*)	0.3
Rolling resistance coefficient in dynamic state (*C0*)	1.6e-^{6}
Rolling resistance coefficient in static state (*C1*)	0.008
***Incline angle of the road* (α)**	2.5%

Since the land vehicles are designed to move primarily in one direction, only single dimensional lateral dynamics are considered. There are five lateral force components: inertial force, longitudinal traction force, air drag, tire rolling resistance, and gravity when the vehicle is moving up or down a hill.

IV.4 Forces applied to the vehicle:

The forces applied to the vehicle consist of:

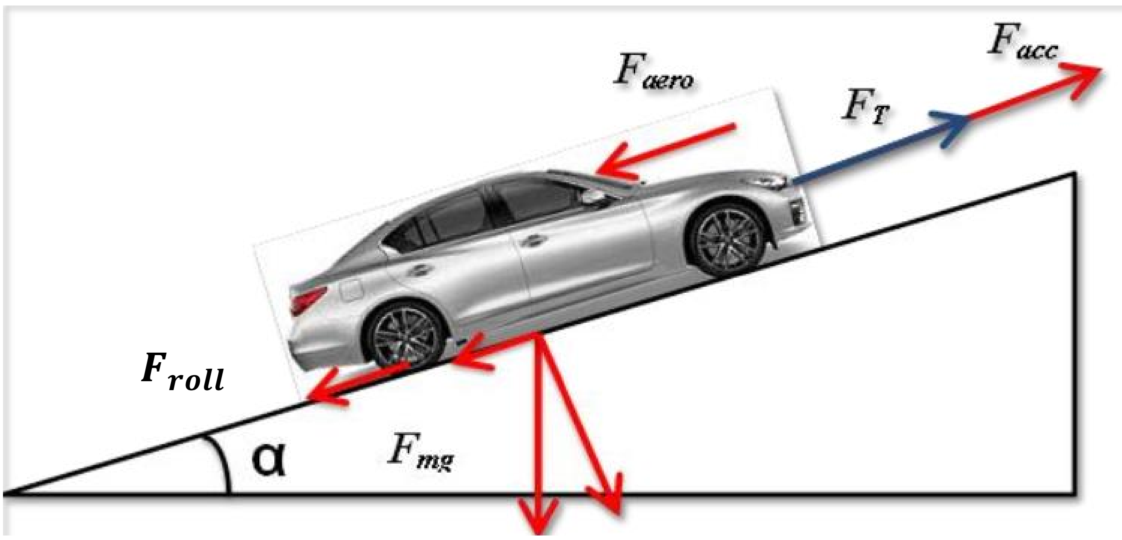

Fig.IV.5 Forces applied to a rolling electric vehicle **[29].**

The power at the wheel P_{EV} which can be expressed by:

$P_{EV} = T_T \, \Omega_{roll}$

The total traction torque T_T and the rotation speed of the wheel Ω_{roll}:

$T_T = F_T \, r$

$\Omega_{roll} = \frac{V_{ev}}{r}$

With: r the radius of the wheel.

Finally we have:

$P_{EV} = F_T \, V_{ev}$

The total force is then written in the following form:

$$F_T = F_{slope} + F_{aero} + F_{roll} + F_{acc}$$

A. **Rolling Resistance:**

As the tire rotates, a part of the tire is continuously depressed at the bottom, and then released back to its original shape after it leaves the contact region. These depressing and releasing processes are not totally elastic. That is, due to the damping action, energy is consumed during the deforming and recovering processes. Such a loss of energy in the tire is reflected as a rolling resistance that opposes the motion of the vehicle. Obviously, the amount of deformation depends on the vehicle's weight. Typically,

$$F_{roll} = M_{ve} \, g \, (C_0 + C_1) \, v_x^{\,2}$$

B. **Aerodynamic Drag Force :**

When a headwind blows at a speed of V_{wind} to a moving vehicle [3], the aerodynamic drag force exerted on a vehicle is calculated as

$$F_{aero} = \frac{\rho \, C_d \, A_F}{2} (V_x + V_{wind})^2$$

where ρ is the mass density of air, Cd is the aerodynamic drag coefficient, and AF is the equivalent frontal area of the vehicle. The mass density of air is equal to ρ = 1.225 kg/m3 at the commonly used standard set of conditions (15◦C and a 101.32 kPa).

To investigate the aerodynamic effect separately, we assume in the following that a vehicle is traveling a horizontal road when the headwind is equal to zero. Neglecting the rolling resistance

$$F_{aero} = \frac{\rho \, C_d \, A_F}{2} (V_x)^2$$

C. Force due to road profile

The force of the road dynamics is the force of gravity obtained when the vehicle is moving on a sloping road

$$F_{slope} = m_v g \sin\alpha$$

D. Force due to acceleration :

The force due to acceleration ensures the dynamic behavior desired by the driver.

$$F_{acc} = m_v \frac{dV_x}{dt}$$

IV.5 Transmission and mechanical reducer:

The reducer is a very important element often allowing a consequent saving on the mass of the motor whose dimensions are determined mainly by the torque to be supplied as shown in figure :

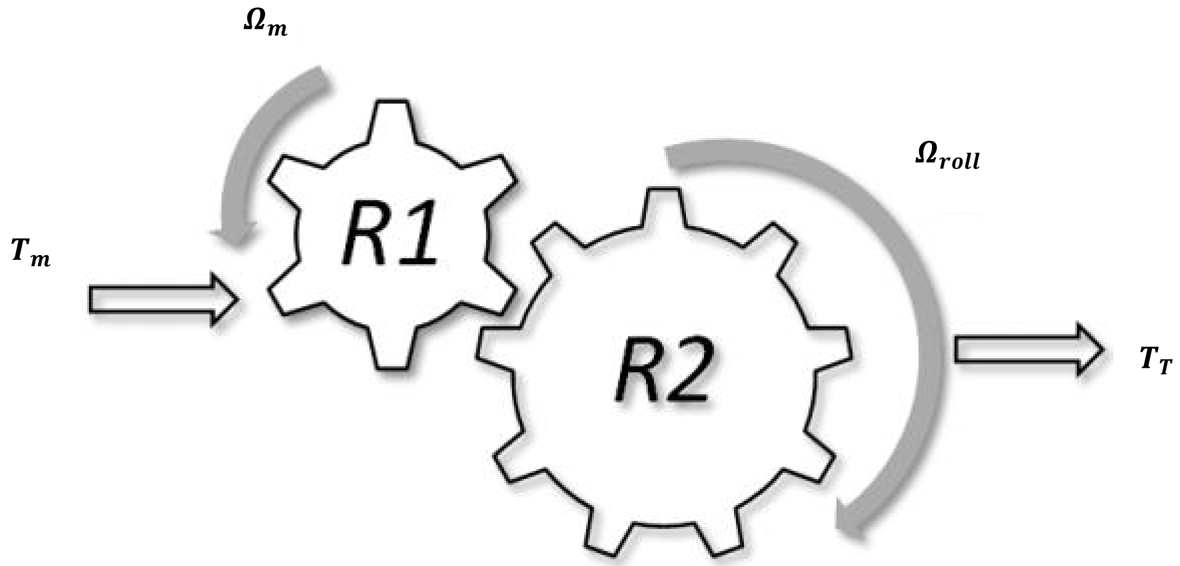

Fig.IV.6 The gear mechanism

$$T_T = g_{dr}\, T_m$$

$$\omega_m = \frac{1}{g_{dr}}\, \omega_{roll}$$

g_{dr}: The gear ratio

IV.6 Vehicle Dynamic Model simulation:

The powertrain system transfer function obtained in the previous section was created in the MATLAB/Simulink program in this section. Calculation of the angular velocity of the electric motor is provided. At this point the momentary torque and efficiency of the electric motor is determined. The angular velocity of the motor is divided by the differential ratio. Then the vehicle speed is obtained by multiplying by the radius of the wheel. By taking the integral of the vehicle speed, the distance traveled by the vehicle is calculated. The derivation of the vehicle speed gives the acceleration of the vehicle.

In this part, we want to simulate the dynamic model of the vehicle to know the load torque (Tr) based on the speed profile (NEDC), we made the choice of the European profile because of its characteristics (constant speed acceleration and braking) and how our vehicle will be used as an urban vehicle

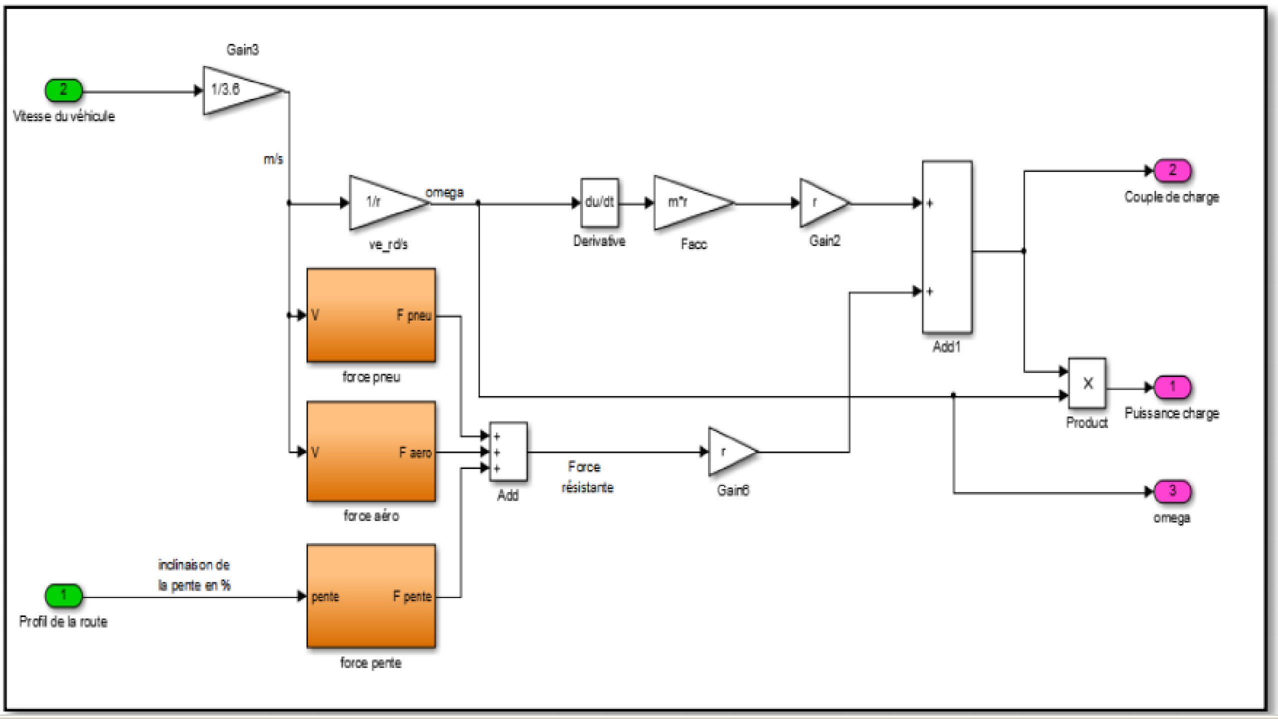

Fig.IV.7. Vehicle Dynamic Model with Simulink

1. **Simulation result**

The **Fig.IV.7** showed the reference speed and the load torque, as long as the load torque was calculated from this velocity profile using the mechanical characteristics and vehicle aerodynamics

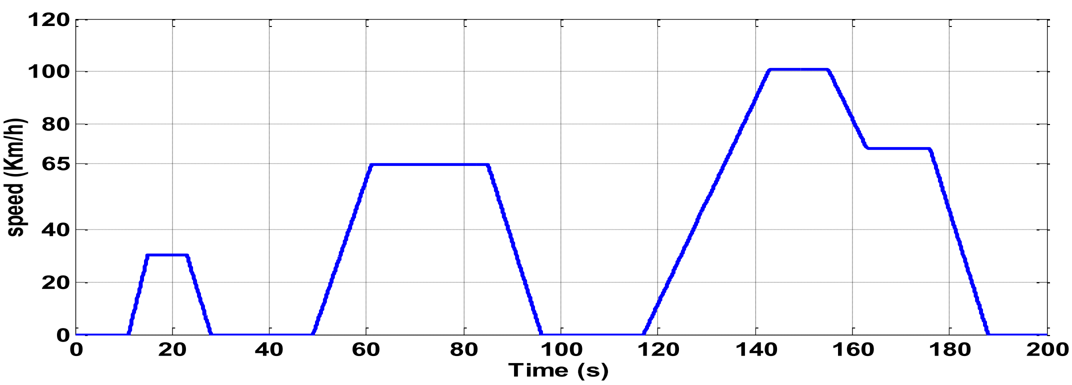

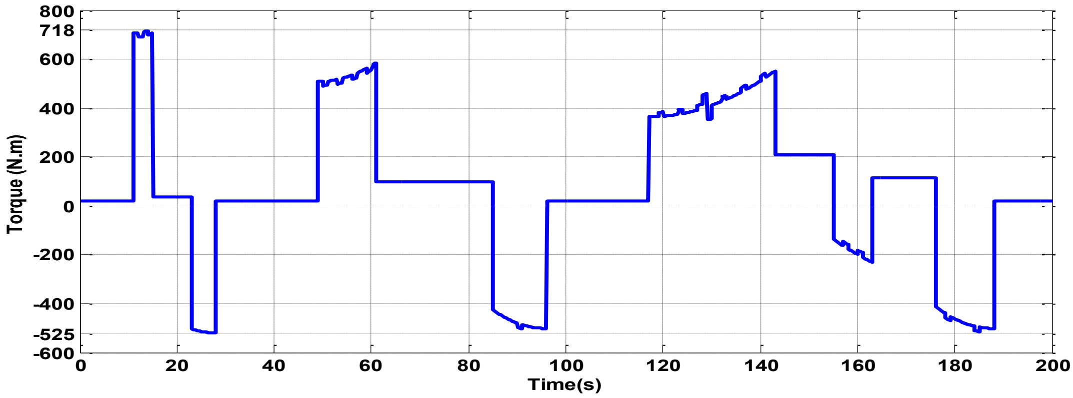

Fig.IV.8 Result of speed and torque simulation setpoints (Vref and Tref)

Note:

1- To apply our control technique, the reference speed must be reset to (rad/s). So :

(Km/h) $\times \frac{1}{3.6}$ = (m/s)

(m/s) $\times \frac{1}{r}$ = (rad/s)

2- The motor power of our syudy is equal to 60kw, so we calculate the torque nominal as follows:

We have P=4 number of poles; the nominal speed is equal to 240 rad /s

$T_m = \frac{P_u}{\Omega} = \frac{60000}{240} = 250$ N.m

We notice that the maximum load torque in the results equals almost 718N.m, so we calculates the gear ratio to maximize the torque in the wheel.

$$T_m = g_{dr}\, T_T \;\rightarrow\; g_{dr} = \frac{T_\omega}{T_e} = \frac{720}{250} = 2.87$$

$$\omega_m = \frac{1}{g_{dr}}\, \omega_T$$

Result of the torque, speed and power simulation setpoints:

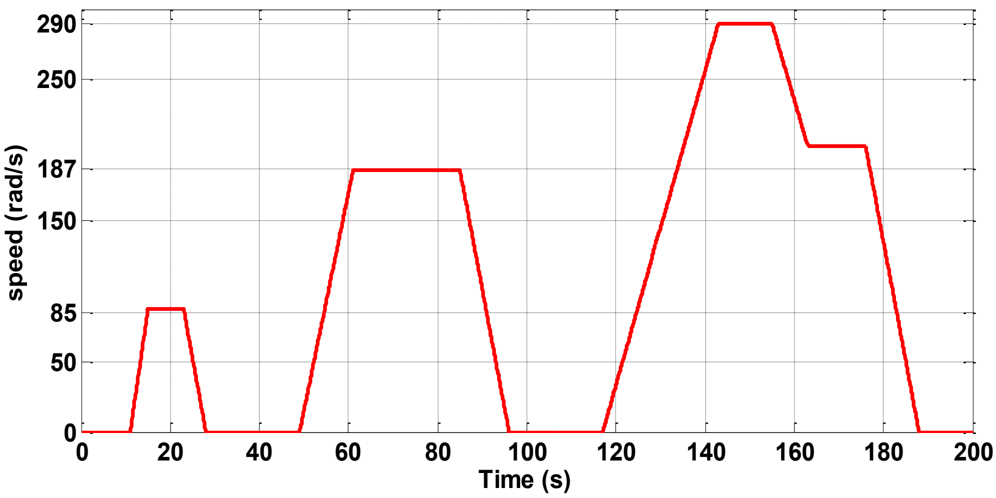

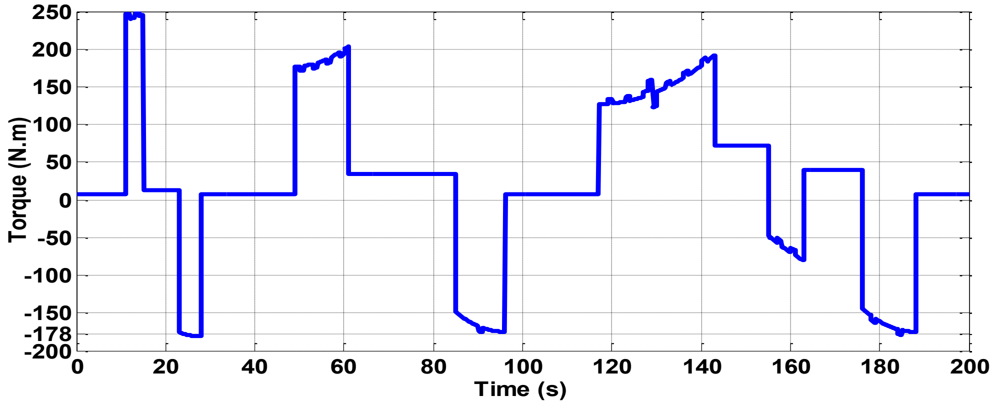

Fig.IV.9 Result of the speed and torque references simulation (Vref and Tref)

According to these results (**Fig.IV.9**) and the power equation (P_{ve} = T_{ω} Ω_{roll}) we can deduce the power demanded by the vehicle as shown in the figure: $\boldsymbol{P_{EV} = T_T\ \Omega_{roll}}$

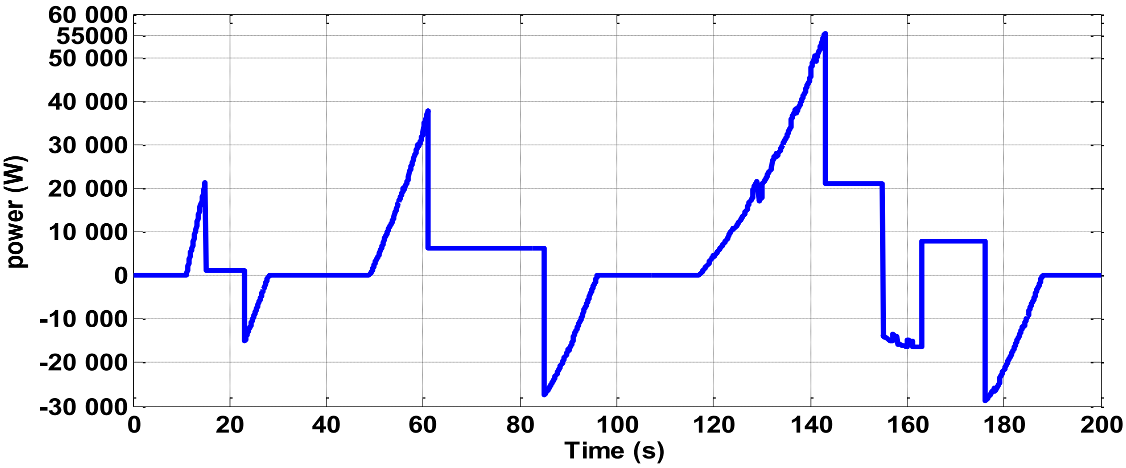

Fig.IV.10 The power requested by the vehicle (Pref)

2. Application of the driving cycle to the sensorless FOC control of pmsm :

Simulation results

Here we consider the application as a reference speed a European driving cycle standardized (the extra urban part), on the other hand, a resistive torque is applied which is obtained from the dynamic model of the vehicle.

The following figures show the results of the response of our traction chain with the two control techniques, namely vector control with sensor (in red) and vector control without sensor (in green) There is a 5-second interval [55s.60s] between the failure happen and the moment when the observer start work.

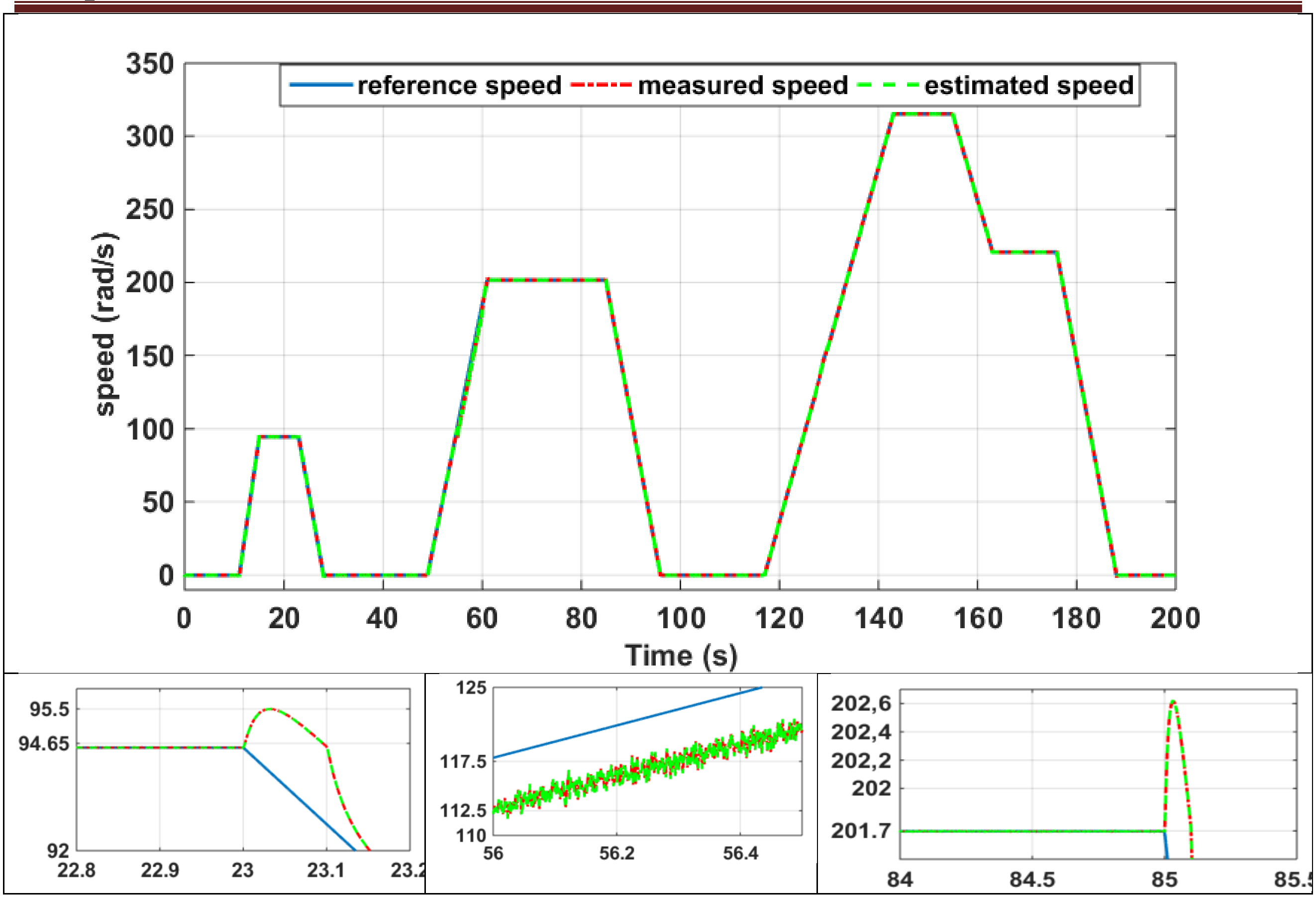

Fig.IV.11 vehicle speed simulation results in rad/s, with the scenario of the speed sensor failure

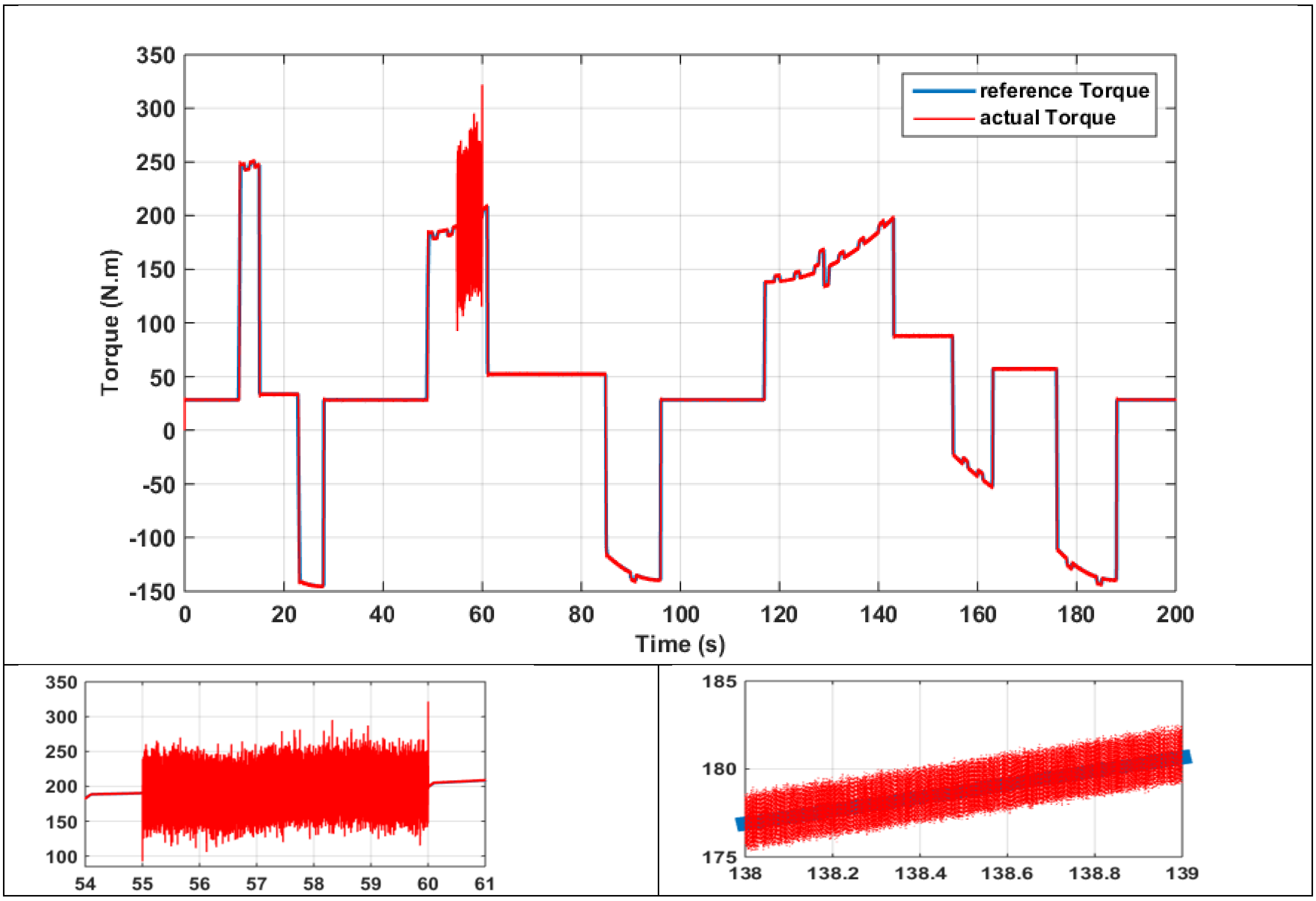

Fig.IV.12 vehicle Torque simulation results in N.m, with the scenario of the speed sensor failure

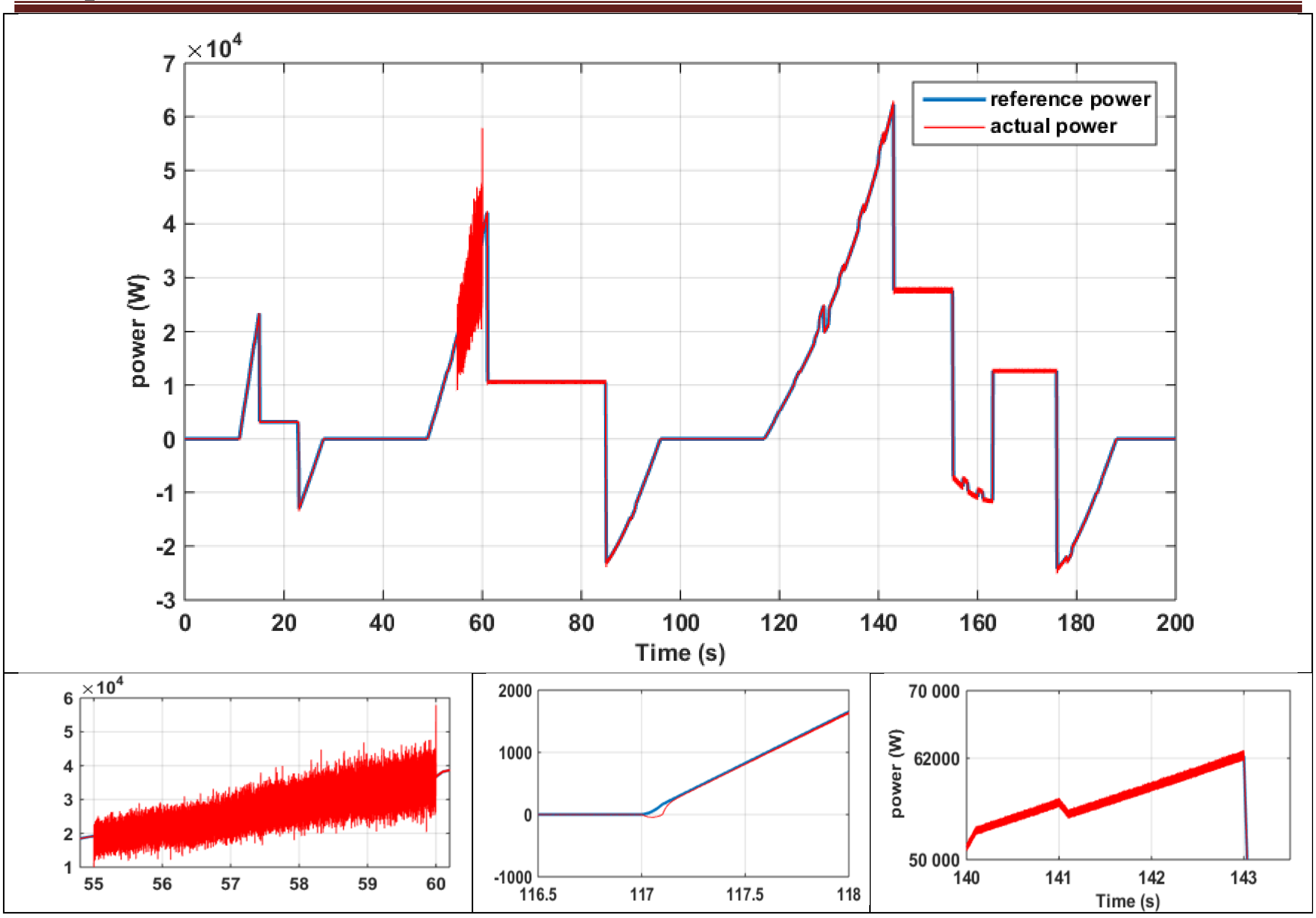

Fig.IV.13 vehicle Power simulation results in W, with the scenario of the speed sensor failure

Simulation results under NEDC driving cycles:

It can be observed in **Fig.IV.11** that the estimated speed follow track rapidly their reference value with an average speed estimation error approximately equal to zero with some overshoots When changing speed(**acceleration and deceleration**), which confirms the effectiveness of the MRAS observer work,

As shown in **Fig.IV.12**. The estimated electromagnetic torque follows perfectly the load torque generated by the machine in all of the speed range, with some fluctuations around 2%, and there is also a very clear response at failure happen. As for power comparing the reference **Fig.IV.13** gives us the desired response with also some small fluctuations but it is generally acceptable.

IV.7 Conclusion:

This chapter has been dedicated to the application of the FOC control techniques with the scenario of the speed sensor failure on the Traction chain of a real Extra urban-type vehicle. At the beginning, is represented by an overview about driving cycles such as the NEDC European Standard Driving and vehicle dynamics model we discussed the specifications of the vehicle for complete our study. Then. By using these last two parameters, we had the load torque setpoints and of the mechanical speed to be applied to the motor. Subsequently, we applied just one of the three techniques control observation in the previous chapter, The simulation results obtained have proven the vector control ensures acceptable performance in terms of stability and tracking of the setpoint and its robustness is good especially with respect to the rejection of disturbances. It is noted that the good performance in term of precision speed and robustness are ensured by the MRAS observer compared to the speed sensor mode. These performances are reflected in the application vehicle on the comfort of the car as well as the performance of the traction chain.

General Conclusion

The subject of this thesis is to make a contribution to the mechanical sensorless control of permanent magnet synchronous machines. This study is placed in the context of the electric vehicle and has the primary application of the traction chain control

The first chapter contains an overview of the electric car and its different types, structures and sensors, the second chapter, we briefly saw the modeling of the MSAP. We have used the Park transformation to present the three-phase machine in a frame at two axes in order to simplify the resolution of the electromagnetic equations of the machine. By Next, we determined the control laws of the vector control of the MSAP associated with a standard PI regulator. With this technique we obtains a decoupled model of the machine. The training simulation results are overall acceptable. They show the performance of the vector control well: pursues it and satisfactorily in parametric variations and load changing, the disturbance is rejected in a very short time, the response is fast

The third chapter presents the study of the sensorless control of the MSAP with the observer by sliding mode and model reference adaptive system (MRAS), the extended Kalman filter (EKF) which eliminates the sensor and its drawbacks.

We have obtained satisfactory results in terms of speed pursuit. Of the more robust this control is with respect to the load torque since it is determined assuming that the load torque is unknown; But I had a problem in terms of the negative torque in EKF observer and the SMO observer, which took me some time. However, the results need to be improved of course.

For our part, we can affirm on the basis of the results obtained that the command without mechanical sensor with the technique of model reference adaptive system MRAS, sliding mode and extended Kalman filter observation based on the modeling (d-q) is a feasible and interesting technique for controlling the MSAP.

Bibliographic references

[1] El Hadji Sidath Diao. Fault Tolerant Control for Critical machine-inverter systems used in automotive industry. Engineering Sciences [physics]. Université Paris Sud - Paris XI, 2014. English. NNT : 2014PA112311. tel-01127062

[2], Chris Mi, Fang Z. Peng, Kenneth J. Kelly, Michael O'Keefe and Vahab Hassani, Topology, design, analysis and thermal management of power electronics for hybrid electric vehicle applications, Vol. 1, No. 3, 2008

[3]. Per Enge, Nick Enge, Stephen Zoepf,,Electric vehivle engineering, edition 01e éd. . New York, NY : McGraw-Hill Education, 2021

[4] Rinkesh. 2020 July 05. Various Advantages and Disadvantages of Electric Cars .Conserve Energy Future.https://www.conserve-energy-future.com/advantages-and-disadvantages-of-electric-cars.php

[5] Chunhua Liu, K. T. Chau, Diyun Wu, Shuang Gao. Opportunities and Challenges of Vehicle-to-Home, Vehicle-to-Vehicle, and Vehicle-to-Grid Technologies. Vol. 101, No. 11, November 2013 | Proceedings of the IEEE

[6] Ashok Jhunjhunwala , Prabhjot kaur Kaur, Neha Yadav. A Guidance Document on Accelerating Electric Mobility in India. Written for Shakti Sustainable Energy Foundation by IIT Madras (CBEEV) & WRI India.September 2019

[7] Sun, Z.; Wen, Z.; Zhao, X.; Yang, Y.; Li, S. Real-World Driving Cycles Adaptability of Electric Vehicles. World Electr. Veh. J. 2020, 11, 19. https://doi.org/10.3390/wevj11010019

[8] Pandav Kiran Maroti Sanjeevikumar Padmanaban Mahajan Sagar Bhaskar Vigna K. Ramachandaramurthy Frede Blaabjerg. The state-of-the-art of power electronics converters configurations in electric vehicle technologies. Published by Elsevier Ltd. November 2021

[9] Hemanth Kumar, 2022 July 19. Electric Vehicle(EV) Configurations. Mass Foundation. https://mass-foundation.org/electric-vehicleev-configurations/

[10] Yuche Chen, Ruixiao Sun, Guoyuan Wu, A Review and Outlook of Energy Consumption Estimation Models for Electric Vehicles, SAE International Journal of Sustainable Transport., Energy, Environment, & Policy..March 2020

[11] Tom Harbid, 2021 May 18, Common Speed Sensor Problems Symptoms, Causes, and How to Fix It. Cash Cars Buyer.https://www.cashcarsbuyer.com/speed-sensor-problem/

[12]: Abhisek Karki, Sudip Phuyal, Daniel Tuladhar, Subarna Basnet, Bim Prasad Shrestha. Status of Pure Electric Vehicle Power Train Technology and Future Prospects. Appl. Syst. Innov. 2020, 3, 35; doi:10.3390/asi3030035

[13] : Mehrdad Ehsani. Krishna Veer Singh. Ramin Tafazzoli Mehrjard. State of the Art and Trends in Electric and Hybrid Electric Vehicles. Vol. 109, No. 6, June 2021. IEEE International Dealers IEL+

[14]: Aviru Kumar Basu. Shantanu Bhattacharya. Shreyansh Tatiya. Overview of Electric Vehicles (EVs) and EV Sensors. January 2019. DOI: 10.1007/978-981-13-3290-6_7

Bibliographic references

[15]: Fuad Un-Noor, Sanjeevikumar Padmanaban, Lucian Mihet-Popa, Mohammad Nurunnabi Mollah, Eklas Hossain. A Comprehensive Study of Key Electric Vehicle (EV) Components, Technologies, Challenges, Impacts, and Future Direction of Development. Energies 2017, 10, 1217; doi:10.3390/en10081217.

[16]: Leszek Jarzebowicz, Krzysztof Karwowski, Wlodek J. Kulesza. Sensorless algorithm for sustaining controllability of IPMSM drive in electric vehicle after resolver fault. Control Engineering Practice · January 2017. DOI: 10.1016/j.conengprac.2016.10.004

[17]: Mohamed Saied, M. Z. Mostafa, T. M. Abdel-Moneim, Hasan A. Yousef, New 13-Space Vector Diagram for the Three-Phase Six Switches Voltage Source Inverter. May 2012. DOI:10.1109/ISIE.2012.6237120

[18]: Enrique L. Carrillo Arroyo.'' MODELING AND SIMULATION OF PERMANENT MAGNET SYNCHRONOUS MOTOR DRIVE SYSTEM''.2006

[19]: Dmitry Levkin. 2022 July 19. Permanent magnet synchronous motor. Permanent Magnet Synchronous Motor. https://en.engineering-solutions.ru/motorcontrol/pmsm/

[20]: IQBAL HUSAIN, SARIFUL ISLAM, EMRE GURPINAR, Burak Ozpineci, Shajjad Chowdhury, Lincoln (Lingxiao) Xue, Gui-Jia Su, Dhrubo Rahman, Wensong Yu, Raj Sahu. Electric Drive Technology Trends, Challenges, and Opportunities for Future EVs. Vol. 109, No. 6, June 2021

[21]: Ramesh T Ramamoorthy, Brett Larimore, Manish Bhardwaj. Sensored Field Oriented Control of 3-Phase Permanent Magnet Synchronous Motors Using TMS320F2837x. Texas Instruments Incorporated. 2021

[22]: SENHADJI Nawel, CHALABI Ammaria. COMMANDE DU MOTEUR SYNCHRONE A AIMANTS PERMANENTS PAR BACKSTEPPING.2015

[23]: A. Glumineau and J. de León Morales, Sensorless AC Electric Motor Control, Advances in Industrial Control, DOI 10.1007/978-3-319-14586-0

[24]: Li, Y.; Wu, H.; Xu, X.; Sun, X.; Zhao, J. Rotor Position Estimation Approaches for Sensorless Control of Permanent Magnet Traction Motor in Electric Vehicles: A Review. World Electr. Veh. J. 2021, 12, 9. https:// doi.org/10.3390/wevj12010009

[25]. Jiaxin Wu, Yi Zhang, Hanpei Wei, Haifeng Wei, Sensorless Vector Control of Permanent Magnet Synchronous Motor Based on Model Reference Adaptive System, 2017 IEEE 978-1-5090-6352-9

[26], Marcel NICOLA, Claudiu-Ionel NICOLA, Adrian VINTILĂ, Sensorless Control of Multi-Motors PMSM using Back-EMF Sliding Mode Observer, 2019 IEEE 978-1-7281-0791-2

[27], Zdenek Peroutka, Design Considerations for Sensorless Control of PMSM Drive Based on Extended Kalman Filter, EPE 2005,90-75815-08-5

[28]:T J Barlow,S Latham,I S McCrae and P G Boulter.A reference book of driving cycles for use in the measurement of road vehicle emissions.Version:3.June 2009

[29] Baadj Lakhdar, Ibrahimibrahimi Ayman, Etude d'une chaine de traction d'un véhicule électrique. University of Amar Thelidji-Laghouat

Bibliographic references

[30]. Murali, A.; Wahab, R.S.; Gade, C.S.R.; Annamalai, C.; Subramaniam, U. Assessing Finite Control Set Model Predictive Speed Controlled PMSM Performance for Deployment in Electric Vehicles. *World Electr. Veh. J.* 2021, *12*, 41. https://doi.org/10.3390/wevj12010041